



AFTAC

Headquarters, Air Force Technical Applications Center
Patrick Air Force Base FL 32925-6001
Directorate of Nuclear Treaty Monitoring
Research Division



Discrimination of Earthquakes and Explosions at Regional Distances Using Complexity

DTIC
S **ELECTE** **D**
AUG 06 1993
A

Robert R. Blandford
HQ AFTAC/TT

17 June 1993

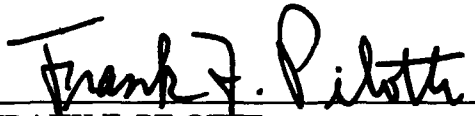
This document has been approved
for public release and sale; its
distribution is unlimited.

93-17763



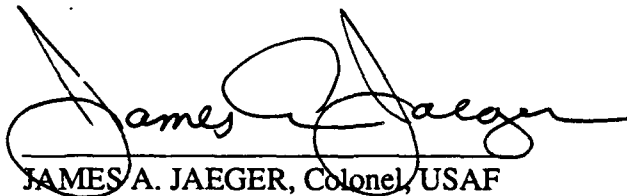
93 3 3 3 17763

Report AFTAC-TR-93-044 has been reviewed and is approved for publication.

A handwritten signature in black ink, appearing to read "Frank F. Pilotte". The signature is written in a cursive style with a horizontal line underneath.

FRANK F. PILOTTE

Director, Nuclear Treaty Monitoring Directorate

A handwritten signature in black ink, appearing to read "James A. Jaeger". The signature is written in a cursive style with a horizontal line underneath.

JAMES A. JAEGER, Colonel, USAF
Commander

If you change your address, wish to be removed from the mailing list, or your organization no longer employs the addressee, please notify HQ AFTAC/TTR, 1030 S. Highway A1A, Patrick AFB FL 32925-3002.

REPORT DOCUMENTATION PAGE			Form Approved OMB No. 0704-0188	
<small>Public reporting burden for this collection of information is estimated to average 1 hour per response, including the time for reviewing instructions, searching existing data sources, gathering and maintaining the data needed, and completing and reviewing the collection of information. Send comments regarding this burden estimate or any other aspect of this collection of information, including suggestions for reducing this burden, to Washington Headquarters Services, Directorate for Information Operations and Reports, 1215 Jefferson Davis Highway, Suite 1204, Arlington, VA 22202-4302, and to the Office of Management and Budget, Paperwork Reduction Project (0704-0188), Washington, DC 20503.</small>				
1. AGENCY USE ONLY (Leave blank)		2. REPORT DATE 17 Jun 93		3. REPORT TYPE AND DATES COVERED Technical
4. TITLE AND SUBTITLE Discrimination of Earthquakes and Explosions at Regional Distances Using Complexity			5. FUNDING NUMBERS	
6. AUTHOR(S) Robert R. Blandford				
7. PERFORMING ORGANIZATION NAME(S) AND ADDRESS(ES) HQ Air Force Technical Applications Center (HQ AFTAC/TTR) 1030 S. Highway A1A Patrick AFB FL 32925-3002			8. PERFORMING ORGANIZATION REPORT NUMBER AFTAC-TR-93-044	
9. SPONSORING / MONITORING AGENCY NAME(S) AND ADDRESS(ES)			10. SPONSORING / MONITORING AGENCY REPORT NUMBER	
11. SUPPLEMENTARY NOTES				
12a. DISTRIBUTION / AVAILABILITY STATEMENT Unlimited			12b. DISTRIBUTION CODE	
13. ABSTRACT (Maximum 200 words) Earthquakes on land in Scandinavia are shown to typically have emergent <i>P</i> -wave signals in the distance range 1.5 to 15 degrees and in the frequency range 2-10 Hz at the single center elements of one or more of the arrays ARCESS, NOR-ESS, and FINNESS; while explosions show impulsive signals. For reasons similar to teleseismic complexity, the causes for this discriminant involve earthquake <i>P</i> -wave nulls, and <i>sP</i> for the deeper earthquakes. The <i>S</i> -converted phases, including <i>sP</i> , are more prominent at regional than at teleseismic distances because of the greater <i>S</i> to <i>P</i> conversion resulting from the greater angles of incidence on the approximately horizontal interfaces. Where there are <i>P</i> wave nulls there is an emergent <i>P</i> wave deriving from <i>S</i> to <i>P</i> conversions. It appears that such an emergent signal can arise only by scattering in 2D or 3D heterogeneities and, for vertical faults, along the fault strike, only by conversion of transverse <i>S</i> to vertical or radial <i>P</i> . The discriminant seems to be more robust at regional than at teleseismic distances. This may be because at high frequencies (2-5 Hz) at regional distances there are multiple paths along which the <i>P</i> wave may arrive in the first five seconds of the signal. Even if one of these paths is defocussed so that the amplitude is low, the other paths may not be defocussed. As a result, as compared to a 1 Hz teleseismic explosion signal, it may be less likely that a high-frequency regional signal will appear emergent due to heterogeneity in the earth. The discriminant may also be more robust because there can be more <i>S</i> to <i>P</i> conversions at many high-wavenumber heterogeneities which scatter only weakly at lower frequencies. The discriminant also appears to work well for several other regions.				
14. SUBJECT TERMS Regional Discrimination Complexity		Scandinavia Quarry Blasts Spall		15. NUMBER OF PAGES 82
		Scattering AFTAC-TR-93-044		16. PRICE CODE
17. SECURITY CLASSIFICATION OF REPORT UNCLASSIFIED	18. SECURITY CLASSIFICATION OF THIS PAGE UNCLASSIFIED	19. SECURITY CLASSIFICATION OF ABSTRACT UNCLASSIFIED	20. LIMITATION OF ABSTRACT UNCLASSIFIED	

(This page intentionally left blank)

CONTENTS

	<u>Page</u>
LIST OF FIGURES	iv
LIST OF TABLES	x
ACKNOWLEDGEMENTS	xi
ABSTRACT	1
INTRODUCTION	2
DATA SELECTION	6
DATA ANALYSIS	11
SYNTHETIC CALCULATION METHODS	30
SYNTHETIC CALCULATION RESULTS	34
CONCLUSIONS	58
REFERENCES	61
DISTRIBUTION	66

Accession For	
NTIS CRARI	<input checked="" type="checkbox"/>
DTIC TAB	<input type="checkbox"/>
Unannounced	<input type="checkbox"/>
Justification	
By	
Distribution/	
Availability Codes	
Dist	Avail and/or Special
A-1	

DTIC QUALITY INSPECTED 3

LIST OF FIGURES

	<u>Page</u>
Figure 1. Reference map showing locations of stations, earthquakes, and explosions analyzed in this report. Asterisks (*) indicate explosions; octagons with a cross indicate earthquakes.	7
Figure 2a. Explosion profile, 1 Hz highpass. The signals are ordered by distance in the range 1.8 to 6.5 degrees as seen in Table 3. The explosions are seen to have impulsive arrivals in the first 1-10 seconds and to have a large P/L_g amplitude ratio as compared to the explosions seen in Figure 2b. The most emergent of the explosions is FIA1/199285. The signals for explosions in the range 7 to 12.7 degrees are seen in Figure 5a.	12
Figure 2b. Earthquake profile, 1 Hz highpass. The signals are ordered by distance in the range 1.6 to 6.9 degrees as seen in Table 4. The earthquakes are seen to have emergent arrivals in the first 1-10 seconds and to have a small P/L_g amplitude ratio as compared to the earthquakes seen in Figure 2a. The most impulsive of the earthquakes is ARA0/1991157. The signals for earthquakes in the range 7.2 to 14.9 degrees are seen in Figure 5b.	13
Figure 3a. First 20 seconds of the explosion signal in Figure 2a. The explosions are seen to have impulsive arrivals in the first 1-10 seconds and may be seen to have a large P/L_g amplitude ratio as compared to the earthquakes seen in Figure 3b by virtue of the fact that in each figure the maximum S phase is normalized to a constant magnitude, and the P amplitude is greater in Figure 3a than in Figure 3b. The most emergent of the explosions is FIA1/199285.	15
Figure 3b. First 20 seconds of the earthquake signal in Figure 2b. The earthquakes are seen to have emergent arrivals in the first 1-10 seconds and may be seen to have a low P/L_g amplitude ratio as compared to the explosions seen in Figure 3b by virtue of the fact that in each figure the maximum S phase is normalized to a constant amplitude, and the P amplitude is greater in Figure 3a than in Figure 3b. The most impulsive of the earthquakes is ARA0/1991157.	16
Figure 4a. Transverse component of the explosion signals in Figure 2a. The explosions are seen to have more impulsive arrivals in the first 105 seconds as compared to the earthquake transverse components seen in Figure 4b. We see that the signal for FIA1/199285 is here also the most emergent explosion signal as it was in Figure 2a.	17

- Figure 4b. Transverse component of the earthquake signals in Figure 2b. The earthquakes are seen to have more emergent arrivals in the first 1-5 seconds as compared to the explosion transverse components seen in Figure 4a. The most impulsive of the earthquakes seems to remain ARA0/1991157 as seen in Figure 2b, but it is difficult to be certain due to the small amplitudes of the transverse component P wave.18
- Figure 5a. Explosion profile, 1 Hz highpass. The signals are ordered by distance in the range 7.0 to 12.7 degrees as seen in Table 3. The explosions are seen to have impulsive arrivals in the first 1-10 seconds and to have a large P/L_g amplitude ratio as compared to the earthquakes seen in Figure 5b. The signals for explosions in the range 1.8 to 6.5 degrees are seen in Figure 2a. ARA0/19915 can be seen to be impulsive in Figure 6a where a 2 Hz highpass filter is applied. The small impulse near 55 seconds in FLA1/199116 is regarded as significant and is characteristic of explosion signals.20
- Figure 5b. Earthquake profile, 1 Hz highpass. The signals are ordered by distance in the range 7.2 to 14.9 degrees as seen in Table 4. The earthquakes are seen to have emergent arrivals in the first 1-10 seconds and to have a small P/L_g amplitude ratio as compared to the explosions seen in Figure 5a. The signals for earthquakes in the range 1.6 to 6.9 degrees are seen in Figure 2b.21
- Figure 6a. The same as Figure 5a except as seen through a 2 Hz highpass filter. The event ARA0/19915 is now seen to be impulsive.22
- Figure 6b. The same as Figure 5b except as seen through a 2 Hz highpass filter.23
- Figure 7a. First 20 seconds of signal from explosions in the distance range 7.0 to 12.7 degrees. By comparison with Figure 7b it may be seen that explosions typically have an initial pulse of 2-5 Hz waves, whereas earthquake signals are more emergent. Similarly, since the maximum S amplitude has been normalized to a constant amplitude in Figures 7a and 7b, and the amplitudes in Figure 7b are substantially smaller than in Figure 7a, it may easily be seen that earthquakes have smaller P/S amplitudes ratios as pointed out by Dysart and Pulli (1990).24
- Figure 7b. First 20 seconds of signal from earthquakes in the distance range 7.2 to 14.9 degrees. By comparison with Figure 7a it may be seen that explosions typically have an initial pulse of 2-5 Hz waves, whereas earthquake signals are more emergent. Similarly, since the maximum S amplitude has been normalized to a constant amplitude in Figures 7a and 7b, and the amplitudes in Figure 7b are substantially smaller than in Figure 7a, it may easily be seen that earthquakes have smaller P/S amplitudes ratios as pointed out by Dysart and Pulli (1990).25

Figure 8a.	Transverse waves from explosions in the distance interval 1.8 to 6.5 degrees, aligned on the <i>S</i> arrival and highpass filtered at 1 Hz. By comparison with the similar Figure 8b for earthquakes we see that the earthquakes do not have more impulsive <i>S</i> arrivals than do the explosions.	26
Figure 8b.	Transverse waves from earthquakes in the distance interval 1.6 to 6.9 degrees, aligned on the <i>S</i> arrival and highpass filtered at 1 Hz. By comparison with the similar Figure 8a for explosions, we see that the earthquakes do not have more impulsive <i>S</i> arrivals than do the explosions.	27
Figure 9.	From Wuster (1992). The upper trace is an earthquake and the lower trace is an explosion as recorded at GERESS from the Vogtland district 180 km Northwest of GERESS. The impulsive explosion and emergent earthquake fit the pattern seen in Scandinavia.	29
Figure 10.	From Ryaboy (1990 and 1992, personal communication). The vertical profile <i>P</i> velocity derived from DSS data was used in this study for the structure below 50 km. Also shown are the <i>P</i> profiles used routinely in DARPA's Intelligent Monitoring System (IMS) and in the Helsinki seismic bulletin.	32
Figure 11.	Broadband velocity vertical component synthetics for an explosion and a 45° dip-slip earthquake at 10 km depth for distances ranging from 100 to 1500 km. Amplitudes are scaled to a common maximum. The earthquakes are seen to have larger shear wave amplitudes.	35
Figure 12.	Broadband velocity vertical component synthetics for an explosion and a 45° dip-slip earthquake Green's function source at 10 km depth for distances ranging from 100 to 1500 km. Amplitudes are scaled to a common maximum. The earthquakes are seen to be more emergent due in large measure to a large <i>sP</i> phase. The large pulse on explosions at 300 and 1200 km at a 3-second delay is a reflection from the upper and lower boundary of a low velocity zone.	36
Figure 13a.	Radial (<i>v</i>) and transverse (<i>u</i>) signals from a Ricker wavelet compressional source in a random exponential medium with 2% rms variation in the <i>P</i> and <i>S</i> velocities is seen at distances of 50, 100, 150, and 200 km. The <i>u</i> scale have been increased by a factor of 2. At all distances the <i>P</i> arrival is impulsive on both radial and transverse components, although at 200 km the <i>P</i> arrival is apparently followed by a rather large second arrival.	38

- Figure 13b. Radial (v) and transverse (u) signals from a Ricker wavelet shear source in a random exponential medium with 2% rms variation in the P and S velocities as seen at distances of 50, 100, 150, and 200 km. The v amplitudes have been increased by a factor of 2. At all distances the P arrival is emergent on both radial and transverse components while the S arrival is impulsive on the transverse, but not on the radial. Calculations by Fisk (personal communication, 1992).39
- Figure 14. Broadband velocity 3-component synthetics for a spall source at 0 km, an explosion at 1 km depth, and three earthquake Green's function sources at 10 km. All non-zero components are plotted. The instrument response is broadband velocity. The spall shear phases are seen to be larger than those for an explosion of equal P amplitude.41
- Figure 15. 1-Hz highpass filtered velocity 3-component synthetics for a spall source at 0 km, an explosion at 1 km depth, and three earthquake Green's function sources at 10 km. All nonzero components are plotted. The instrument response is broadband velocity. The spall shear phases are seen to be larger than those for an explosion of equal P amplitude.42
- Figure 16. Broadband velocity vertical component P synthetics for a spall source at 0 km, an explosion at 1 km depth, and three earthquake Green's function sources at 10 km. A 3-4 second window beginning at the P arrival could be used to define an initial P amplitude for purposes of defining a complexity discriminant. The vertical strike-slip and dip-slip earthquake sources do not generate signals as emergent as the 45° dip-slip source. The phase at approximately a 5 second delay for the earthquakes is sP43
- Figure 17. The 1-Hz highpass filtered, amplitude equalized, velocity 3-component synthetics for a spall source at 0 km, an explosion at 1 km depth, and three earthquake Green's function sources at 10 km from Figure 14, centered on the arrival of the S phase. The S arrival is more impulsive for the spall and earthquake sources than for the explosion sources, and more impulsive for the vertical (transverse with respect to the source) than for the actual radial.44
- Figure 18a. Broadband velocity vertical component P synthetics for an explosion source at 1 km depth, and the vertical strike-slip (SS) Green's source at 1, 5, 10, 20, 30, 40, and 50 km depth. The moveout of the sP phase for the earthquake source is apparent, as is the weakness of pP47

Figure 18b. Broadband velocity vertical component P synthetics for an explosion source at 1 km depth, and the vertical dip-slip (DS) Green's source at 1, 5, 10, 20, 30, 40, and 50 km depth. The moveout of the sP phase for the earthquake source is apparent, as is the weakness of pP .	48
Figure 18c. Broadband velocity vertical component P synthetics for an explosion source at 1 km depth, and the 45° dip-slip (DD) Green's source at 1, 5, 10, 20, 30, 40, and 50 km depth. The moveout of the sP phase for the earthquake source is apparent, as is the weakness of pP .	49
Figure 18d. Broadband velocity vertical component P synthetics for an explosion source at 1, 5, 10, 20, 30, 40, and 50 km depth. The weakness of sP and pP is apparent.	50
Figure 19a. Broadband velocity vertical component synthetics for an explosion source at 1 km depth, and the vertical strike-slip (SS) Green's source at 1, 5, 10, 20, 30, 40, and 50 km depth. The decrease of the Rayleigh amplitude with depth is apparent. The L_g amplitudes for the earthquake do not significantly decrease until the Moho is reached at 40 km. Even there the S wave amplitudes remain large.	51
Figure 19b. Broadband velocity vertical component synthetics for an explosion source at 1 km depth, and the vertical dip-slip (DS) Green's source at 1, 5, 10, 20, 30, 40, and 50 km depth. The L_g amplitude at 1 km is low enough that the L_g to P discriminant would not work, but then increases and subsequently does not decrease until the source below the Moho is reached at 50 km. Even there the S wave amplitudes remain large and the L_g to P discriminant would likely work well.	52
Figure 19c. Broadband velocity vertical component synthetics for an explosion source at 1 km depth, and the 45° dip-slip (DS) Green's source at 1, 5, 10, 20, 30, 40, and 50 km depth. The decrease of the Rayleigh amplitude with depth is apparent. The L_g amplitudes for the earthquake do not significantly decrease until the Moho is reached at 50 km. Even there the S wave amplitudes remain large.	53
Figure 19d. Broadband velocity vertical component for an explosion source at 1 km and 3 components for the vertical dip-slip (DS) Green's source function at 1 km. While the L_g to P discriminant would not work well for the vertical components only, it is apparent that if the discriminant were applied using some average over all three components; or if the transverse component were scattered into the vertical component, then the discriminant would work.	54

- Figure 20a. 1 Hz highpass velocity vertical component synthetics for an explosion source at 1 km depth, and the vertical strike-slip (SS) Green's source at 1, 5, 10, 20, 30, 40, and 50 km depth. The L_g amplitudes for the earthquake do not significantly decrease until the Moho is reached at 40 km. Even there the S wave amplitudes remain large and a suitably defined discriminant would work.55
- Figure 20b. 1 Hz highpass velocity vertical component synthetics for an explosion source at 1 km depth, and the vertical dip-slip (DS) Green's source at 1, 5, 10, 20, 30, 40, and 50 km depth. The L_g amplitude at 1 km is low enough that the L_g to P discriminant would not work, but then increases and subsequently does not decrease until the source below the Moho is reached at 40 km. Even there the S wave amplitudes remain large and a suitably defined discriminant would work.56
- Figure 20c. 1 Hz highpass velocity vertical component synthetics for an explosion source at 1 km depth, and the 45° dip-slip (DD) Green's source at 1, 5, 10, 20, 30, 40, and 50 km depth. The L_g amplitudes for the earthquake do not significantly decrease until the Moho is reached at 40 km. Even there the S wave amplitudes remain large and a suitably defined discriminant would work.57

LIST OF TABLES

	<u>Page</u>
Table 1. Explosions	6
Table 2. Earthquakes	8
Table 3. Explosion-Station Distance/Radial Azimuth at Station (degrees)	9
Table 4. Explosion-Station Distance/Radial Azimuth at Station (degrees)	10
Table 5. DSS Structure for Synthetics	31

ACKNOWLEDGMENTS

Mark Fisk calculated phase-screen waveforms resulting from shear and compressional sources in random media, showing that the P signals from shear sources were emergent while from compressional sources they remain impulsive. Florence Riviere-Barbier and Lori Grant helped me to understand the differences between signals from different quarries and to determine which events were earthquakes and which were explosions. Bob Herrmann guided me through the use of his wavenumber integration program package for computing synthetics, and David Bonnett and John Coyne helped me learn to use the CenterView and Geotool software at the CSS. Keith McLaughlin and Steve Day helped me understand the proper specification of a source function for spall. Ivan Henson's Geotool program proved to be very valuable in analyzing and plotting both the experimental and the synthetic waveforms.

(This page intentionally left blank)

Abstract

Earthquakes on land in Scandinavia are shown to typically have emergent P -wave signals in the distance range 1.5 to 15 degrees and in the frequency range 2-10 Hz at the single center elements of one or more of the arrays ARCESS, NORESS, and FINESS; while explosions show impulsive signals. For reasons similar to teleseismic complexity, the causes for this discriminant involve earthquake P -wave nulls, and sP for the deeper earthquakes. The S -converted phases, including sP , are more prominent at regional than at teleseismic distances because of the greater S to P conversion resulting from the greater angles of incidence on the approximately horizontal interfaces. Where there are P wave nulls there is an emergent P wave deriving from S to P conversions. It appears that such an emergent signal can arise only by scattering in 2D or 3D heterogeneities and, for vertical faults, along the fault strike, only by conversion of transverse S to vertical or radial P . The discriminant seems to be more robust at regional than at teleseismic distances. This may be because at high frequencies (2-5 Hz) at regional distances there are multiple paths along which the P wave may arrive in the first five seconds of the signal. Even if one of these paths is defocussed so that the amplitude is low, the other paths may not be defocussed. As a result, as compared to a 1 Hz teleseismic explosion signal, it may be less likely that a high-frequency regional signal will appear emergent due to heterogeneity in the earth. The discriminant may also be more robust because there can be more S to P conversions at many high-wavenumber heterogeneities which scatter only weakly at lower frequencies. The discriminant also appears to work well for several other regions.

Introduction

Teleseismic Complexity

From the earliest days of attempts to discriminate between the seismic recordings of earthquakes and explosions it has been thought that earthquake seismograms would be more complex than those of explosions and, to this day, some analysts assert that by use of human pattern recognition capabilities they are able to distinguish between the two source types, using the general concept of complexity, when presented with comprehensive sets of network teleseismic seismograms.

The earthquake has been expected to be a source more extended in space, and it has been expected that there could be multiple events. In addition, it was anticipated that the earthquakes would be deeper than the explosions so that the surface-reflected depth phases, pP and sP , would complicate the P coda, and that some stations might see the P -wave null, thus inevitably leading to an emergent seismogram.

It was recognized early-on that, at teleseismic distances, a shallow, 45° dip-slip thrust earthquake mechanism could look like an explosion source from the point of view of complexity and first motion since the P wave compressional first motion would be directed to teleseismic distances and the surface reflected phases would follow too quickly after the initial phase to be easily distinguished. In addition, there would be no S to P converted phases from interfaces below the epicenter because an S wave null would be directed to teleseismic distances.

It was expected, however, that only an earthquake could create a complex waveform, so that most earthquakes could be identified, if observed at a well-distributed network, by searching the network for one or more complex waveforms. If no complex waveforms were found the event would be classified as undetermined since the possibility would remain that it was one of the 45° dip-slip events discussed above.

Since explosions would have a short time duration, be shallow, and emit no S waves, it was anticipated that they would be simple so long as array beams were used to suppress waves scattered near the receiver; such scattering can greatly increase the complexity of signals, see, e.g., Key (1968) and Gupta and Wagner (1992). Since an earthquake could be simple, an explosion would have to be placed in the undecided category as far as complexity was concerned, but at least it would not be identified as an earthquake and, if in an area of interest, could be investigated with other discriminants such as M_s , m_b . Existence of a complex explosion signal would clearly, however, very much weaken the applicability of the discriminant.

Early observations seemed to bear out this approach. Most of the publications in the field have been by United Kingdom researchers, beginning with Thirlaway (1963, 1966), Carpenter (1963), and UKAEA (1965).

However, in September 1964 a seismogram was recorded at YKA in Canada from a nuclear test at Novaya Zemlya in which the coda following the initial P wave was comparable in amplitude to the P wave itself, see for example, Marshall (1972). This seismogram required explanation since

without a satisfactory approach to this problem the explosion might be identified as an earthquake.

Subsequent publications by Douglas and co-workers, Douglas (1967, 1981), Douglas et. al. (1971, 1974, 1981, 1990) developed the ideas that this and other complex explosion seismograms resulted from a weak initial *P*. Their preferred explanation for this weak *P* wave is that the initial *P* ray passes through a relatively small volume of low *Q* material, thus lowering its frequency and amplitude, so that subsequent scattered phases appeared large and high-frequency by comparison. These authors also have noted that for complex signals from explosions the station m_b values are small. However, since this could be due to a *P* wave null if the event had been an earthquake it has not seemed reasonable to restrict complexity analysis to those stations with high m_b values.

In the same series of publications these authors discussed how the same mechanism could generate both complex and simple seismograms from an earthquake (e.g., 45° dip-slip) which would otherwise have only simple teleseismic signals. In Douglas et. al. (1990, 1992), the larger coda phases are identified as *S* to *P* conversions at interfaces below the epicenter such as the Moho or a descending plate. An explanation for the *P*-coda from explosions is that it is comprised of Rayleigh to *P* scattering near the source, e.g., Greenfield (1971), Gupta and Wagner (1992).

If the emergent earthquake teleseismic coda is comprised of *pP* and of *S* to *P* conversions at relatively sharp interfaces, while the emergent explosion coda are comprised of Rayleigh to *P* conversion, it is possible that the coda in emergent explosion signals will have more of a "rolling" character which can be distinguished from the "impulsive" coda of the emergent earthquake. This may account for the apparent ability of analysts to use teleseismic complexity for discrimination even in the cases where explosions exhibit complex signals at some stations.

A competing possible explanation for the existence of weak, low-frequency initial *P* for some explosion signals is that the initial ray is defocused by a structure relatively near the source such as that discussed by McLaughlin et. al. (1992). In an earlier publication, McLaughlin and Anderson (1987) showed both theoretically and empirically that scattering preferentially delays high frequencies; Fisk and McCartor (1991) and Fisk et. al. (1992) showed the same effects using phase screen techniques on vector elastic waves. Thus the initial wave may be both weak and low frequency even in the absence of low-*Q* material.

In this case, to result in a complex signal, the direct *P* would have to be defocused while the later phases were not similarly affected. This difficulty was also recognized by Douglas and colleagues and could be the case in the geometry discussed by McLaughlin et. al. (1992). One important point to consider is that while *P* and *pP* from an earthquake 10 km deep may have sufficiently different paths near the source to be differently focused, two explosions one or two kilometers apart, which might be used to simulate an earthquake *P* and *pP* in an evasion attempt, would in most cases not have such different paths. However, for a possible counterexample see the events in the Northeast corner of Shagan discussed by Barker and Murphy (1992).

Another mechanism which can alter the amplitude relationship between *P* and *pP* and *sP* is a Doppler effect associated with the direction of fault plane rupture, as discussed by Douglas et. al. (1990). They discuss the E. Kazakhstan event of 25 September 1979. There may be similar problems with the 20 March 1976 event discussed by Pooley et. al. (1983).

If the Doppler shift increases the frequency of P but decreases the frequency of the pP and sP signals so that the response to the latter in the short-period passband is small, an earthquake may look like a simple explosion (as do 45° dip-slip events seen only at teleseismic distances, see, e.g., Cullen and Douglas (1975)). While Doppler effects may be a problem for events in the magnitude range 5-6, it may not be a problem for smaller events with higher corner frequencies.

Whatever the cause of the weakening of the first arriving P wave, the possibility of this (or the weakening or strengthening of a later pP or sP arrival) occurring strikes at the heart of the approach to discrimination outlined by Pearce (1977, 1980), Pooley et. al. (1983), McLaughlin et. al. (1983), and Pearce et. al. (1988). In these papers it is implicitly or explicitly hypothesized that if no double couple mechanism can fit the array of relative amplitudes of P , pP , and sP , then the event is likely to be an explosion.

Despite the unfortunate implication that this promising discrimination method would be unreliable, it nonetheless seems that the perception of strikingly different relative amplitudes and/or polarities for P , pP , and sP as examined over a focal sphere, even if not strictly consistent with a double couple mechanism, is good evidence for a definite conclusion that the event is an earthquake, and perhaps means may yet be determined to formalize such a decision process. An initial study along these lines was performed by Smart and McLaughlin (1985), see also Douglas et. al. (1992), who attempted to develop a systematic method to detect differences in P wave polarity with respect to pP or other P waves. As discussed above, a large variation in relative amplitudes could likely not be attained by a shot array.

In addition to the work cited above, studies which have restricted themselves to a single array, e.g., LASA or NORSAR, and to a basically statistical approach have found that a time-series type of definition of complexity serves as a useful discriminant between earthquakes and explosions, especially in combination with the observed deficit of explosion energy below 1 Hz as compared to the energy near 1 Hz, (note *not* an excess of energy above 1 Hz) see, for example, Shumway and Blandford (1974) and Tsvang et. al. (1993). However, these authors have not attempted to explain the failures of the complexity method in physical terms such as earthquake mechanisms or defocused P waves from explosions.

Regional Complexity

It does not seem that complexity, *per se*, has been previously suggested as a discriminant for regional phases. It seems likely that most workers in the field have felt that scattering would be so severe that all events would be complex. This would certainly be a reasonable supposition given, for example, the results of Gupta and Blandford (1983) and Fisk and McCartor (1991), in which it is suggested that the observed heterogeneity in the earth is sufficient to equilibrate the energy between the two shear modes in a distance of a few hundred wavelengths.

It would also be a reasonable assumption if one considered that the P_g or L_g phases are generally regarded as being made up of many individual rays and would thus be "complex" if generated by *either* an explosion or earthquake.

However, several authors have felt that discriminants might be found via a detailed examination of the regional P_n which, in simple structures, can be analyzed with only a few rays. For example, Barker (1991) shows that after P_n an earthquake shows the phases pP_n , sP_n , and SP_n quite prominently. All of these phases would not appear in the coda of a shallow explosion, and their absence should result in a simpler P_n - P_n -coda signal for explosions than for earthquakes. Saikia and Burdick (1991) have performed similar calculations.

One might also hope that at high frequencies for regional distances in complex structures the actual P_n arrival would be made up of several rays along many paths so that the defocussing of a single path from an explosion would not result in an emergent signal, as it apparently does for some paths at teleseismic distances.

The SP_n phase is, of course, converted at the Moho and sP_n at the free surface, and should there be other interfaces in the crust, additional complexity could result. The higher the frequency the more the conversions if there are high wavenumber heterogeneities in the crust; so that one might expect that extensive S wave scattering would result in much more complex, or even emergent signals at regional distances for shallow earthquakes as compared to explosions. At teleseismic distances the effects might not be so great, even for high frequencies, because, as pointed out by Pearce (1980), S to P conversion is very weak at small incidence angles; it is only for regional distances that the S waves impinge upon the predominantly horizontal heterogeneities at substantial angles. Thus, for these reasons, we might actually expect complexity to work better for P_n at regional distances than for P at teleseismic distances.

Data Selection

The best source of high-frequency regional data available today is that from the arrays NORESS, ARCESS, and FINESS in Scandinavia. Figure 1 shows the locations of these arrays together with the locations of the explosions and earthquakes examined for discrimination.

Table 1 shows the explosions selected and Table 2 the earthquakes.

Table 1: Explosions

Latitude	Longitude	mo/day/year	julian day	origin time	local magnitude
61.4333	34.9744	01/05/91	005	14:19:45.7	2.34
58.7722	10.3969	03/05/91	064	12:42:35.6	2.36
69.2327	34.3002	03/23/91	082	14:14:13.1	2.85
61.8100	30.6573	04/13/91	103	11:52:34.4	2.60
67.6445	33.8702	04/26/91	116	09:34:53.1	2.95
67.6181	30.6171	08/03/91	215	11:18:01.6	2.13
67.0742	20.9543	09/05/91	248	15:30:39.7	2.32
59.4760	24.1442	12/10/91	344	09:14:59.6	2.59
69.3599	30.7596	12/29/91	363	14:06:36.0	2.96
64.6750	30.7476	03/25/92	085	10:00:08.6	2.94
59.3855	27.3022	05/11/92	132	11:26:58.8	2.64

The events were selected with consideration for having sufficient S/N at single elements so that all phases could be clearly seen on all components of a single instrument at the most distant station in order to obtain the clearest picture of the true relationships between phases without extensive beamforming.

This required accepting only the largest events. Because the analysis in this report is of the nature of a survey, only one event from each major quarry was selected for analysis, although comparisons were made using the data cited in the study of Riviere-Barbier and Grant (1992) to ensure that the general character of each selected event was typical of those from the same quarry. We may remark that inspection of the plots in Riviere-Barbier and Grant shows that the general character of the complexity of the explosion P_n waveforms is quite reliably different from the complexity of the earthquake P_n waveforms which we shall examine below.

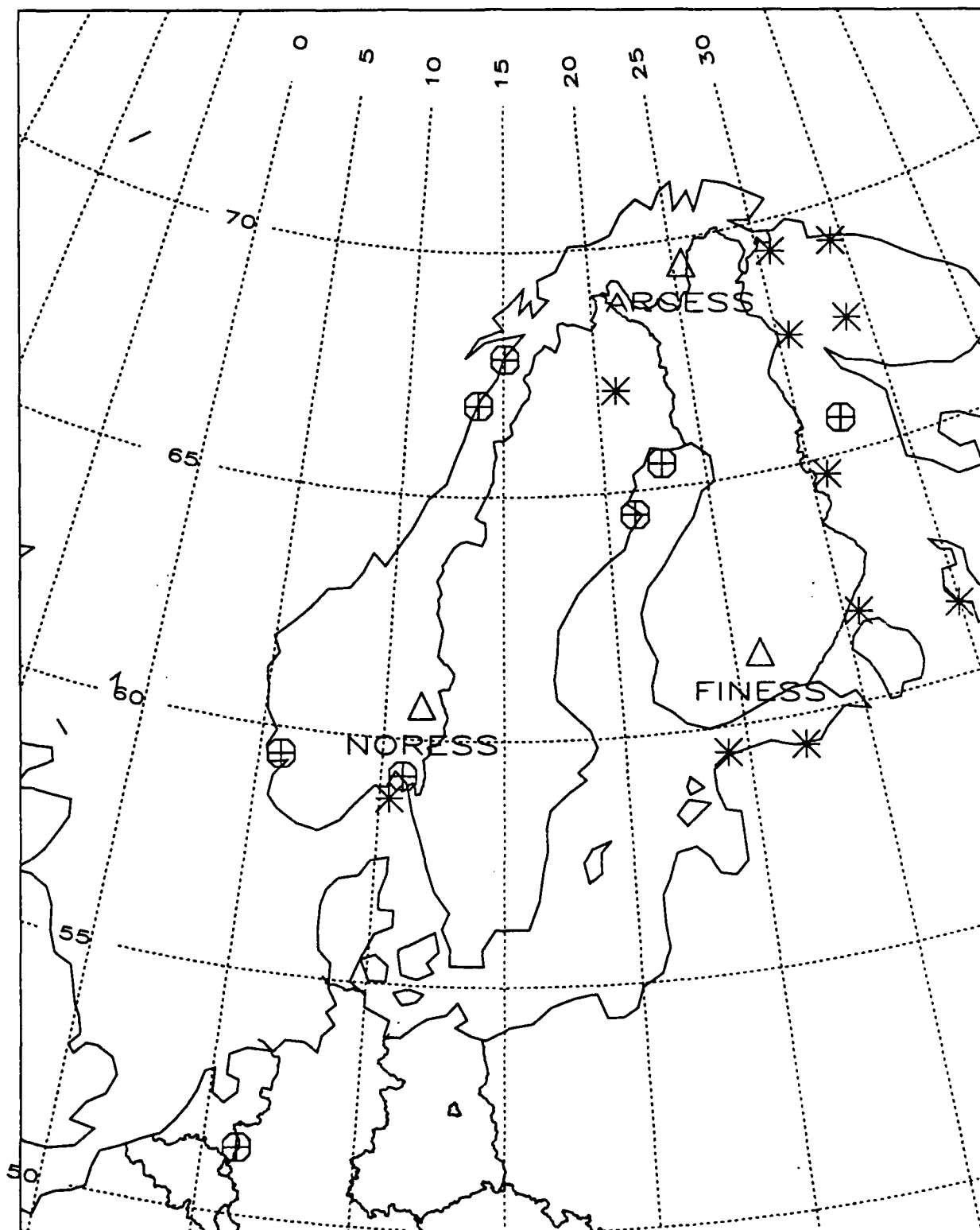


Figure 1. Reference map showing locations of stations, earthquakes, and explosions analyzed in this report. Asterisks (*) indicate explosions; octagons with a cross indicate earthquakes.

In addition, the explosions were selected with a view to distributing them about Scandinavia as uniformly as possible in order to minimize any bias due to source area.

Table 2: Earthquakes

Latitude	Longitude	mo/day/year	julian day	origin time	local magnitude
65.4978	22.8995	06/06/91	157	12:46:11.5	3.22
65.7122	32.0997	08/24/91	236	10:56:28.5	3.18
64.5198	21.3412	09/23/91	266	19:20:28.3	3.15
67.8151	15.0871	01/04/92	004	06:00:51.7	3.60
59.2399	10.8856	02/19/92	050	06:39:32.9	3.26
51.3740	6.1325	04/13/92	104	01:20:05.0	4.40
59.4524	5.8739	04/14/92	105	13:10:07.3	3.38
66.8591	13.7072	05/18/92	139	13:47:01.8	2.74

As seen in Figure 1, in selecting the earthquakes, in addition to looking for large events well distributed over Scandinavia, a requirement was imposed that the event epicenter be on, or very close to, land. This is not a simple requirement to meet since the large majority of events occur in the Atlantic west of Norway and, as a result, the earthquakes in most Scandinavian discrimination data bases, e.g., Dysart and Pulli (1990), Sereno et. al. (1992), consist predominantly of oceanic earthquakes.

An event in the ocean is very unlikely to be a clandestine nuclear explosion and, in addition, it is plausible that its seismic signature could have distinctive features different from those occurring for earthquakes on land but which might come to be relied upon as a discrimination feature. For example, it is well established in the teleseismic literature, e.g., Pearce (1981), that reverberations in the low-velocity water layer can greatly complicate the P signal. It is, therefore, very plausible that such events would be much more complex in their P_n signals than land earthquakes and thereby make the complexity criterion look *too* good. It is possible also, of course, that other discriminants based on L_g frequency and on L_g to P amplitude ratios, as discussed, for example, by Dysart and Pulli (1990), might also be biased by the water layer; such effects should be looked for both empirically and theoretically.

Also, by requiring that the earthquakes epicenters be on land, it is ensured that the source-receiver paths for the two source types have much in common and that one can be more certain that differences in discrimination are not simply path effects. In Figure 1 we see that there are many pairs of different source types whose source-station paths are quite close to each other.

Care was taken by means of consulting the Helsinki bulletins, researchers in Scandinavia, and by examining the temporal patterns of testing of quarries near events of interest, to ensure that the events were in fact identified correctly as explosions or earthquakes.

Note that the magnitudes of the earthquakes in Table 2 are generally greater than the explosion magnitudes in Table 1. This reflects the fact that in Scandinavia there are very few explosions with magnitude greater than 2.5 (1 kt decoupled) except from a very few quarries. Thus the predominant practical discrimination problem in areas like Scandinavia will be to determine that earthquakes not near quarries are not explosions; most of the ambiguous explosions will be below the magnitude threshold of interest and hence need not be discriminated. If in a test-ban on-site inspection is negotiated for the few quarries at which blasts with magnitudes greater than 2.5 are detonated, then the problem of distinguishing between quarry blasts and nuclear blasts may not be severe.

Tables 3 and 4, below, give the distance and radial azimuth at the station for the events in Tables 1 and 2, respectively.

Table 3: Explosion-Station Distance/Radial Azimuth at Station (degrees)

mo/day/year	julian day	ARAO	F1A1	NRA0
01/05/91	005	09.0/329	04.2/266	11.3/256 low S/N
03/05/91	064	12.6/038 low S/N	08.3/078 low S/N	02.1/016
03/23/91	082	03.1/271	08.5/200	12.7/218
04/13/91	103	08.0/342	02.1/258	09.2/255
04/26/91	116	03.6/297	070/204 mixed S	11.9/224
08/03/91	215	02.7/318	06.5/195	10.7/222
09/05/91	248	03.0/036	06.0/160	07.5/209
12/10/91	344	10.1/003 mixed S	02.2/026	06.4/275
12/29/91	363	01.8/272	08.1/191	11.7/214
03/25/92	085	05.3/334	03.8/211	09.6/237
05/11/92	132	10.3/354	02.2/343	08.0/272

The signals indicated above to have low S/N have not been subsequently plotted in this study. The events with signals which are mixed with those from other events can be used for some purposes, e.g., for P_n analysis if the event of interest arrives before the mixing event.

For the 4.4 magnitude 04/13/92 earthquake in Belgium the recording at ARA0 is not plotted in the profiles in this report because it is at a greater distance (20.4 degrees) than is usually regarded as regional and is also at much greater distances than all other waveforms treated. For example, there are no explosion waveforms observed at those distances for single components because a larger magnitude than is available would be required for sufficient S/N. It is, however, of interest to note that, even though 04/13/92 is an earthquake, its P_n arrival at ARA0 is one of the most impulsive, in agreement with the argument given above that earthquakes may seem more impulsive at teleseismic distances than at regional distances due to the decrease in S to P conversion for steeper incidence angles.

For unknown reasons data was not available for 08/24/91 at NRA0 or for 02/19/92 at FIA1.

Table 4: Earthquake-Station Distance/Radial Azimuth at Station (degrees)

mo/day/year	julian day	ARA0	FIA1	NRA0
06/06/91	157	04.2/015	04.2/162	06.9/222
08/24/91	236	04.6/323	05.0/209	10.4/132 NA
09/23/91	266	05.3/019	03.7/147	05.8/225
01/04/92	004	04.1/070	07.9/148	07.2/190
02/19/92	050	12.1/038	07.9/080 NA	01.6/012
04/13/92	104	20.4/036	14.9/056	09.9/020
04/14/92	105	13.1/049	10.2/087	03.1/068
05/18/92	139	05.1/064	07.6/140	06.1/187

Data Analysis

In Figure 2a we see the explosion events in the distance range from 1.8 to 6.5 degrees. The events are ordered from bottom to top in order by increasing distance. The waveforms are plotted with equal maximum amplitude and are spaced evenly in the vertical; the actual distance and back-azimuth to the event (radial azimuth at the station minus 180 degrees) can be determined by reference to Table 3.

The data have been filtered with a 3-pole highpass Butterworth filter with the corner frequency at 1 Hz. This was done to improve the S/N.

Figure 2b is a similar profile for earthquakes. It is immediately apparent by comparison with Figure 2a that the explosions are characterized by an impulsive *P* wave and the earthquakes by an emergent *P* wave. It seems clear that all but a few of the explosions are more impulsive than all of the earthquakes and that all but a few of the earthquakes are more emergent than all of the explosions. In particular, over the network of three stations, at least one of the waveforms from each earthquake is more emergent than the most emergent single explosion signal. The most emergent explosion signal appears to be ARA0/199182. The most difficult earthquake to discriminate is 19924 for which the ARA0 signal, the most emergent of the three signals for this event (See Figure 5b for the other two.), is only slightly more emergent than that most emergent explosion signal. In fact, the 19924 earthquake might best be regarded as one of the earthquakes that must fall in the undecided category. All in all, it appears that a large proportion of both types of events may be safely discriminated on the basis of complexity, leaving some events unidentified.

As we have seen in the previous section, however, on the basis of theoretical considerations we should expect only to identify most earthquakes, leaving explosions in the unidentified category since we expect that some earthquakes could look like explosions. While this restriction seems irksome in a research study, in many practical applications, where the actual number of explosions of interest is small and the number of earthquakes is very large, the restriction results in a procedure in which unidentified events are subsequently examined using other seismic and non-seismic techniques by leaving only a very few events above some threshold which could be explosions.

In addition to the basic ideas suggesting that complexity should work at teleseismic distances which have been discussed in the previous section, calculations by Fisk (personal communication, 1992) using the phase screen methods discussed by Fisk and McCartor (1991) and Fisk et. al. (1992), show that an impulsive shear source in a scattering medium generates an emergent *P* wave, while an impulsive compressional source generates an impulsive *P* wave. These interesting results will be discussed further in the following theoretical section. Thus, since earthquakes emit approximately five times the shear amplitude as compressional amplitude and, since along *P* wave nulls, only scattered *S* wave will be available to generate *P*, it will be the rare earthquake that is not emergent, while it would be the rare explosion which was emergent. The statistics of these theoretical results should be further investigated in different media to see how often a compressional source might result in an emergent *P* signal.

Explosion profile, 1 Hz HP

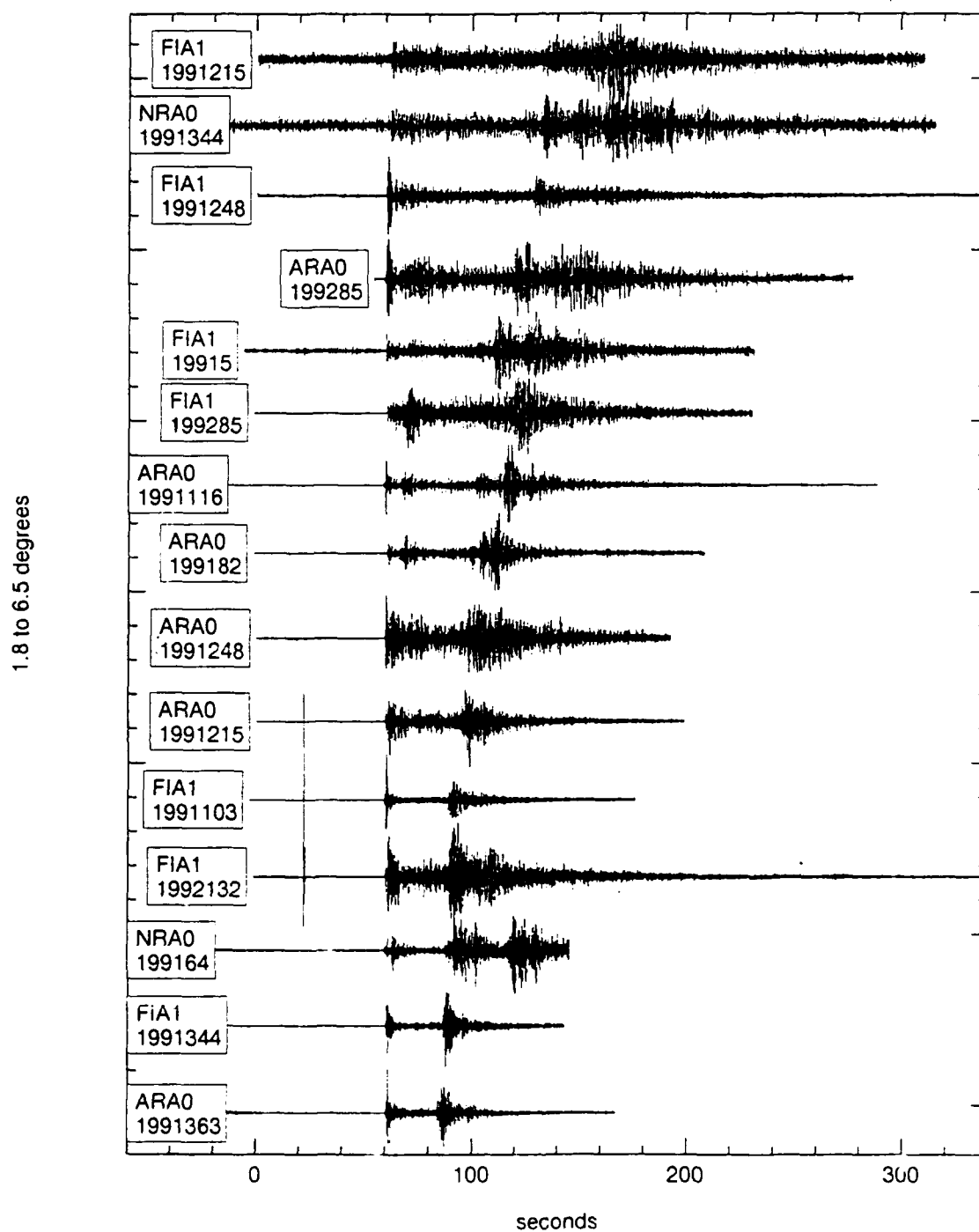


Figure 2a. Explosion profile, 1 Hz highpass. The signals are ordered by distance in the range 1.8 to 6.5 degrees as seen in Table 3. The explosions are seen to have impulsive arrivals in the first 1-10 seconds and to have a large P/L_g amplitude ratio as compared to the explosions seen in Figure 2b. The most emergent of the explosions is FIA1/199285. The signals for explosions in the range 7 to 12.7 degrees are seen in Figure 5a.

Earthquake profile, 1 Hz HP

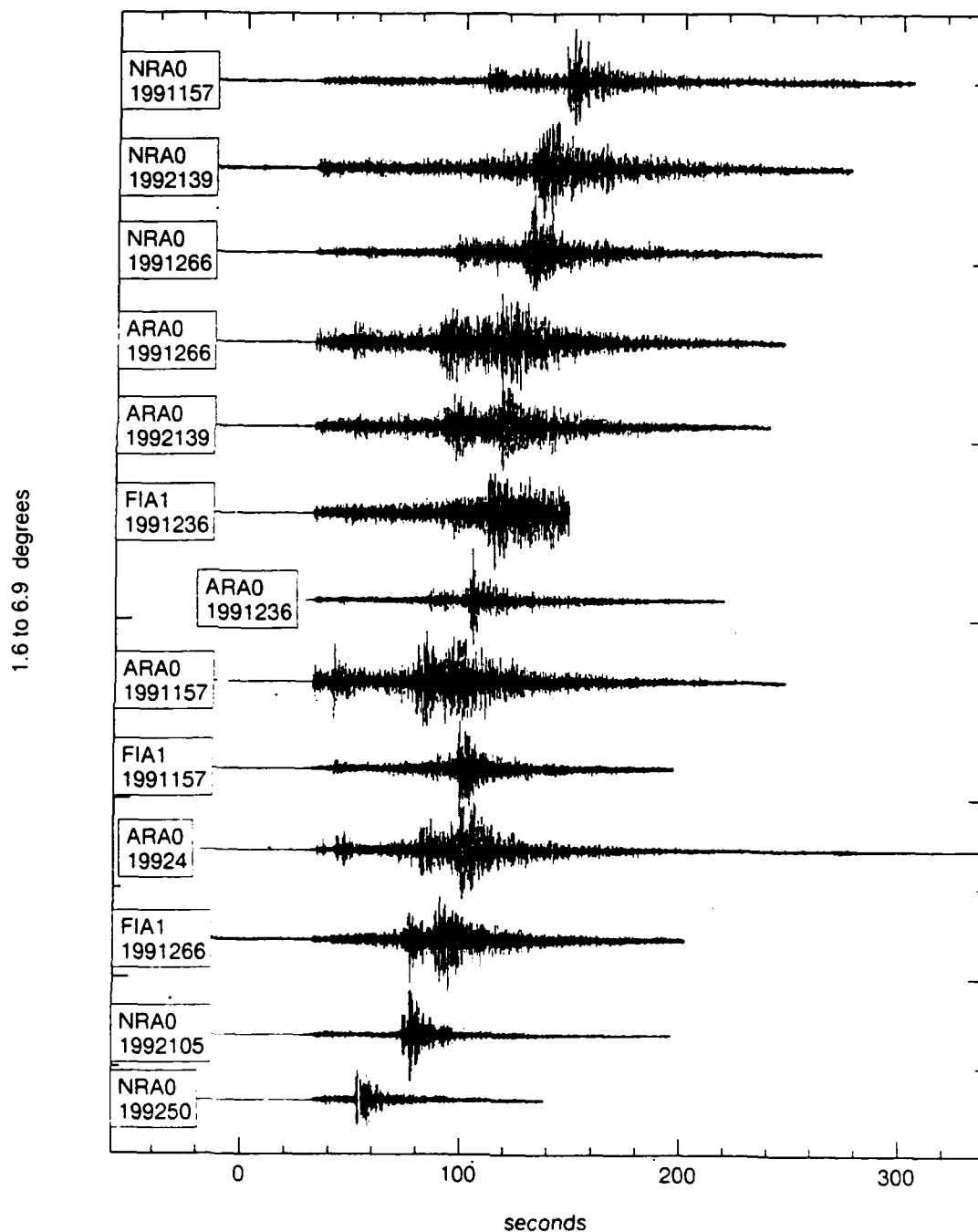


Figure 2b. Earthquake profile, 1 Hz highpass. The signals are ordered by distance in the range 1.6 to 6.9 degrees as seen in Table 4. The earthquakes are seen to have emergent arrivals in the first 1-10 seconds and to have a small P/L_g amplitude ratio as compared to the earthquakes seen in Figure 2a. The most impulsive of the earthquakes is ARA0/1991157. The signals for earthquakes in the range 7.2 to 14.9 degrees are seen in Figure 5b.

One might hope that in a sufficiently complex medium even those regional stations toward which an S wave null, and a corresponding P wave maximum, was directed would have emergent signals because of strong back-scattering near the source. However, in addition to earthquake 19924 in this study, there is at least one other example in Scandinavia (V. Schulte-Pelkum, personal communication, 1992) for which a regional earthquake has a strikingly impulsive signal at one station but clearly emergent signals at two others as could be expected as a result of earthquake radiation patterns. Thus it does not seem that in Scandinavia the crustal complexity is sufficient for this idea to be valid.

One of the most emergent explosion signals in Figure 2a appears to be FIA1/199285; and the most impulsive earthquake signal in Figure 2b appears to be ARA0/1991157. Note that the signal at another station for explosion 199285, ARA0, is quite impulsive; and that another station for earthquake 1991157, NRA0, is quite emergent. Therefore it does not seem likely that the events have been misidentified with respect to their source type.

It is likely, by analogy with the teleseismic problem, that it is emergent explosion signals which will place the most severe restriction on the applicability of the complexity discriminant. This is because there is no well-understood cause for an emergent explosion signal whereas, as we have discussed with respect to teleseisms and as we shall see for regional signals, there are theoretical calculations which predict impulsive earthquake signals.

Thus, the more emergent a signal that is recorded from an explosion, the fewer the number of earthquakes that can be identified unambiguously. And, in most applications, it will be the number of unidentified earthquakes which will place the major load on a discrimination system.

It is also clear from inspection of Figures 2a and 2b that the high-frequency L_g to P amplitude ratio serves as a good discriminant as has been noted previously by e.g., Blandford et. al. (1981) using the Long-Range-Seismic-Measurements (LRSM) system which peaked near 3 Hz, and implicitly in the same tectonic area by Murphy and Bennett (1982) and Bennett and Murphy (1986) since they noted that earthquakes had higher frequency L_g than explosions while the P_g spectra were similar. Similar, more recent results in Scandinavia and other areas have been obtained by Dysart and Pulli (1990), Chan et. al. (1990), Lynnes and Baumstark (1991), and Bennett et. al. (1990, 1992). In many of these studies, especially Lynnes and Baumstark (1991), there is considerable overlap in the populations even at high frequencies; however, usually a large proportion of both populations can be identified, leaving the remainder to be discriminated by other techniques, perhaps complexity if the two discrimination approaches should prove to be at least somewhat independent.

Figures 3a and 3b show the first 20 seconds of the P waves from Figures 2a and 2b. We see that the dominant frequency of the signal is around 5 Hz and that, for the explosion, the impulsive P is actually a pulse of 2-5 cycles.

Interestingly, we see in Figures 4a and 4b that the transverse P wave is also more impulsive for explosions than for earthquakes. This is as expected since transverse P must be locally scattered and as such will be proportional to longitudinal P . (This is also seen in the theoretical calculations by Fisk (personal communication, 1992) referred to above.) In particular we see that the explosion signal FIA1/199285 is also the most emergent of the explosion signals in this set.

Explosion profile, 1 Hz HP, Smax equalized

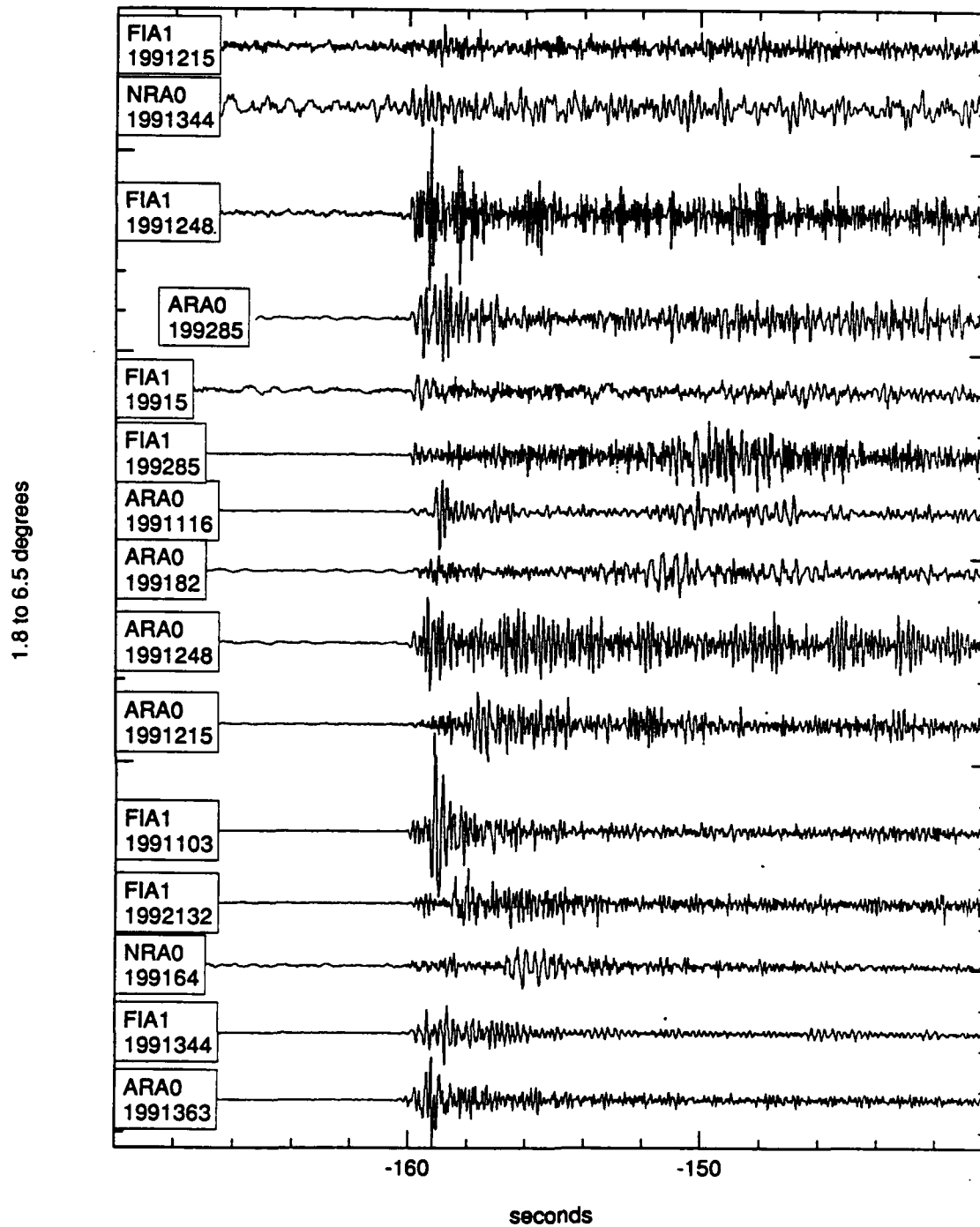


Figure 3a. First 20 seconds of the explosion signal in Figure 2a. The explosions are seen to have impulsive arrivals in the first 1-10 seconds and may be seen to have a large P/Lg amplitude ratio as compared to the earthquakes seen in Figure 3b by virtue of the fact that in each figure the maximum S phase is normalized to a constant magnitude, and the P amplitude is greater in Figure 3a than in Figure 3b. The most emergent of the explosions is FIA1/199285.

Earthquake profile, 1 Hz HP, Smax equalized

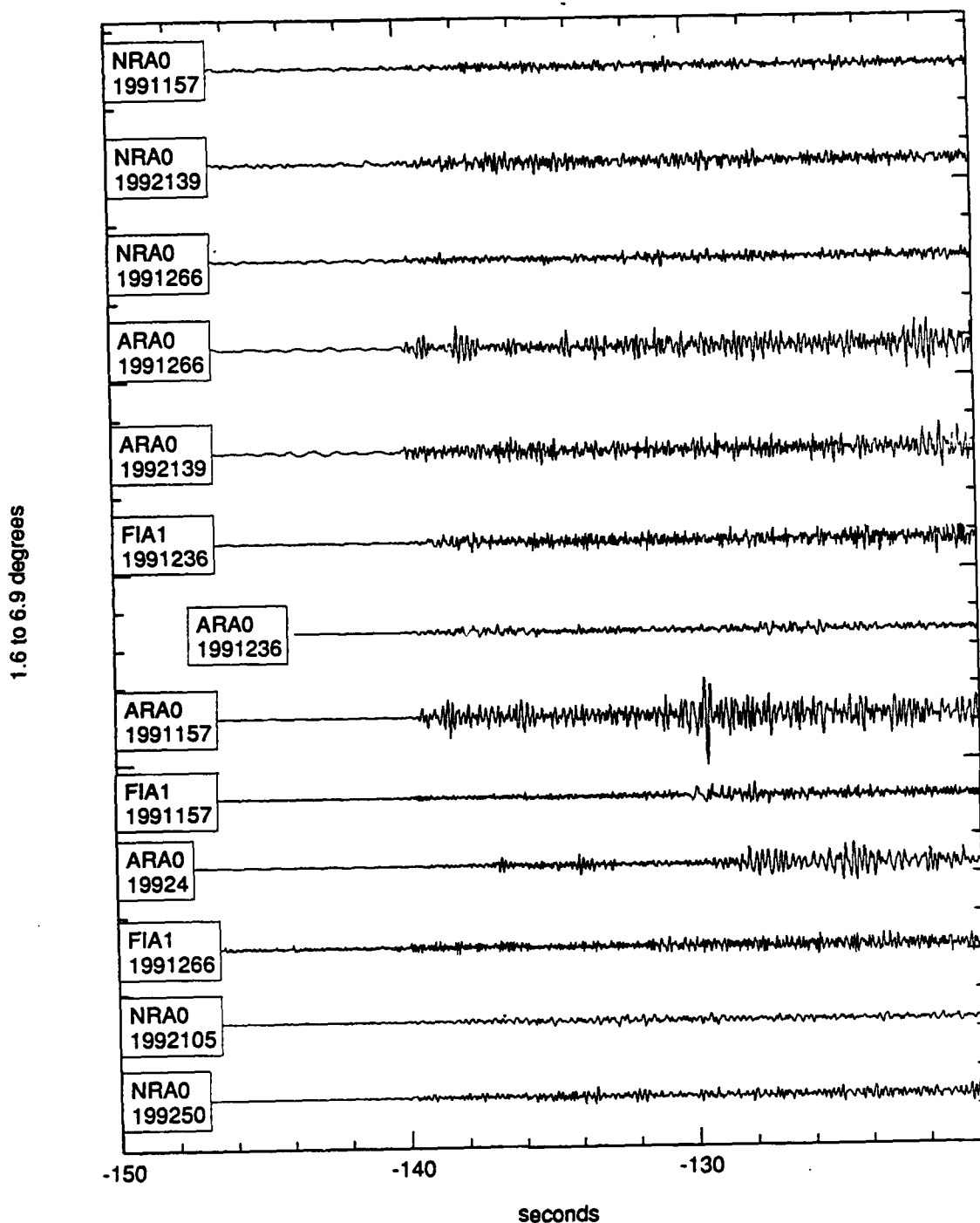


Figure 3b. First 20 seconds of the earthquake signal in Figure 2b. The earthquakes are seen to have emergent arrivals in the first 1-10 seconds and may be seen to have a low P/L_g amplitude ratio as compared to the explosions seen in Figure 3b by virtue of the fact that in each figure the maximum S phase is normalized to a constant amplitude, and the P amplitude is greater in Figure 3a than in Figure 3b. The most impulsive of the earthquakes is ARA0/1991157.

Explosion profile, 1 Hz HP, Transverse

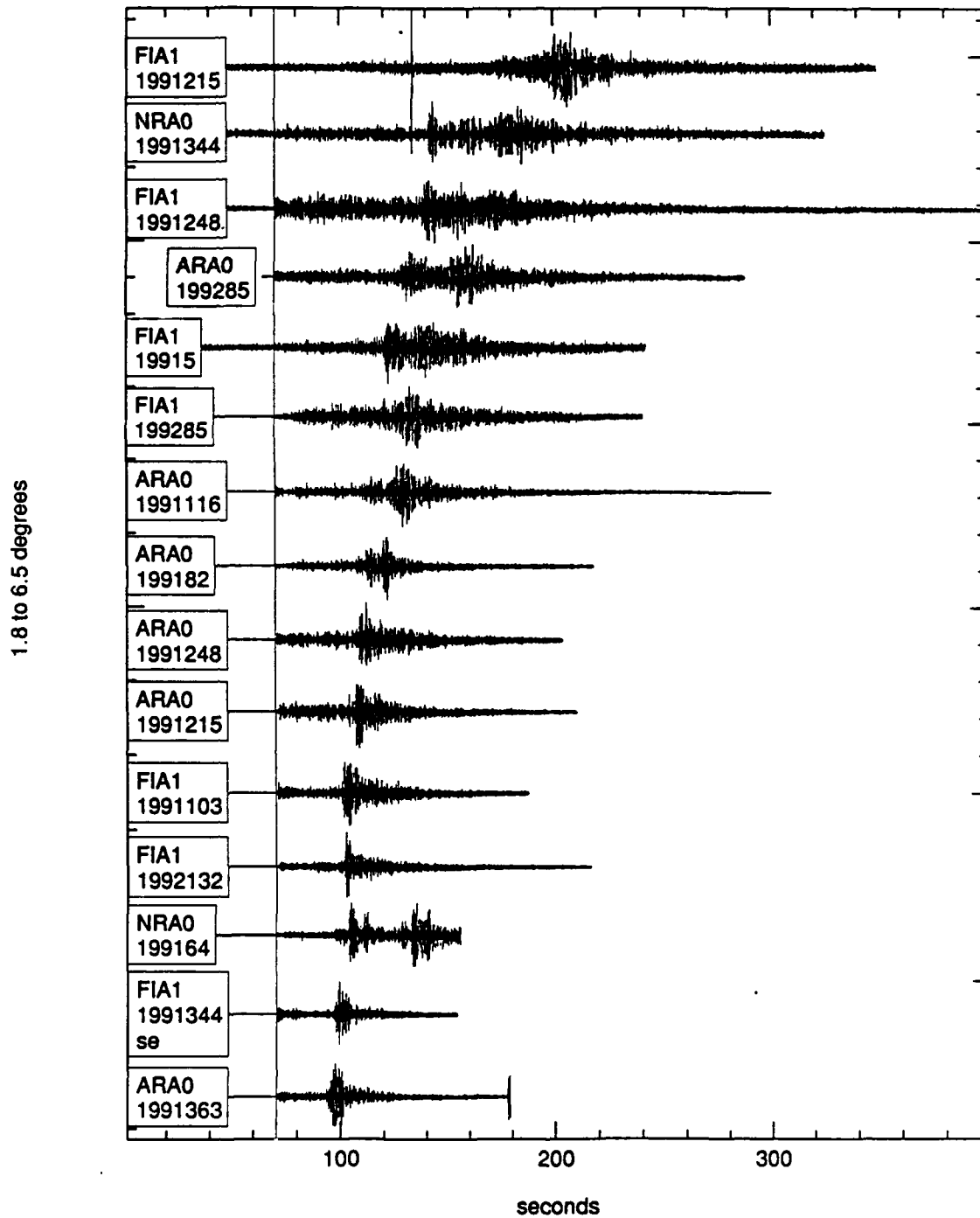


Figure 4a. Transverse component of the explosion signals in Figure 2a. The explosions are seen to have more impulsive arrivals in the first 105 seconds as compared to the earthquake transverse components seen in Figure 4b. We see that the signal for FIA1/199285 is here also the most emergent explosion signal as it was in Figure 2a.

Earthquake profile, 1 HP, Transverse

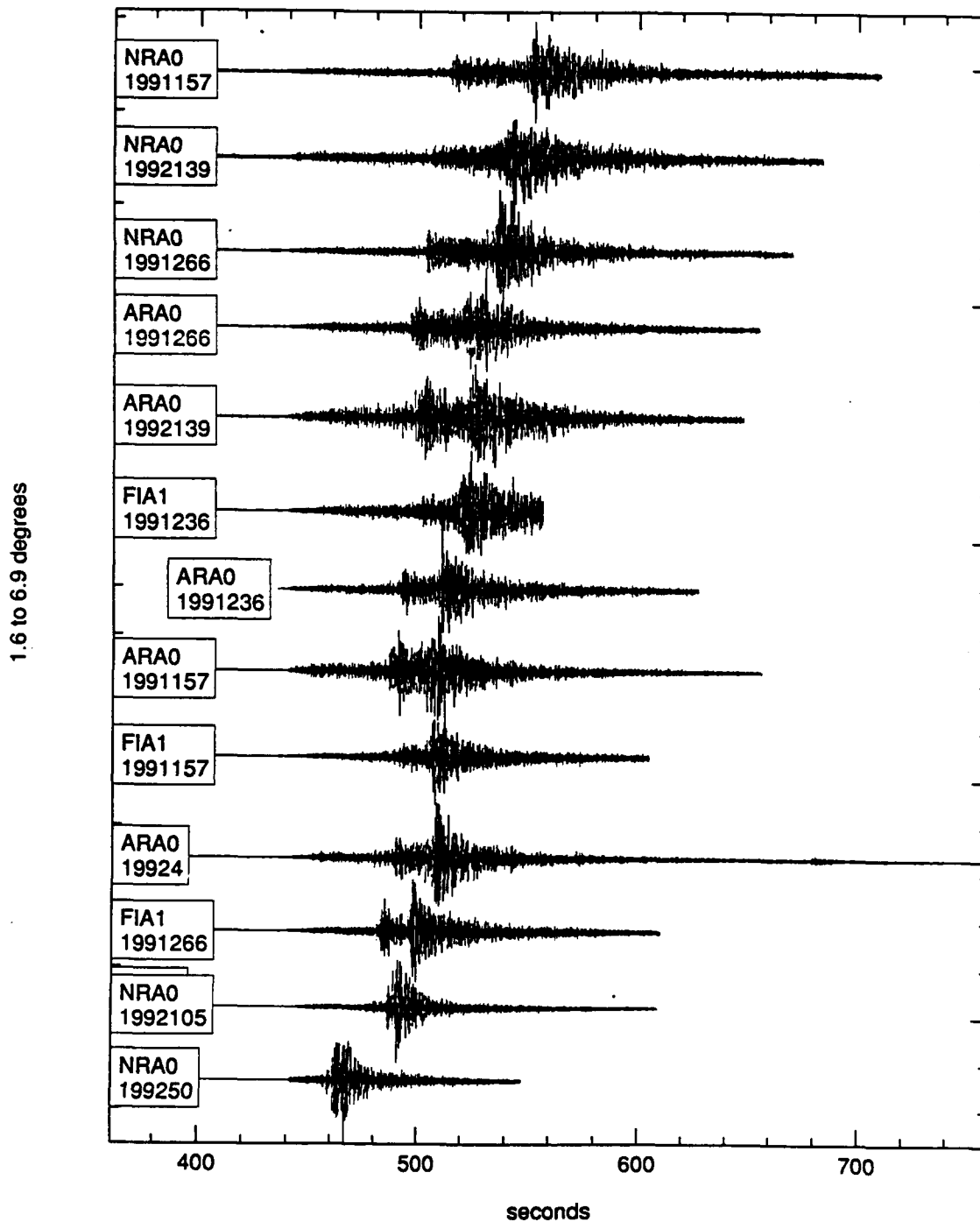


Figure 4b. Transverse component of the earthquake signals in Figure 2b. The earthquakes are seen to have more emergent arrivals in the first 1-5 seconds as compared to the explosion transverse components seen in Figure 4a. The most impulsive of the earthquakes seems to remain ARA0/1991157 as seen in Figure 2b, but it is difficult to be certain due to the small amplitudes of the transverse component *P* wave.

By examination of Figures 5a and 5b we see that in the distance range between roughly 7 and 14 degrees it still appears that explosions are more impulsive than earthquakes. Figures 6a and 6b are highpass filtered at 2 Hz instead of 1 Hz and we see in that the resulting improvement in S/N results in the explosion ARA0/19915, which is too noisy in Figure 5a to determine if it is emergent or impulsive, being seen in Figure 6a to be impulsive, as expected for an explosion.

The impulsive signal for ARA0/19915 in Figure 6a is only a single cycle and would likely be insignificant in a discrimination approach which relied on rms measurements.

In Figures 7a and 7b we see the first 20 seconds of the 7 to 14-degree earthquake and explosion signals plotted in Figures 5a and 5b. Similarly to what was seen in Figures 3a and 3b for the closer distances, we see that the impulsive P signal from explosions in Figure 7a is often a 2-5 Hz pulse of waves extending over 2-5 seconds. This lends some encouragement to the idea that complexity may be a more stable discriminant at regional distances because the P wave is made up of multiple rays all of which may not be defocused at once.

In Blandford (1981), noting the characteristics of the SALMON explosion and of a nearby earthquake as observed at an eastern United States station approximately 1000 km distant, it was noted that the onset of the L_g phase, especially on the transverse components, was more impulsive for the earthquake than for SALMON, perhaps due to the fact that the earthquake S phases would be generated at the source instead of being created by scattering. The earthquake onset was also characterized by a shift to lower frequency. This then would argue for the utility of transverse data, both for more accurate location estimates using better arrival times, and for discrimination using the impulsiveness of the S onset.

However, Figures 8a and 8b show the explosion and earthquake transverse waveforms from the distance range of 1.6 to 6.9 degrees which were displayed in Figures 4a and 4b, now aligned on the S onset and with an expanded scale. There is no apparent greater impulsiveness at the S_n or L_g onset for the earthquakes than for the explosion; nor is there a distinct change in frequency for either source, a rather surprising result.

Perhaps, as we shall see in the theoretical section, this may be because the explosion signals used in this study are actually from quarry blasts which have generated a large spall signal which theoretically gives a relatively impulsive S onset as compared to explosions. SALMON, and other well-contained explosions, might not be expected to generate such a large spall signal.

Because of the relatively low amplitude of P_n , and of the concentration of discrimination on the larger P_g and L_g amplitudes, and of the technical difficulty until recent years of plotting regional waveforms, it is difficult to find in the literature P_n waveforms from earthquakes and explosions from a common region on a common instrument in order to determine if this discriminant can work in other areas. However, especially more recently, some figures have become available in the literature.

Explosion profile, 1 Hz HP

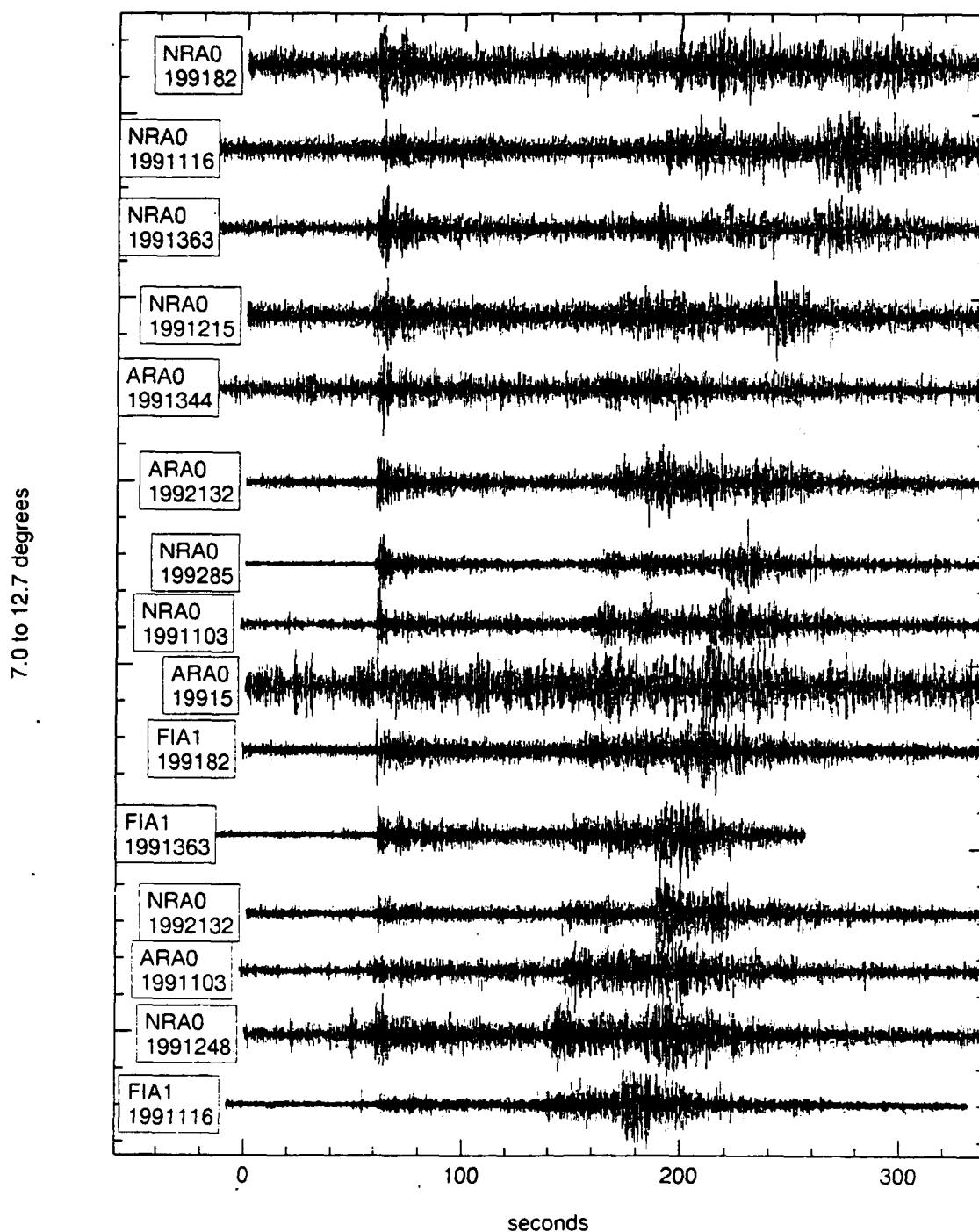


Figure 5a. Explosion profile, 1 Hz highpass. The signals are ordered by distance in the range 7.0 to 12.7 degrees as seen in Table 3. The explosions are seen to have impulsive arrivals in the first 1-10 seconds and to have a large P/L_g amplitude ratio as compared to the earthquakes seen in Figure 5b. The signals for explosions in the range 1.8 to 6.5 degrees are seen in Figure 2a. ARA0/19915 can be seen to be impulsive in Figure 6a where a 2 Hz highpass filter is applied. The small impulse near 55 seconds in FIA1/1991116 is regarded as significant and is characteristic of explosion signals.

Earthquake profile, 1 Hz HP

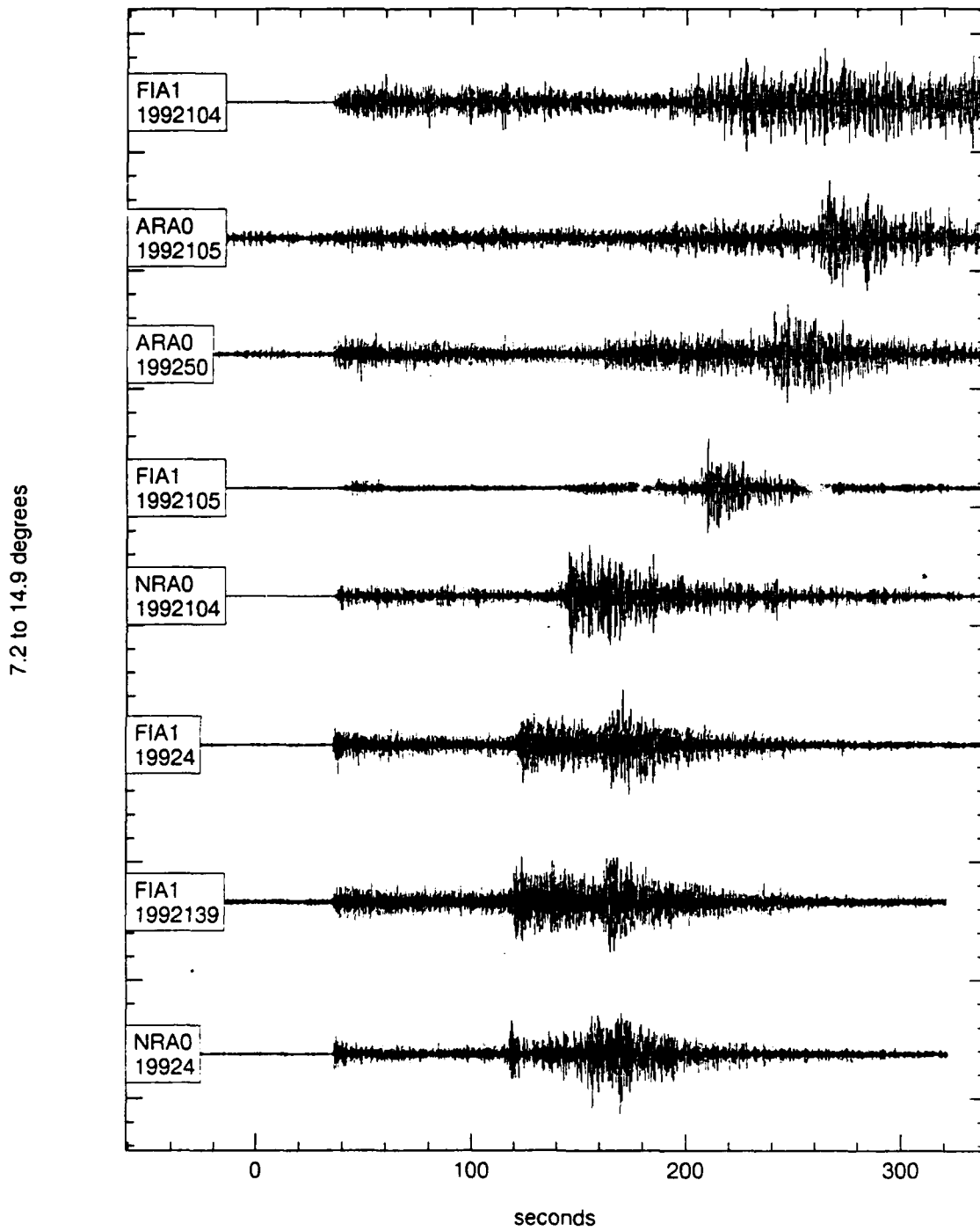


Figure 5b. Earthquake profile, 1 Hz highpass. The signals are ordered by distance in the range 7.2 to 14.9 degrees as seen in Table 4. The earthquakes are seen to have emergent arrivals in the first 1-10 seconds and to have a small P/L_g amplitude ratio as compared to the explosions seen in Figure 5a. The signals for earthquakes in the range 1.6 to 6.9 degrees are seen in Figure 2b.

Explosion profile, 2 Hz HP

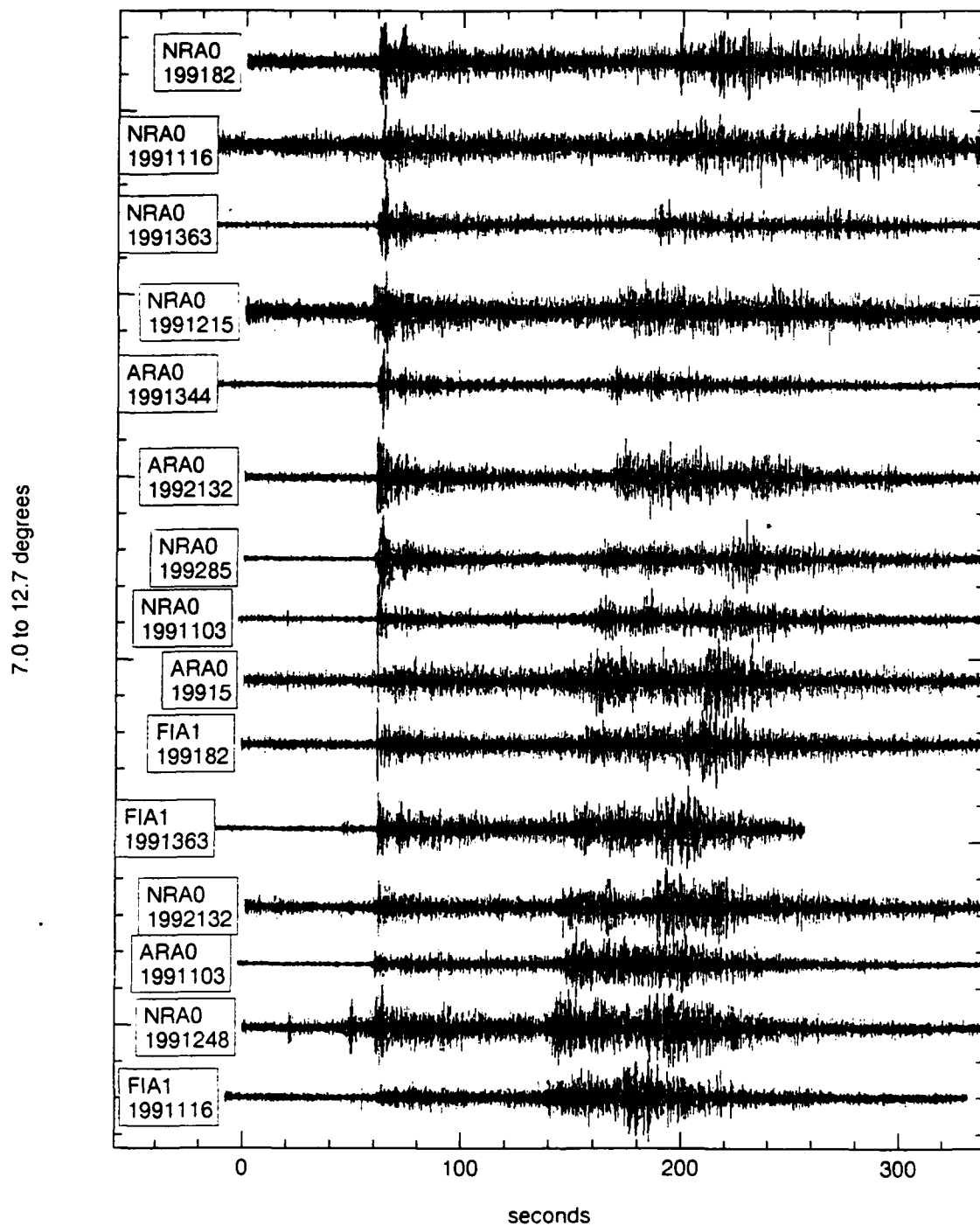


Figure 6a. The same as Figure 5a except as seen through a 2 Hz highpass filter. The event ARA0/19915 is now seen to be impulsive.

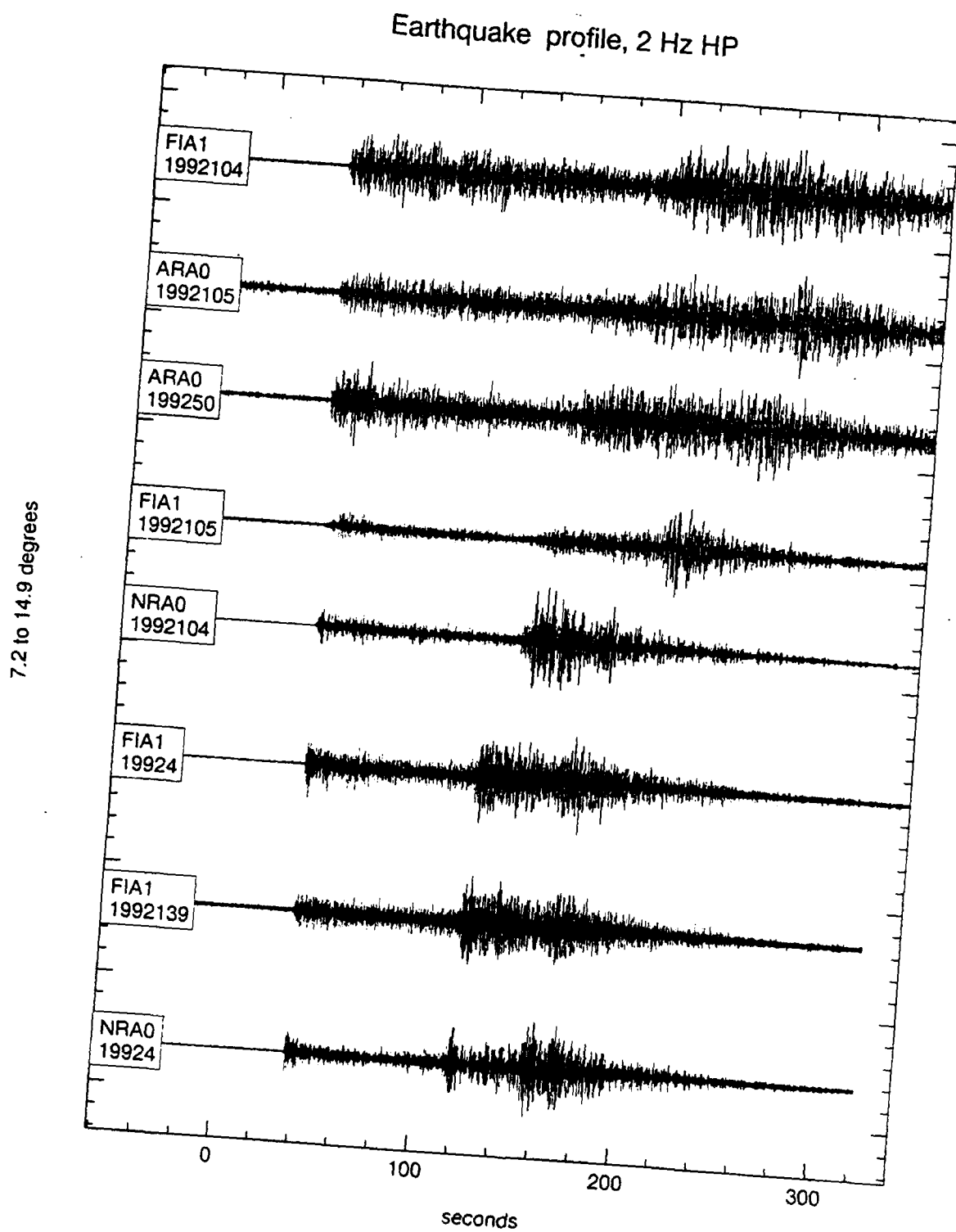


Figure 6b. The same as Figure 5b except as seen through a 2 Hz highpass filter.

Explosion profile, 1 Hz HP, Smax equalized

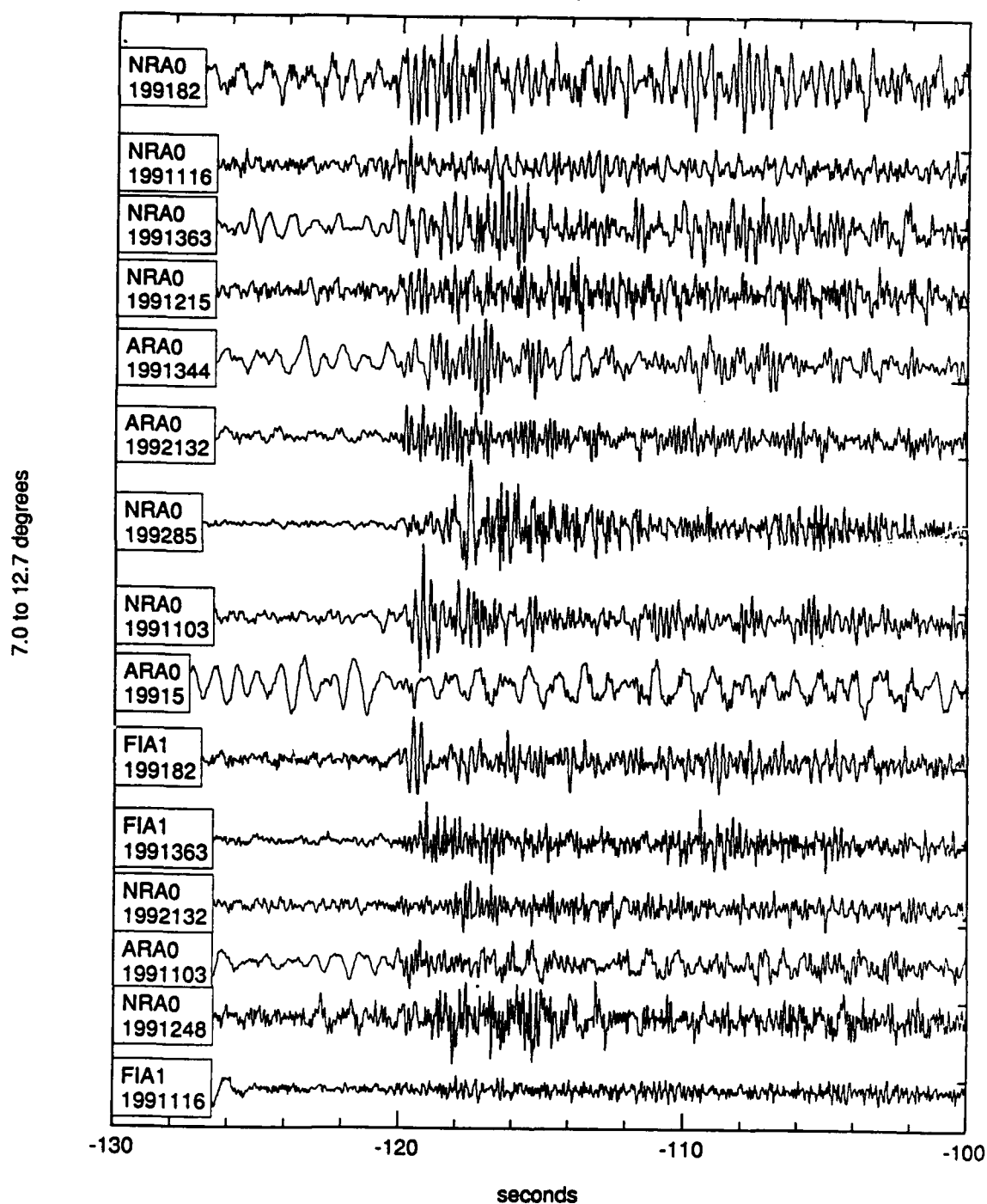


Figure 7a. First 20 seconds of signal from explosions in the distance range 7.0 to 12.7 degrees. By comparison with Figure 7b it may be seen that explosions typically have an initial pulse of 2-5 Hz waves, whereas earthquake signals are more emergent. Similarly, since the maximum *S* amplitude has been normalized to a constant amplitude in Figures 7a and 7b, and the amplitudes in Figure 7b are substantially smaller than in Figure 7a, it may easily be seen that earthquakes have smaller P/S amplitudes ratios as pointed out by Dysart and Pulli (1990).

Earthquake profile, 1 Hz HP, Smax equalized

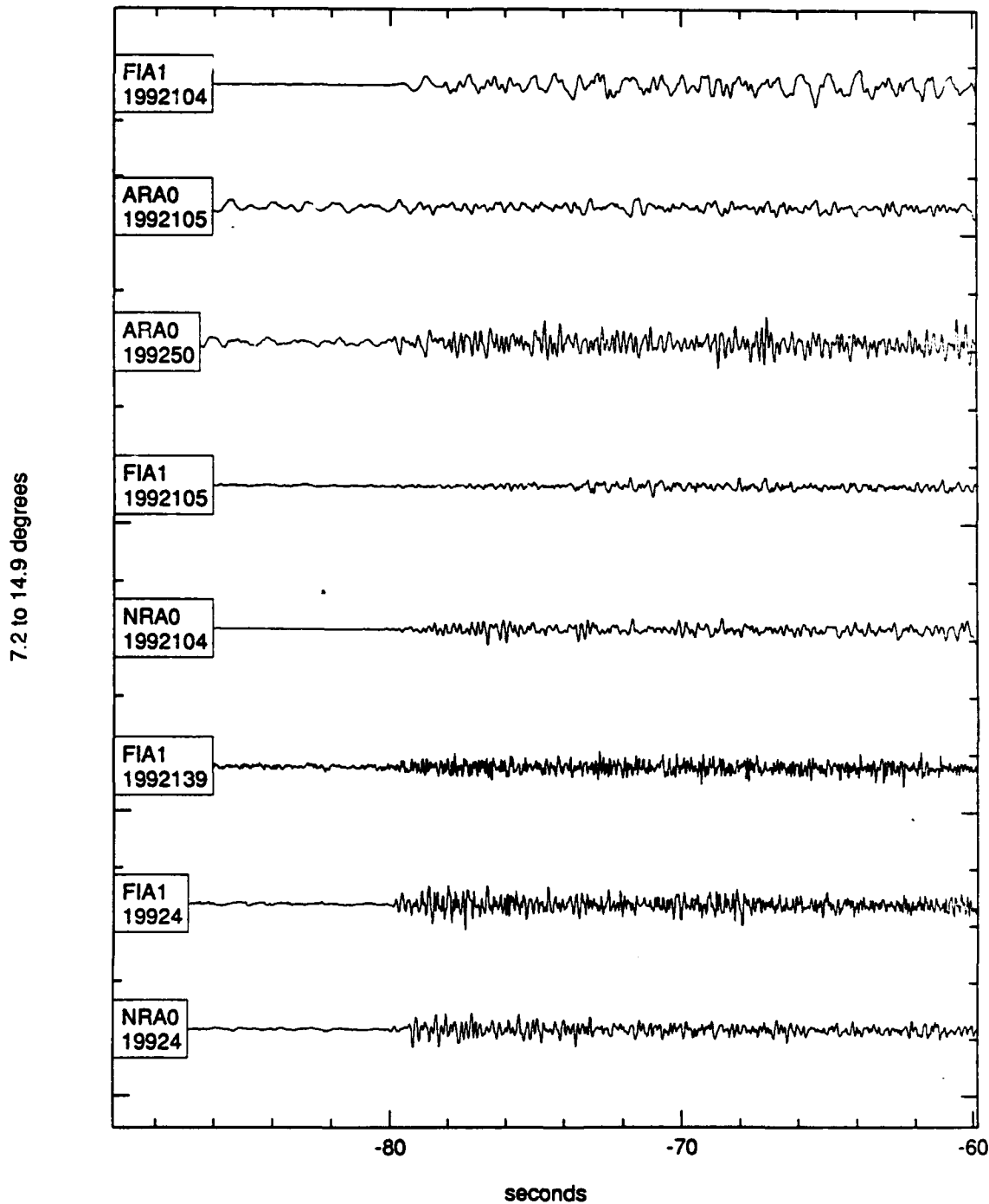


Figure 7b. First 20 seconds of signal from earthquakes in the distance range 7.2 to 14.9 degrees. By comparison with Figure 7a it may be seen that explosions typically have an initial pulse of 2-5 Hz waves, whereas earthquake signals are more emergent. Similarly, since the maximum S amplitude has been normalized to a constant amplitude in Figures 7a and 7b, and the amplitudes in Figure 7b are substantially smaller than in Figure 7a, it may easily be seen that earthquakes have smaller P/S amplitudes ratios as pointed out by Dysart and Pulli (1990).

Explosion profile, 1 Hz HP, Transverse

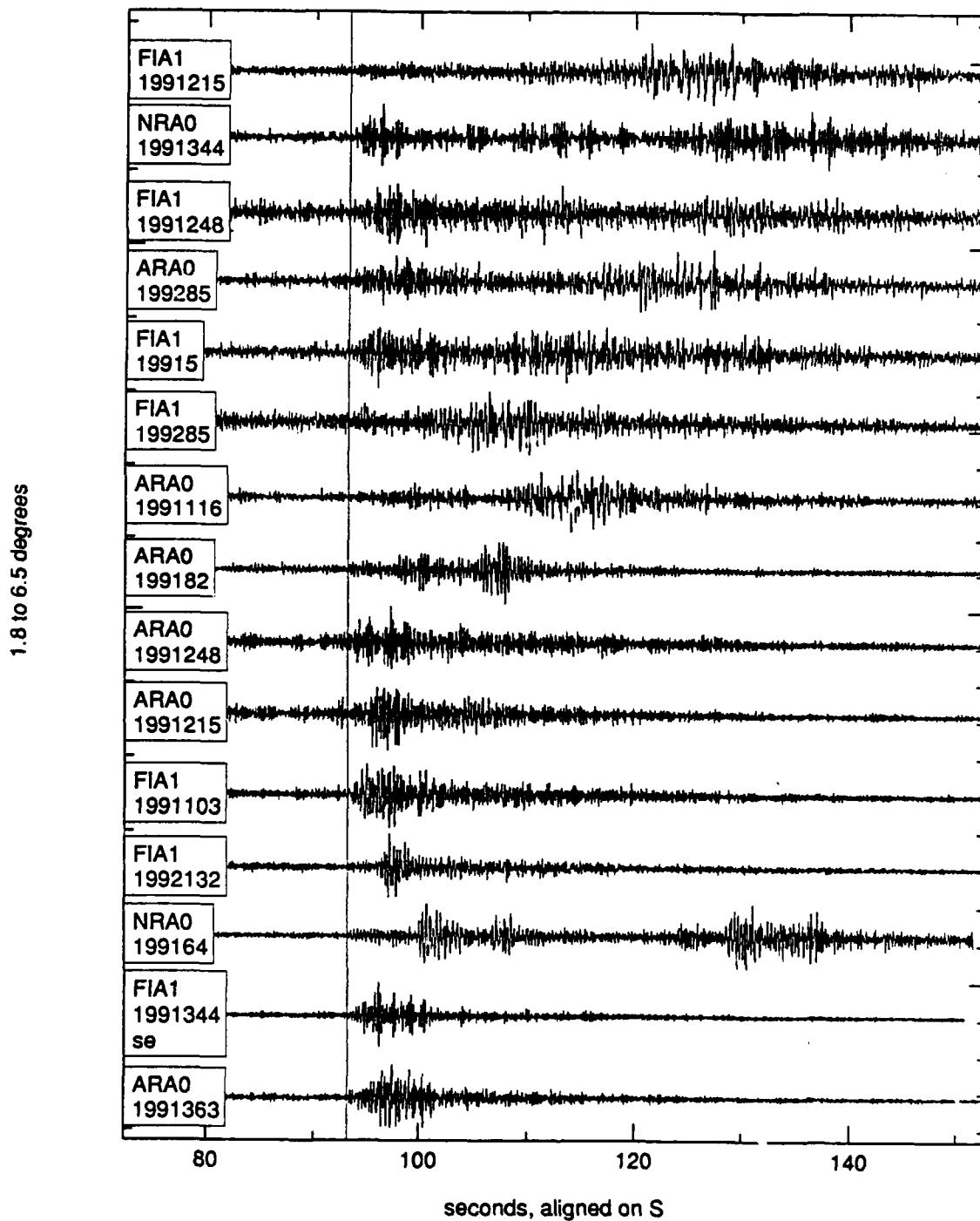


Figure 8a. Transverse waves from explosions in the distance interval 1.8 to 6.5 degrees, aligned on the *S* arrival and highpass filtered at 1 Hz. By comparison with the similar Figure 8b for earthquakes we see that the earthquakes do not have more impulsive *S* arrivals than do the explosions.

Earthquake profile, 1 HP, Transverse

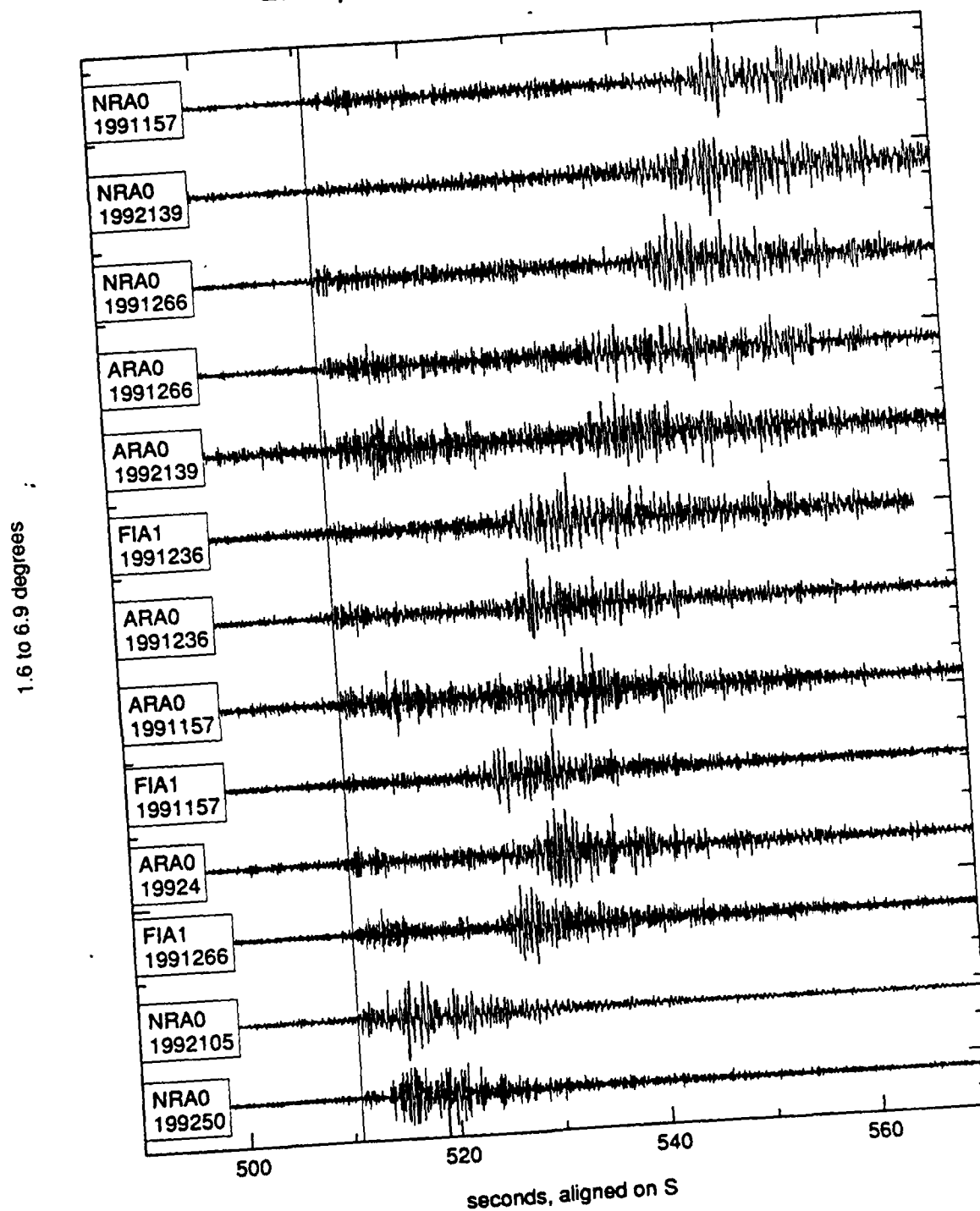


Figure 8b. Transverse waves from earthquakes in the distance interval 1.6 to 6.9 degrees, aligned on the *S* arrival and highpass filtered at 1 Hz. By comparison with the similar Figure 8a for explosions, we see that the earthquakes do not have more impulsive *S* arrivals than do the explosions.

In Blandford (1981) and Blandford et. al. (1981) there are plots of SALMON and a nearby 18 February 1964 earthquake as recorded on LRS systems at distances of approximately 1000 km. However, the P_n amplitude is small and, although the earthquake appears to be more emergent than the explosion, the S/N is not good and it is difficult to be certain. In Blandford et. al. (1981) there is also a plot of the well known 20 March 1976 event which occurred near Semipalatinsk and which is known from studies by Pooley et. al. (1983) to be a simple earthquake, together with a plot of a Semipalatinsk explosion as recorded at station MSH in Iran at a distance of 19°. The explosion P_n is noted to be clearly more impulsive.

Murphy and Bennett (1982) and Bennett and Murphy (1986) present several NTS explosion and near-NTS earthquake signals as recorded at single elements of the Tonto Forest, Uinta Basin, and Blue Mountain Vela Array Observatories (TFO, UBO, and BMO). As they point out, the S/N for P_n is poor (These authors therefore rested their analysis on P_g and L_g .) so that it is difficult to tell if the arrival is emergent or impulsive, perhaps reflecting the difficulty of applying this discriminant in low Q tectonic regions. However, it does seem possible that many of the earthquake P_n arrivals are more emergent than any of the explosions. It may be that for low Q tectonic regions array processing will be required to apply a regional complexity discriminant at the required magnitude levels.

Sereno et. al. (1992) have selected 33 events in Scandinavia to comprise their data set #2 and they attempted to ensure that each of these events is an earthquake. (Only one of the events in Sereno et. al.'s data set are considered in this study: the event ORID 25748 on 6 June 1991 at 12:46:11. All other events in this study occurred after this event which was the last event in the Sereno et. al. data base.) Approximately one-half of the events are well out into the ocean. Plots of six of the events are shown in the report, one of them from the mid-Atlantic Ridge, and one in the Barents Sea. Both of these events are impulsive. Perhaps this is an effect of reverberation in the overlying water column although it could be a radiation pattern effect.

Of the remaining four events plotted only one, ORID 207992 in Southwest Norway, seems to be clearly on land, and it is also clearly emergent. Another clearly emergent event is ORID 191216 in Western Norway which is located approximately 15 km off the Western Coast. It is apparent that it would be interesting to investigate, both theoretically and empirically, the relation between the impulsiveness of a signal and the depth of the overlying water column.

Figure 9, from Wuster (1992), shows a typical earthquake and explosion from the Vogtland area approximately 180 km Northwest of GERESS as recorded at GERESS. We see here the same pattern, in that the explosion P wave is impulsive and the earthquake's is emergent.

In Bennett et. al. (1992) the plot of Eurasian earthquakes and of explosions from three test sites at the station ARU shows the explosions to be impulsive and all but one earthquake record, at 2160 km to be emergent by comparison. At station GAR the record from Semipalatinsk at a distance of 1390 km appears to be not more impulsive than perhaps 1/2 of the earthquakes. At station OBN all of the explosion signals and most of the earthquake signals are at distances greater than 2000 km. The explosions are all quite impulsive as are many of the earthquakes at distances greater than 2000 km. For the six earthquakes at distances less than 2000 km the P_n appear to be emergent, however the S/N is poor for most of them. The story is similar at station KIV.

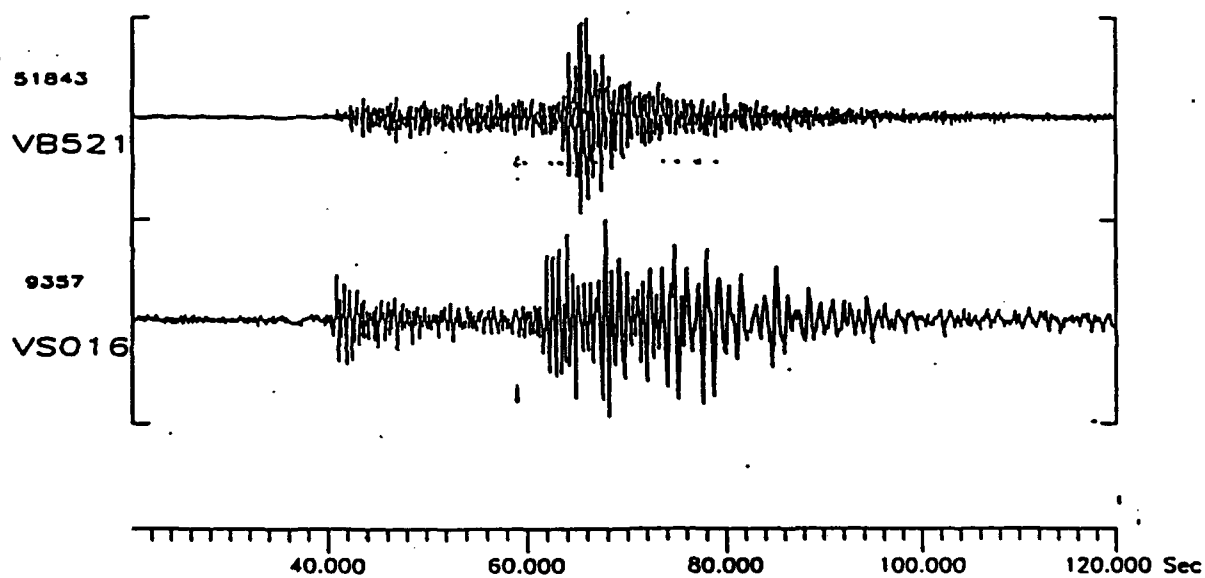


Figure 9. From Wuster (1992). The upper trace is an earthquake and the lower trace is an explosion as recorded at GERESS from the Vogtland district 180 km Northwest of GERESS. The impulsive explosion and emergent earthquake fit the pattern seen in Scandinavia.

Synthetic Calculation Methods

In the previous section we have seen how explosion seismograms appear to be more impulsive than earthquake seismograms at regional distances. It would be useful to see if this is the expected behavior for Scandinavia by computing synthetic seismograms for a structure appropriate for Scandinavia.

Methods for performing these calculations have been developed by Bouchon (1981, 1982), Campillo et. al. (1984, 1985), and discussed and reviewed by, e.g., Herrmann and Wang (1985), Chapman and Orcutt (1985), and Herrmann and Mandal (1986).

The calculations which follow were performed using the seismic synthetic waveform calculation software developed by R. Herrmann.

The structure used for the calculations is given in Table 5 and the P -wave velocity profile from which it is derived for depths below 50 km, is plotted in Figure 10. Figure 10 is taken from Ryaboy (1990) and was derived by analysis of Deep Seismic Sounding (DSS) profiles in Scandinavia. The shear wave velocity below 50 km was taken to be $3^{-1/2}$ times the compressional velocity and the corresponding densities were determined using the formula in Sereno and Given (1990).

The structure above 50 km in Table 5 differs from that of Ryaboy (1992), which was derived only by consideration of DSS P waves, by the inclusion of three lower velocity surface layers with a total thickness of 6 km which have low Q values in accordance with the results of Toksoz et. al. (1990) for Scandinavia who showed that lower Q and velocity values in the upper crust are required to properly model regional R_g seismograms. The velocity values are also generally consistent with those found by Ruud et. al. (1992) by analysis of R_g dispersion at NORESS, ARCESS, and FINESS. These Q values also serve the purpose in this study of reducing the amplitudes of the 1 Hz R_g fundamental surface waves generated by shallow events. Otherwise these waves would dominate the calculated signals at distances beyond 200 km, which is not, in fact, observed.

The estimated velocity gradient below 100 km of 0.01s^{-1} is substantially greater than the value of 0.0013s^{-1} found by Sereno and Given (1990) to be appropriate for an earth flattening approximation and which is certainly within the margin of error of the estimated gradient. Thus it does not seem appropriate to make an additional earthflattening approximation.

The Green's function seismograms were calculated using Herrmann's `hspec91` subroutine with the time domain damping of 0.008sec^{-1} a time step of $1/6.4$ seconds, and a total number of data points of 2048, giving a total time for the calculated waveform of 320 seconds. Green's functions were computed for earthquake, explosion, and point-force sources. (We shall see that the vertical point-force Green's functions may be used to compute the seismograms resulting from a spall source.) The top of the layer stack was specified to be a free surface, and the bottom a half space with the indicated properties. The control of wavenumber sampling, following Bouchon (1981), is 5000 km, and the control on the upper limit of wavenumber integration is 3. The seismograms

Table 5: DSS Structure for Synthetics

Layer h (km)	P-wave Velocity	S-wave Velocity	Density	P-wave Q^{-1}	S-wave Q^{-1}
.5	5.90	3.50	2.70	0.01250	0.0250
4.5	6.00	3.60	2.80	0.00500	0.0100
1	6.10	3.70	2.80	0.00200	0.0050
10	6.20	3.80	2.80	0.00200	0.0050
8	6.70	4.10	3.10	0.00050	0.0010
8	6.80	4.10	3.10	0.00050	0.0010
8	6.90	4.42	3.20	0.00050	0.0010
10	8.00	4.64	3.29	0.00050	0.0010
5	8.05	4.67	3.30	0.00025	0.0005
10	8.10	4.70	3.33	0.00025	0.0005
10	8.15	4.73	3.35	0.00025	0.0005
10	8.25	4.79	3.39	0.00025	0.0005
10	8.40	4.87	3.44	0.00025	0.0005
15	8.00	4.64	3.29	0.01000	0.0200
10	8.45	4.90	3.46	0.00025	0.0005
10	8.47	4.91	3.47	0.00025	0.0005
10	8.49	4.92	3.48	0.00025	0.0005
10	8.51	4.93	3.49	0.00025	0.0005
10	8.53	4.94	3.49	0.00025	0.0005
10	8.54	4.95	3.49	0.00025	0.0005
10	8.55	4.96	3.55	0.00025	0.0005
below	8.55	4.96	3.55	0.00025	0.0005

are computed for a surface instrument, and the maximum distance for which a seismogram is computed is 1500 km. The reduction velocity to determine the first time calculated is 8.5 km/sec, and there is an additional offset to allow 10 seconds before the first arrival. No wavenumber filtering was performed. Computation time for all mechanisms for a single depth was approximately 24 hours on the Center for Seismic Studies Stardent computer while it was being used predominantly only for these calculations.

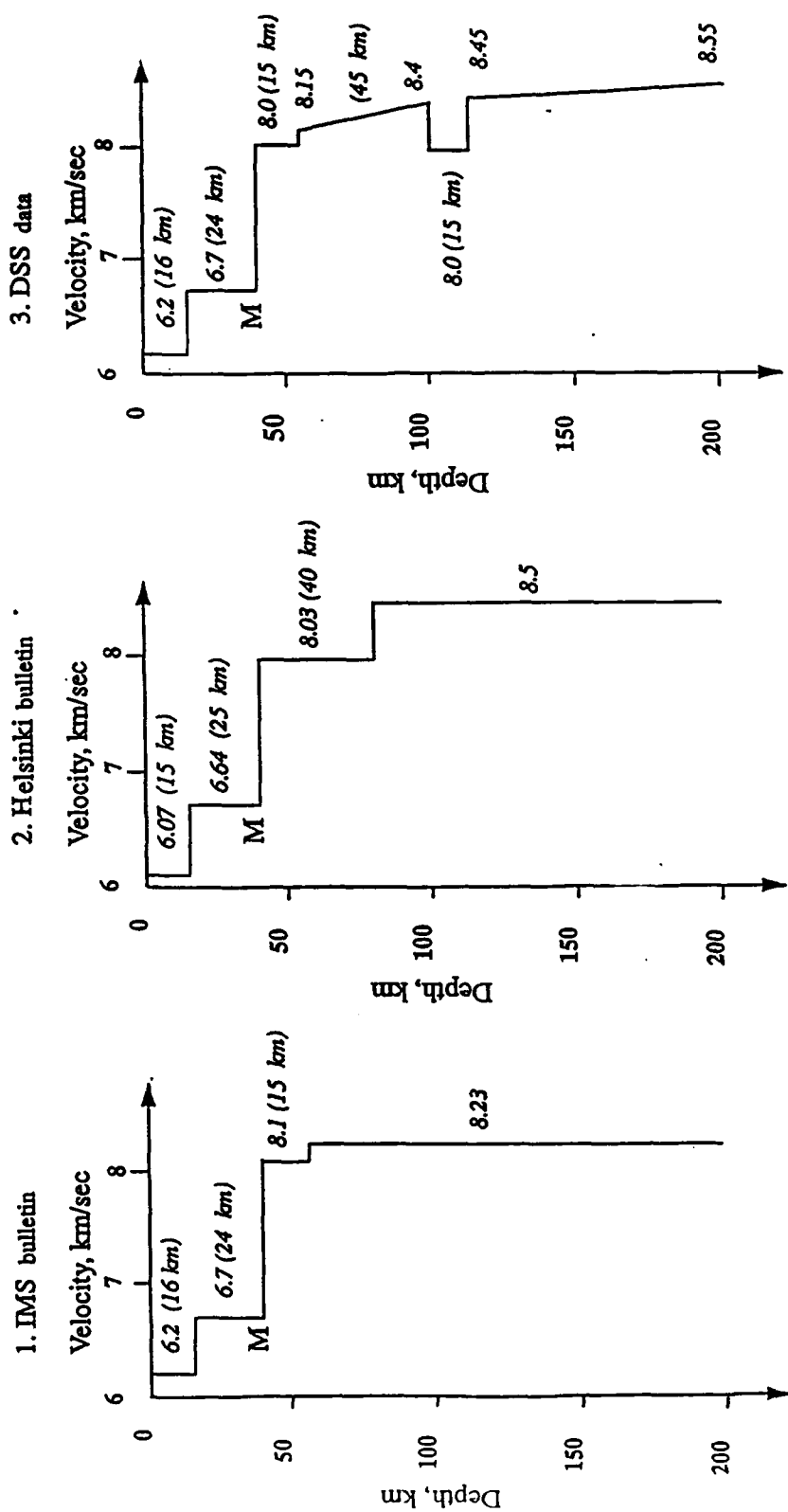


Figure 10. From Ryaboy (1990 and 1992, personal communication). The vertical profile *P* velocity derived from DSS data was used in this study for the structure below 50 km. Also shown are the *P* profiles used routinely in DARPA's Intelligent Monitoring System (IMS) and in the Helsinki seismic bulletin.

The Green's function output of `hspec91` is then passed through Herrmann's program `rhfoc91` with the option to specify the source time function as a one-sided parabola with unit area, as discussed by Herrmann and Mandal (1986), with a duration of 0.625 seconds. One of the favorable features of this time function is that it has a null at the Nyquist frequency so that there are no time-domain ripples introduced by a sharp high frequency spectral cutoff.

For earthquakes the parabolic time function corresponds to the near-field velocity time history, or equivalently to a unit step displacement on the fault. The corresponding moment is 10^{20} dyne-cm. The explosion source has the same moment and a corresponding velocity time history. For the point force source the parabolic time source represents the time derivative of the force as a function of time.

Since the experimental data is recorded on broadband velocity instruments, the option in `rhfoc91` which yields a velocity seismogram is selected. For an earthquake or explosion source this results in the final synthetic seismograms of interest for comparison with observations. For a spall source the situation is more complicated.

The parabolic time series is a good representation of the time history of a typical spall displacement, starting at zero, reaching a finite maximum, and returning to zero. However, in the calculations the parabola actually represents the time derivative of the applied force. The implied actual applied force is then the first integral of the parabola. However, Day and McLaughlin (1991) have shown that the spall force itself is the second derivative of the displacement. Thus the displacement responsible for the computed force seismograms, under the hypothesis that the source of the force is a spall, is the third integral of the parabola. Thus we must differentiate the parabolic point source seismogram *three* (3) times to obtain a spall broadband velocity seismogram to be compared to the explosion or earthquake velocity seismograms.

To compute synthetic seismograms for particular faults one may combine these Green's functions with coefficients appropriate to the fault plane normal and vector slip times cosines and sines of the azimuth and twice azimuth from the event. These formulas may be found, for example, in Herrmann and Mandal (1986).

For the particular cases of vertical strike-slip, vertical dip-slip, and 45° dip-slip, the vertical waveforms are proportional to $ZSS \sin 2\phi$, $ZDS \sin \phi$, and $[ZDD + ZSS \cos 2\phi]$, respectively; while the transverse component is proportional to $TSS \cos 2\phi$, $TDS \cos \phi$, and $TSS \sin 2\phi$, respectively. We note that, for the vertical faults, the vertical waveform vanishes completely 2 or 4 azimuths; and for a fault of any dip with a horizontal slip there is a complete z component null for any 90 degrees. Thus, for such events and azimuths, if there is to be any *P* wave it must come from transverse *S* scattered into the radial and vertical components. This can only happen if there is fully three-dimensional (3D) scattering. It is presumably cases such as this which accounts for the waveforms which seem uniquely characteristic of earthquakes but which cannot be modeled by 1D, or even perhaps by 2D, earth models.

Synthetic Calculation Results

Figure 11 shows the Green's function vertical component synthetics for an explosion at a depth of 1 km, and for an earthquake at a depth of 10 km with a 45° dip-slip (DD) source mechanism for the distance range of 100 to 1500 km.

We see immediately that at all distances the shear phases on the vertical are much larger for the earthquake (the lower of each pair of traces) than for the explosion. Close examination of the P phase, shown in more detail in Figure 12, also shows that the earthquake P phases, even for this 1D model, are more emergent than are those from the explosion. This fact, coupled with the observation that the long-period Rayleigh phases are approximately of equal amplitude for the explosion and earthquake, suggests that if the m_b phase is calculated from the first motion, an $m_b:M_s$ discriminant would be successful at regional distances for this earthquake mechanism.

On the other hand, it is apparent that a SP/LP discriminant based on L_g and M_s would go in the other direction.

Close inspection of the Rayleigh phase for the explosion reveals that the higher frequency R_g is prominent at 100 km but is reduced in amplitude by 300 km and basically absent beyond 500 km. This reflects the action of the low Q values in the upper crustal layers.

The P phases may be examined more easily in Figure 12. Here we see that the earthquake P phases are extremely emergent as compared to the explosion P waves in the distance range 500 to 900 km. At the distances of 300 and 1200 km the explosion P wave seems emergent due to the large pulse at a delay of approximately 3 seconds. This phase, according to Ryaboy (1990), is reflected from the top and bottom of the low velocity layer, while the first arrival is the P_n arrival associated with the upper interface. The phase is also apparent in the earthquake P signals, although, for the earthquake, both the initial and reflected phase are small compared with the following phase which is sP .

It is apparent from these two explosion signals that any simple complexity model in these distance ranges would be most effective were it to define the amplitude of the first arrival as an average over the first 3 seconds, not the first 1 or 2 seconds. In a practical situation it would be important to examine signals from many quarry blasts to discover those paths over which the velocity structure creates emergent explosion signals and to define the first window of a complexity criterion to ensure that those signals are defined as simple.

It is interesting that the 45° dip-slip (DD) source mechanism which gives a more emergent signal at regional distances is the same mechanism which is so difficult to discriminate at teleseismic distances where the takeoff angles all result in compression for thrust faults. Presumably this is because at regional distances the takeoff angles are more oblique. This suggests that regional complexity may nicely complement teleseismic discrimination.

Explosion & Earthquake (DD, 10 km) Synthetics, Vertical, BB

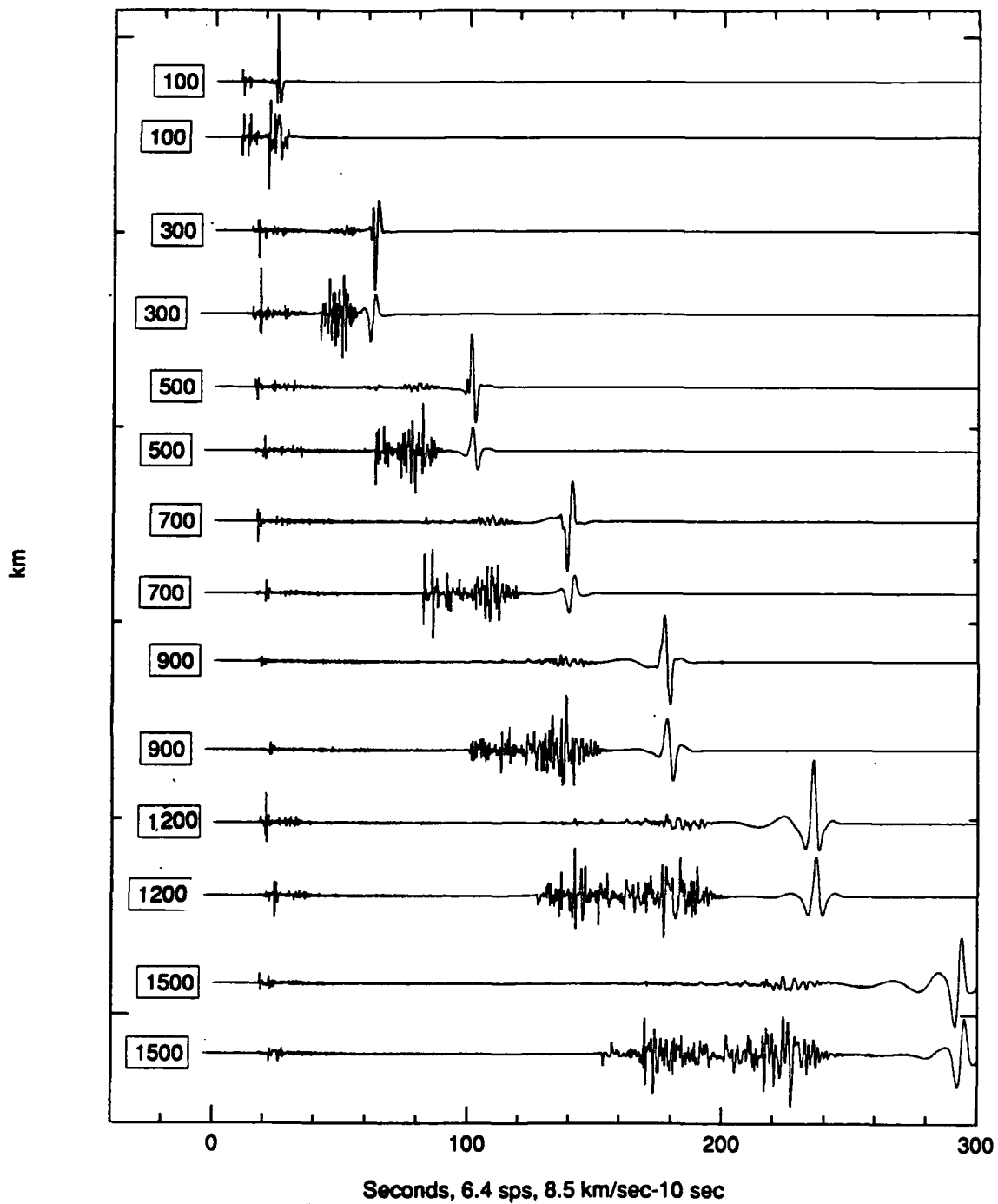


Figure 11. Broadband velocity vertical component synthetics for an explosion and a 45° dip-slip earthquake at 10 km depth for distances ranging from 100 to 1500 km. Amplitudes are scaled to a common maximum. The earthquakes are seen to have larger shear wave amplitudes.

Explosion & Earthquake (DD, 10 km) Synthetics, Vertical, BB

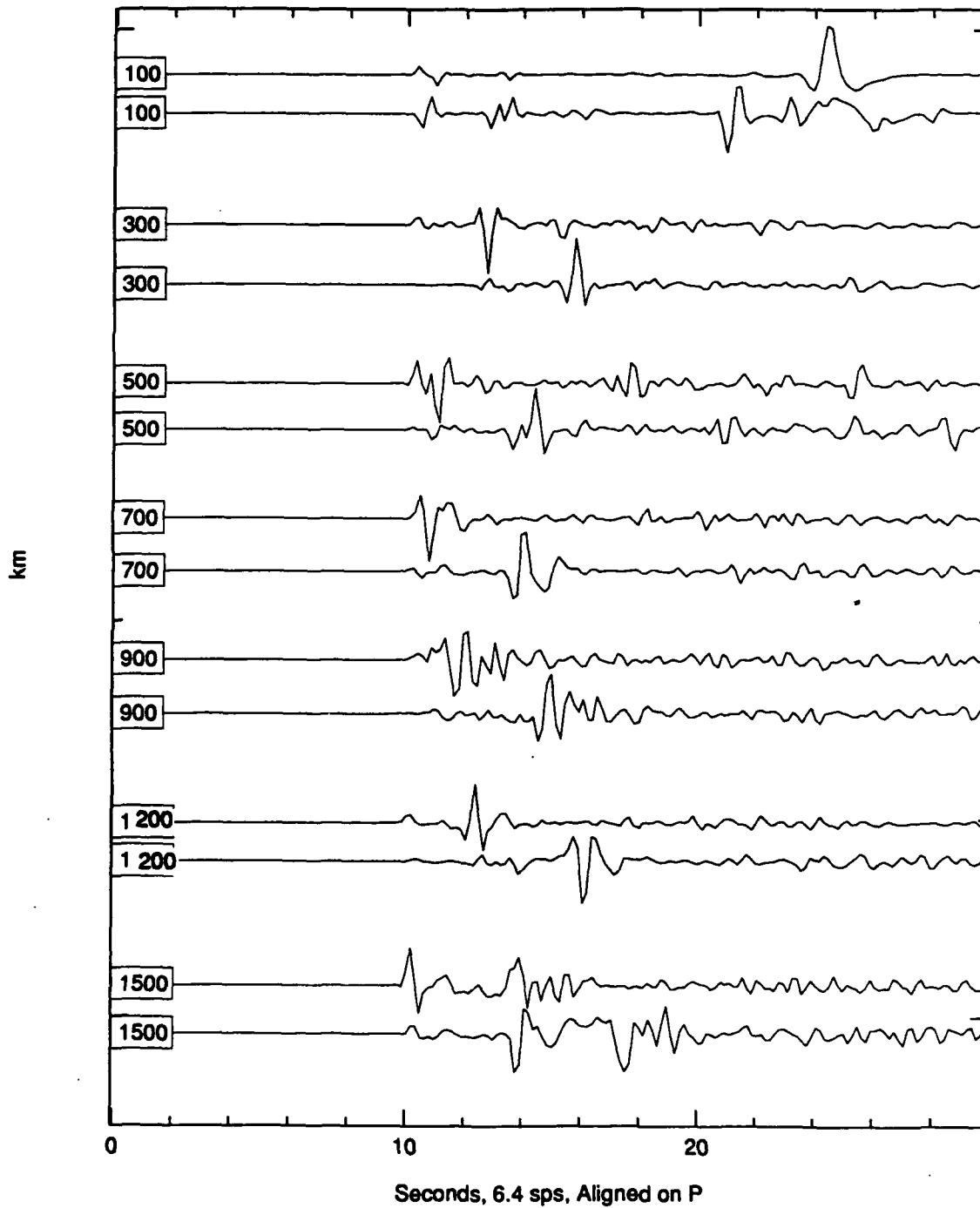


Figure 12. Broadband velocity vertical component synthetics for an explosion and a 45° dip-slip earthquake Green's function source at 10 km depth for distances ranging from 100 to 1500 km. Amplitudes are scaled to a common maximum. The earthquakes are seen to be more emergent due in large measure to a large *sP* phase. The large pulse on explosions at 300 and 1200 km at a 3-second delay is a reflection from the upper and lower boundary of a low velocity zone.

The more oblique takeoff angles result in an approximate P null being directed to regional distances so that the "scattered" sP phase, which arrives later, results in an emergent signal. It is plausible that in more complex earth models the basic idea may be retained but the scattered S phases may derive from sharp discontinuities other than the free surface. In the present earth model the only sharp discontinuity which strongly scatter the typically 1 Hz signals of these P synthetics is the free surface. However, in the real earth, which has produced the observed data presented earlier, other interfaces may exist which strongly scatter the 3-5 Hz frequencies which characterize the signals. Fisk (personal communication, 1992), using the 2D phase screen techniques discussed in Fisk and McCartor (1991) and Fisk et. al. (1992), has calculated the signals resulting from pure 1 Hz Ricker wavelet compressional and shear sources imbedded in an infinite exponential random medium with 2% rms P and S velocity perturbations, a correlation length of 5 km, and mean P and S velocities of 6 and 3.5 km/sec respectively.

Figures 13a and 13b show that while the compressional source still gives an impulsive initial signal on the radial component at 200 km distance, the shear source results in an emergent radial component. Of course, for the shear source the S arrival on the transverse component is impulsive. However, at 200 km it is noticeable that the S arrival is not impulsive on the radial component. This suggests that it would be best to measure S arrival times on the transverse, rather than on the radial component in a random medium; this is, of course, standard practice in observational seismology. Theoretically, this result is understandable because the energy in the radial component just in front of the transverse S arrival is largely comprised of energy recently converted to faster compressional waves from the soon-to-arrive S phase.

It is also of interest in Figure 13a that at 200 km the P wave, though still impulsive, is apparently comprised of two arrivals as compared to the single arrival at 50 -150 km. This suggests a greater stability in the impulsive P arrival in that if one of the arrivals were to be defocused at a greater distance, the other might remain large and maintain the impulsive nature of the onset.

It is of further interest that the initial transverse component of the compressional source is impulsive while the initial transverse component from the shear source is not. This is reasonable since signals on the transverse component arriving at times appropriate to a P signal must be scattered locally and thus be approximately proportional to the radial component.

Since these phase screen calculations are 2D they can only model the situation where a P -wave null, but not an SV null, exists. The SV randomly scatters into P . In the real earth this is often a strong sP phase which does not result in a waveform with an extremely emergent character. These calculations show how the SV can be transformed into an emergent P wave. For a complete waveform null an emergent P could only occur by scattering in 3D. The fact that no complete nulls have been noted by workers in the field suggests that such scattering in 3D does occur. It would be interesting to examine network waveforms from earthquakes known to have vertical fault planes, especially using stations along strike.

As we saw in Figure 11, the short-period shear phases from the earthquake are much greater than for an explosion which has an equal compressional amplitude. McLaughlin et. al. (1988) have suggested that the observed difference in shear excitation is not this great, that the calculated amplitude of explosion L_g is too low, and that the difference is made up for by spall. In this study also the L_g to P ratio difference between earthquakes and explosions is less for observation than in theory.

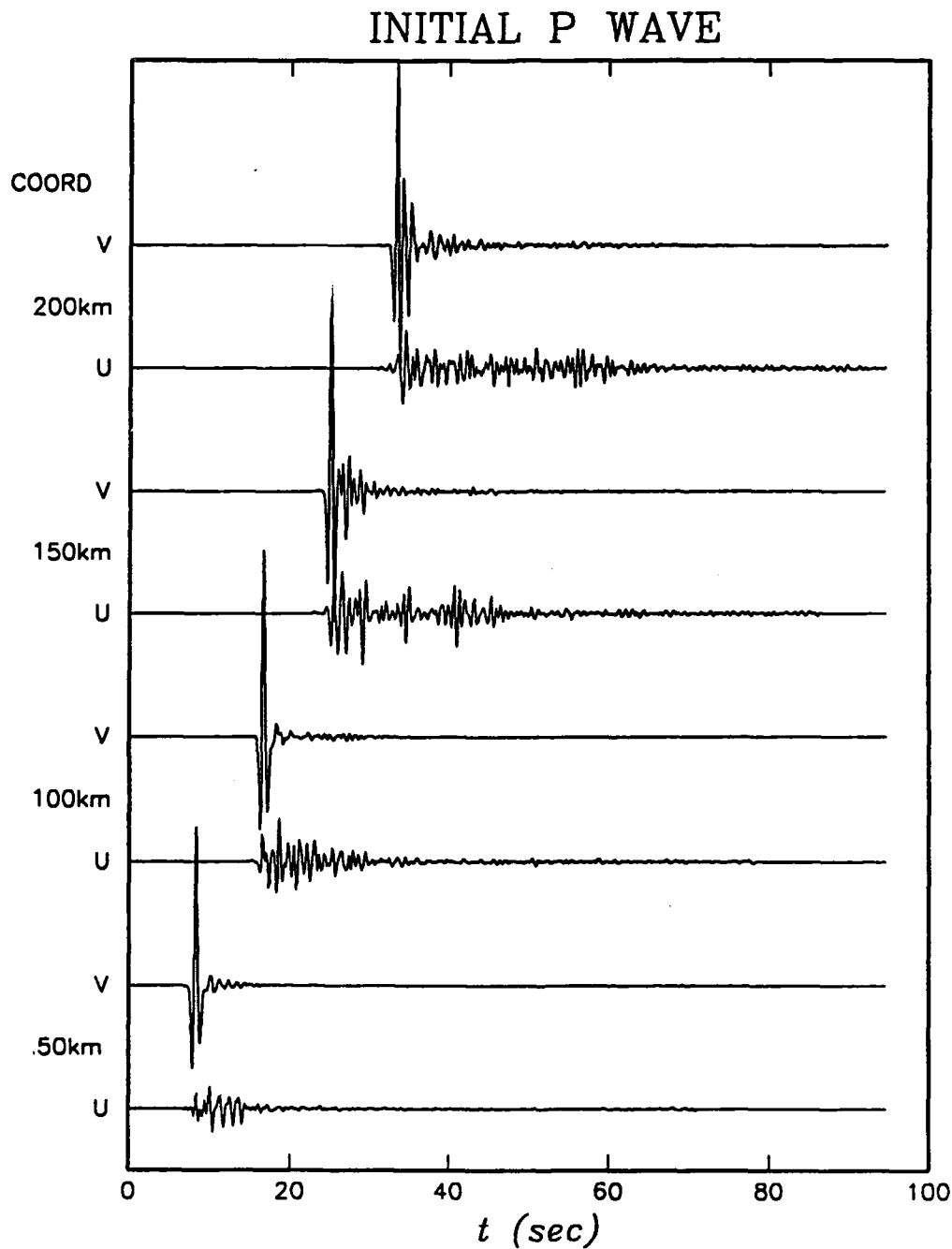


Figure 13a. Radial (v) and transverse (u) signals from a Ricker wavelet compressional source in a random exponential medium with 2% rms variation in the P and S velocities as seen at distances of 50, 100, 150, and 200 km. The u scale have been increased by a factor of 2. At all distances the P arrival is impulsive on both radial and transverse components, although at 200 km the P arrival is apparently followed by a rather large second arrival.

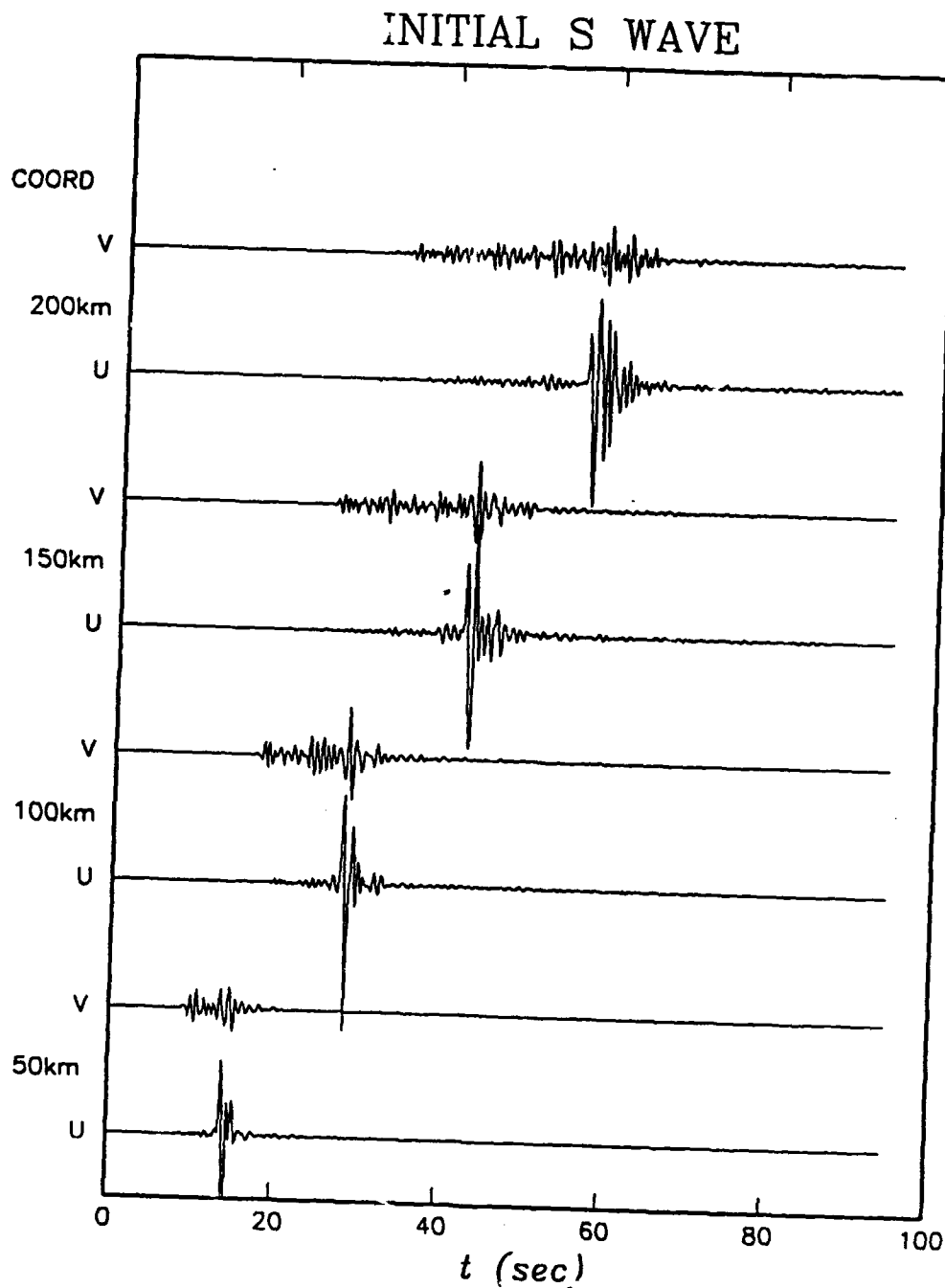


Figure 13b. Radial (v) and transverse (u) signals from a Ricker wavelet shear source in a random exponential medium with 2% rms variation in the P and S velocities as seen at distances of 50, 100, 150, and 200 km. The v amplitudes have been increased by a factor of 2. At all distances the P arrival is emergent on both radial and transverse components while the S arrival is impulsive on the transverse, but not on the radial. Calculations by Fisk (personal communication, 1992).

In Figure 14 we see all non-zero Green's function components at a distance of 900 km from the spall, explosion, and three earthquake sources. The DD earthquake source, as we have seen previously is from a 45° dip-slip source. The SS earthquake is a vertical strike slip, and the DS source is a vertical dip-slip. The explosion source is taken to be at a depth of 1 km, the spall at 0 km, and the earthquake at 10 km.

It is apparent that, at high frequencies, the spall shear waves are much larger, for a fixed P wave amplitude, than are the explosion shear waves. In addition, spectral analysis of the synthetic signals in Figure 14 shows that the explosion L_g signal is lower in frequency than either the spall or the earthquake L_g signals. This provides support, from a linear mechanism, for the discriminant of Bennett and Murphy (1986) who found that explosion L_g was of lower frequency than that of earthquakes. From the present analysis it would appear that extensive spall could, depending on the details of the spall source time function, render this discriminant less effective. On the other hand, well-buried explosions which have little spall would be expected to discriminate well. The physical source of the spectral difference between the theoretical explosion and earthquake L_g spectra have not been determined; however, it is evidently related to depth since the 1 km earthquake spectrum is not different from that of the explosion.

Although the L_g to P ratio as a discriminant seems marginal when comparing the vertical components of spall and the SS (vertical strike-slip) earthquake source, it is important to note that the transverse component is large and that some of this energy will likely scatter into the vertical component, thus improving the discriminant. We shall see later that the DS (vertical dip-slip) source has a small shear amplitude on the vertical component for a depth of 1 km but, there also, the transverse component is approximately 10 times larger. These results suggest that one should investigate extending the L_g to P ratio discriminant to an average over all components; theoretically it will result in better discrimination although for most events it will not be needed and, if there is extensive scattering between components, it may be of little benefit.

Returning to Figure 14. In accord with the results of Day et. al. (1983), we see that there is no detectable long-period Rayleigh wave from the spall.

To examine further the possibility of using complexity as a discriminant, Figure 16 shows the vertical component P signals for the explosion, spall, and the three earthquake Green's functions, all at 900 km distance. It is apparent that a 3-4 second window defining the initial arrival will serve to separate earthquakes from explosions. The SS and DS sources do not generate as emergent a signal as does the DS source. Any actual earthquake can be characterized as a linear superposition of these three sources and, even in the absence of P wave nulls and S to P scattering, would often have a complexity intermediate between them, although studies should be carried out to see if which combinations, e.g., the sum of SS and DS which seem to have the same polarity for P but opposite polarity for sP , are very simple. Of course, under a suitable mode of application of complexity, a simple earthquake will fall in the undecided category and not be classified as an explosion.

In Figure 17 we display on an expanded time scale with amplitudes scaled to a common maximum, all three components of shear onset for these sources. The explosion does not exhibit a sharp onset (although the vertical is sharper than the radial), whereas the spall and earthquakes do.

EX,SP,&EQ(SS,DS,DD,10km) Synthetics,3 Component BB

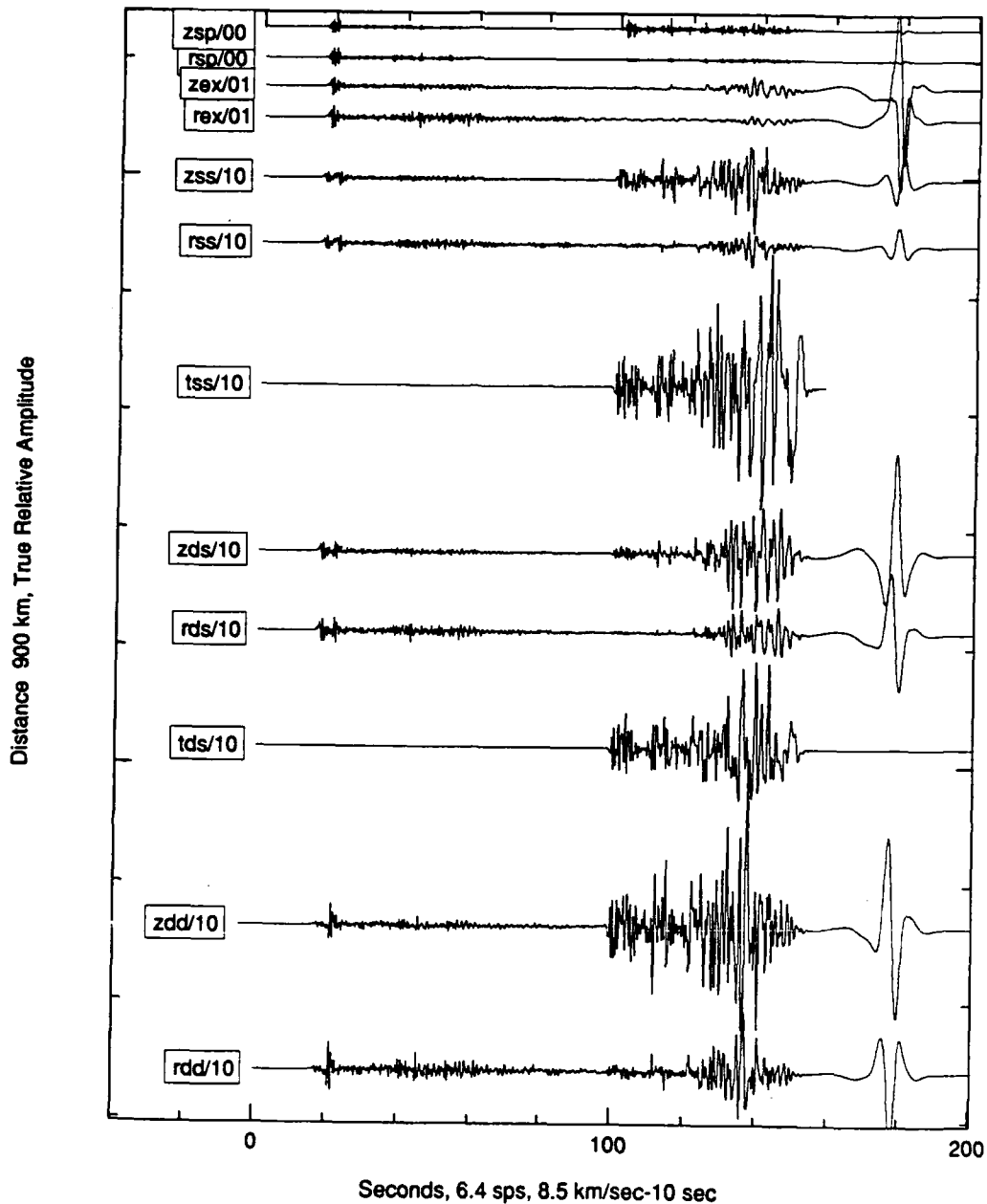


Figure 14. Broadband velocity 3-component synthetics for a spall source at 0 km, an explosion at 1 km depth and three earthquake Green's function sources at 10 km. All non-zero components are plotted. The instrument response is broadband velocity. The spall shear phases are seen to be larger than those for an explosion of equal P amplitude.

EX,SP,&EQ(SS,DS,DD,10km) Synthetics,3 Component 1Hz HP

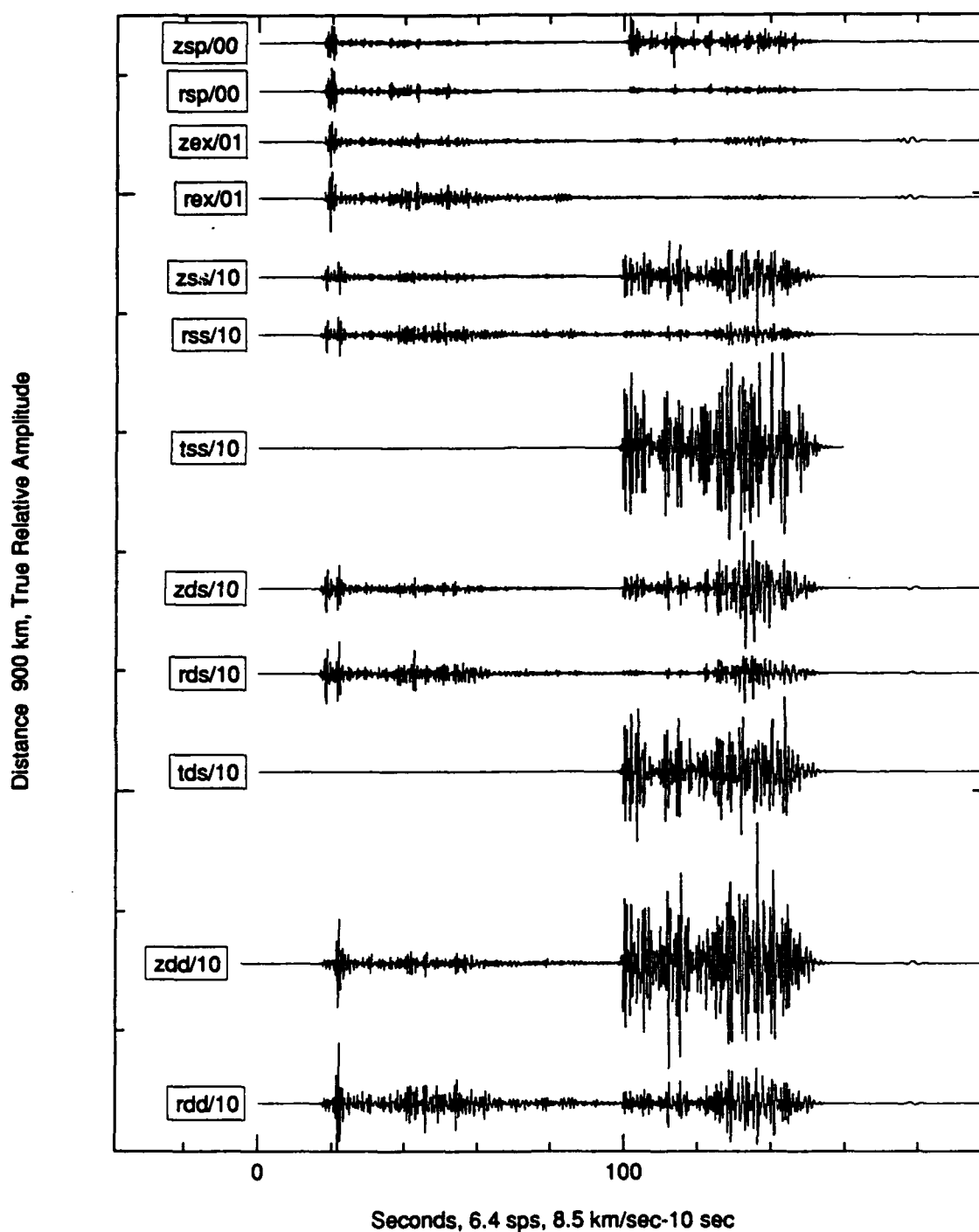


Figure 15. 1-Hz highpass filtered velocity 3-component synthetics for a spall source at 0 km, an explosion at 1 km depth, and three earthquake Green's function sources at 10 km. All nonzero components are plotted. The instrument response is broadband velocity. The spall shear phases are seen to be larger than those for an explosion of equal P amplitude.

EX, SP, & EQ(SS, DS, and DD, 10 km) Synthetics, Vertical Component, Bf

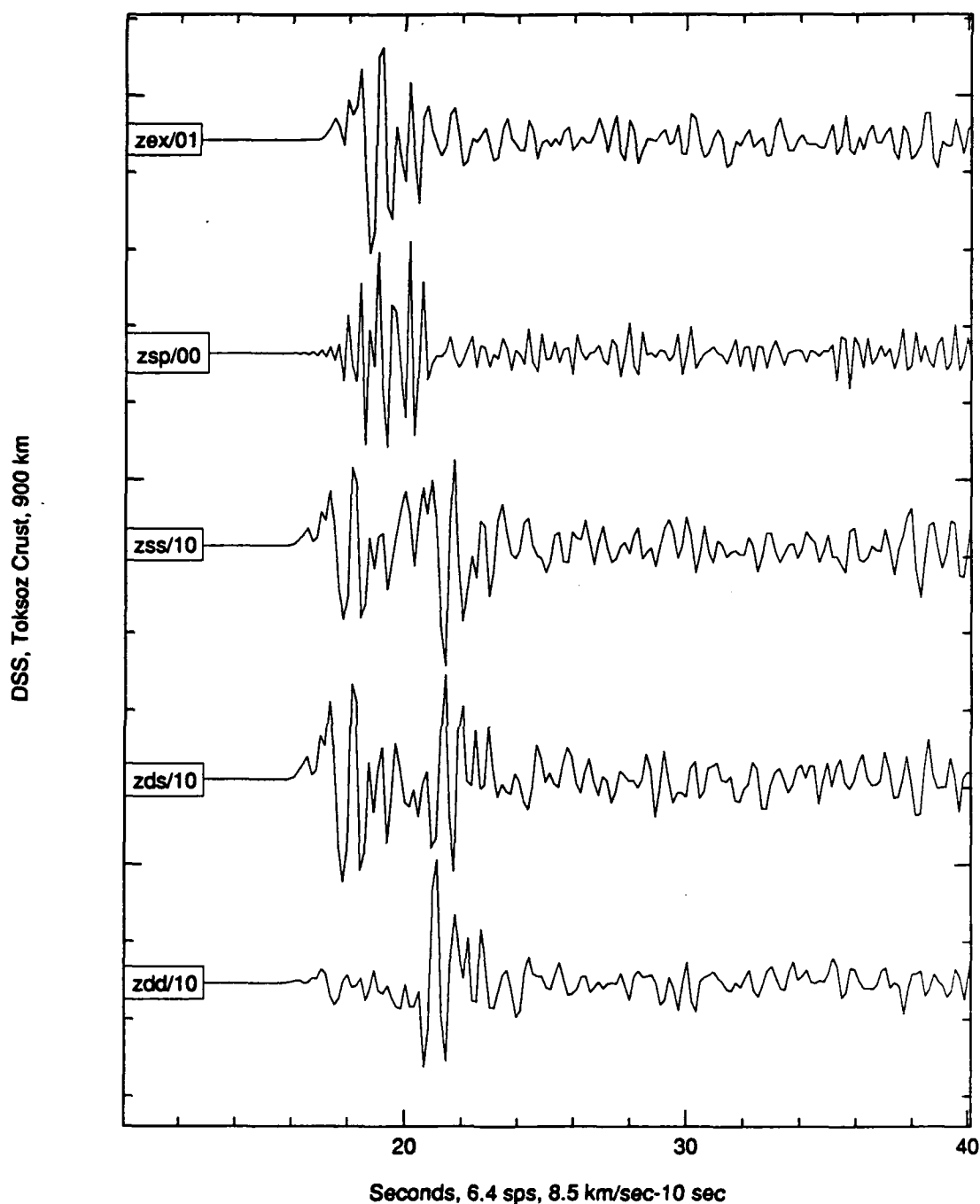


Figure 16. Broadband velocity vertical component P synthetics for a spall source at 0 km, an explosion at 1 km depth, and three earthquake Green's function sources at 10 km. A 3-4 second window beginning at the P arrival could be used to define an initial P amplitude for purposes of defining a complexity discriminant. The vertical strike-slip and dip-slip earthquake sources do not generate signals as emergent as the 45° dip-slip source. The phase at approximately a 5 second delay for the earthquakes is sP .

EX,SP,&EQ(SS,DS,DD,10km) Synthetics,3 Component 1Hz HP

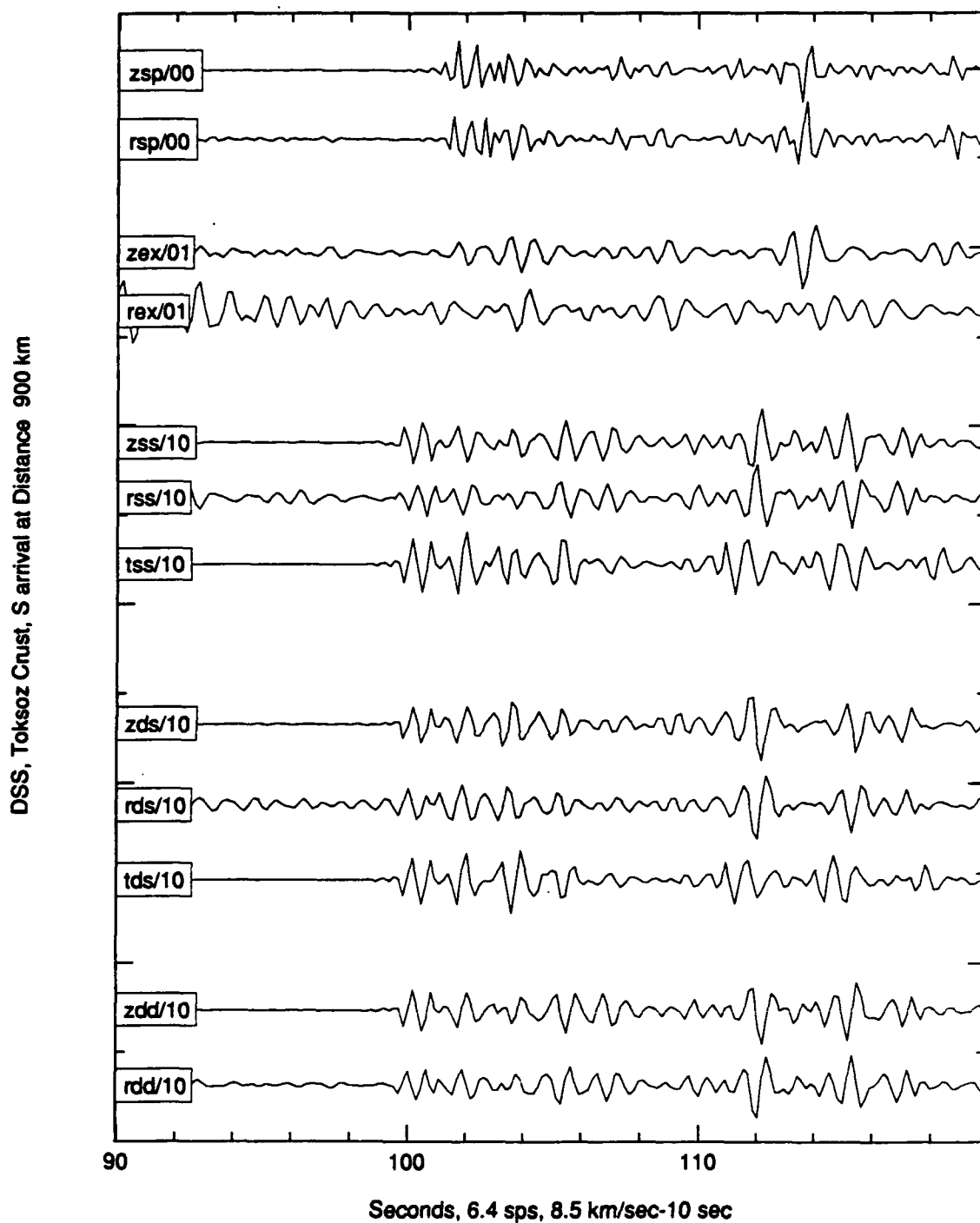


Figure 17. The 1-Hz highpass filtered, amplitude equalized, velocity 3-component synthetics for a spall source at 0 km, an explosion at 1 km depth, and three earthquake Green's function sources at 10 km from Figure 14, centered on the arrival of the *S* phase. The *S* arrival is more impulsive for the spall and earthquake sources than for the explosion sources, and more impulsive for the vertical (transverse with respect to the source) than for the actual radial.

With respect to the vertical/radial difference, referring back to Figure 15 we see that this is due in part to the fact that the vertical component signal amplitude is larger than the radial, and in part to the fact that the pre-arrival signal generated noise is larger on the radial component.

We might expect that the difference in onsets between earthquakes and explosions would be seen in observations and perhaps even serve as a discriminant. However, the fact that the observations discussed earlier did not exhibit this difference suggests that the quarry blasts may have had substantial proportions of spall in their signal thus contributing to a sharper onset than would be expected from an explosion, resulting in the quarry blast signal onsets being more like those from the earthquakes. We might expect signals from a simple explosion to be more emergent than any of the data seen in this study. Thus this remains a topic for further study. A useful experiment would be to detonate a well-buried explosion at a quarry, or a spall-generating conventional explosion near the site of well-confined nuclear test.

To aid in the identification of the different pulses in the P -signal, Figures 18a, 18b, 18c, and 18d show the P phase as a function of depth for the vertical strike-slip (SS), vertical dip-slip (DS), 45° dip-slip (DD), and explosion, respectively. Of course we do not expect to see explosion sources at great depths; the waveforms are presented only to illustrate the fact that the large phase which contributes to the earthquake signal complexity does, in fact, originate from S waves emitted by the source.

One of the most interesting features of these waveforms is the absence of a clearly defined pP phase for the deeper events, even for the explosion source. However, the sP phase, as mentioned previously, is quite prominent for all three earthquake sources and exhibits the expected moveout as depth is increased. However, especially for the DS source, the weakness of the sP phase at 40 and 50 km depth would very likely place these earthquake signals, if seen in isolation in the undecided category. It would be hoped that events this deep could be properly classified by standard depth location means.

In Figures 19a, 19b, and 19c we see that the L_g to P discriminant should remain reliable in Scandinavia for depths from 1 to 30 km since over this range the L_g amplitude is not appreciably reduced. For events at or below the Moho, 40 or 50 km respectively, the L_g amplitude is greatly reduced, as expected from ray trapping considerations; however the earlier S arrivals are still quite large and could serve as a discriminant. The Rayleigh wave amplitude is also seen to decrease more rapidly with depth than the L_g , suggesting that if there were no propagation problems that L_g to P would be more reliable for events of ambiguous depth than would be $M_s:m_b$.

An exception to the overall favorable picture of excellent L_g to P discrimination is found for shallow depths for the vertical dip-slip (DS) source as seen in Figure 19b. At 1 km we see that the earthquake source gives L_g values smaller than that of the explosion. However, in Figure 19d we see that the transverse component for the earthquake is very large. Thus, if scattering converts the transverse energy into the vertical component, or if the discriminant is carried out using a weighting over all components, then the L_g to P discriminant should work well.

Figures 20a, 20b, and 20c show the waveforms of Figures 19a, 19b, and 19c high-pass filtered at 1 Hz. In general this presentation can be used to see more clearly how the signals would appear

on a short-period system. One feature of interest which could not be seen in Figures 19a, 19b, and 19c is how the short period R_g , just barely visible at 900 km due to the attenuation by the low Q in the upper crust, can be seen to decrease in amplitude as the source depth increases.

EX & EQ(SS) Synthetics, Vertical Component, BB

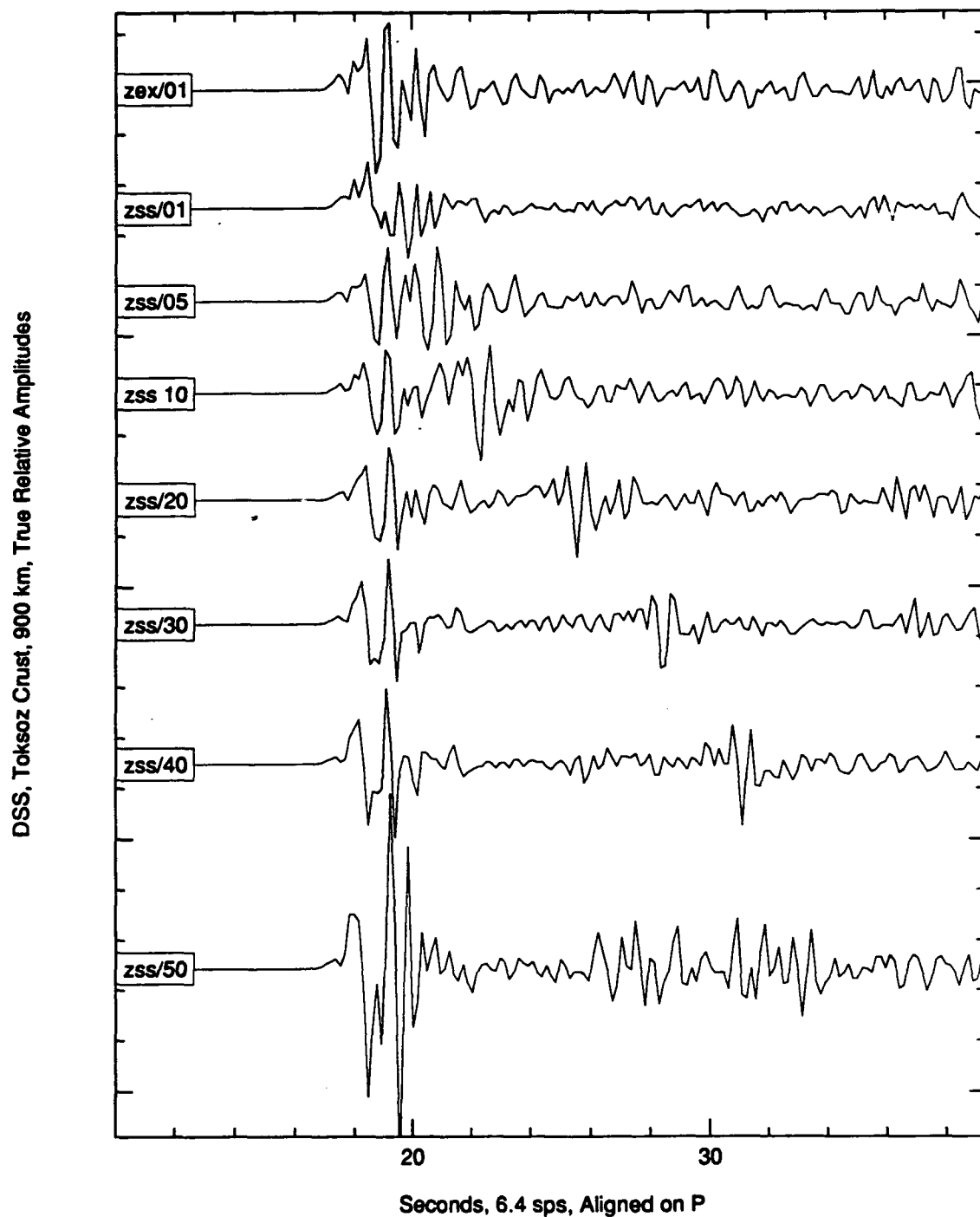


Figure 18a. Broadband velocity vertical component P synthetics for an explosion source at 1 km depth, and the vertical strike-slip (SS) Green's source at 1, 5, 10, 20, 30, 40, and 50 km depth. The moveout of the sP phase for the earthquake source is apparent, as is the weakness of pP .

EX & EQ(DS) Synthetics, Vertical Component, BB

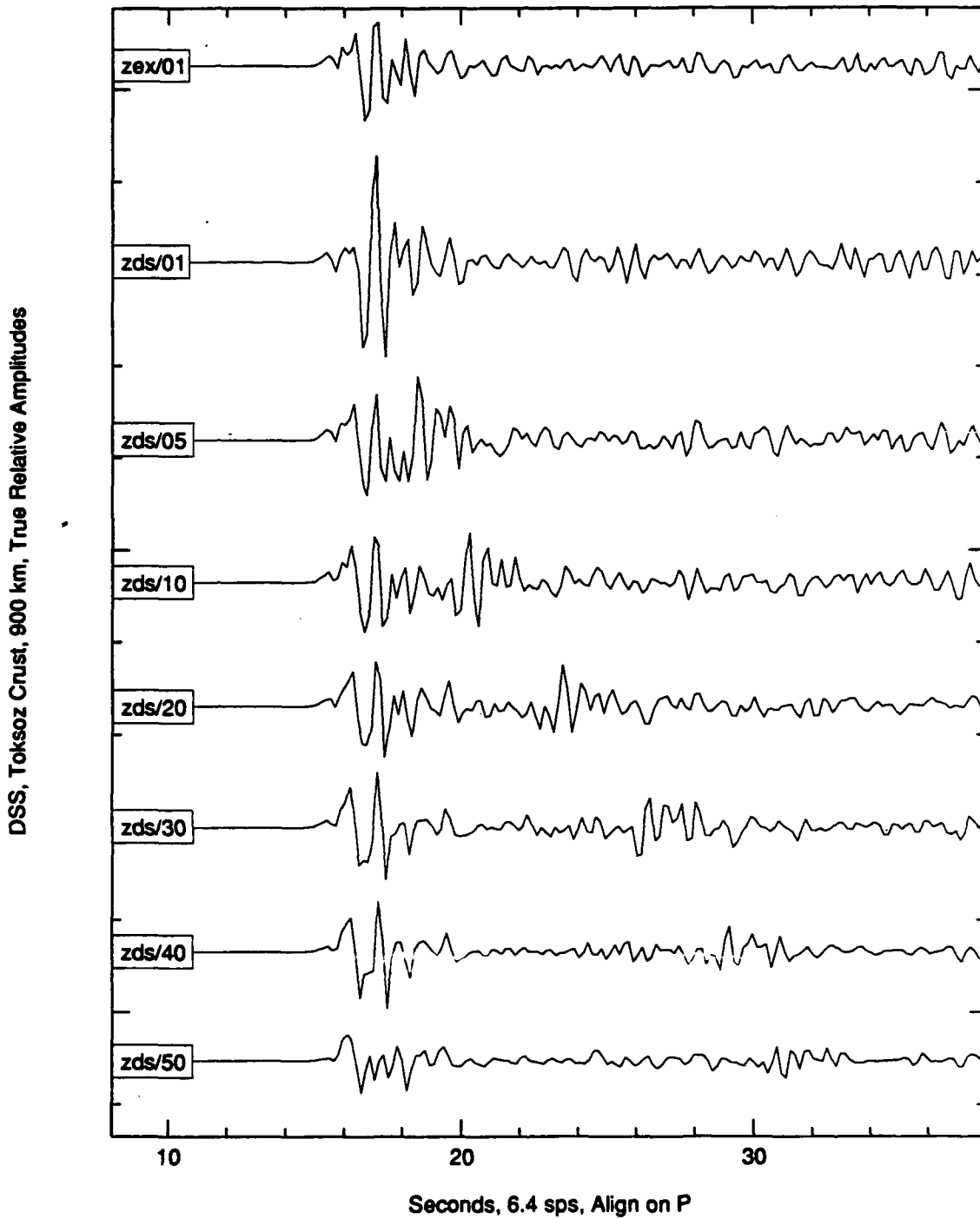


Figure 18b. Broadband velocity vertical component P synthetics for an explosion source at 1 km depth, and the vertical dip-slip (DS) Green's source at 1, 5, 10, 20, 30, 40, and 50 km depth. The moveout of the sP phase for the earthquake source is apparent, as is the weakness of pP .

EX & EQ(DD) Synthetics, Vertical Component, BB

DSS, Toksoz Crust, 900 km, True Relative Amplitudes

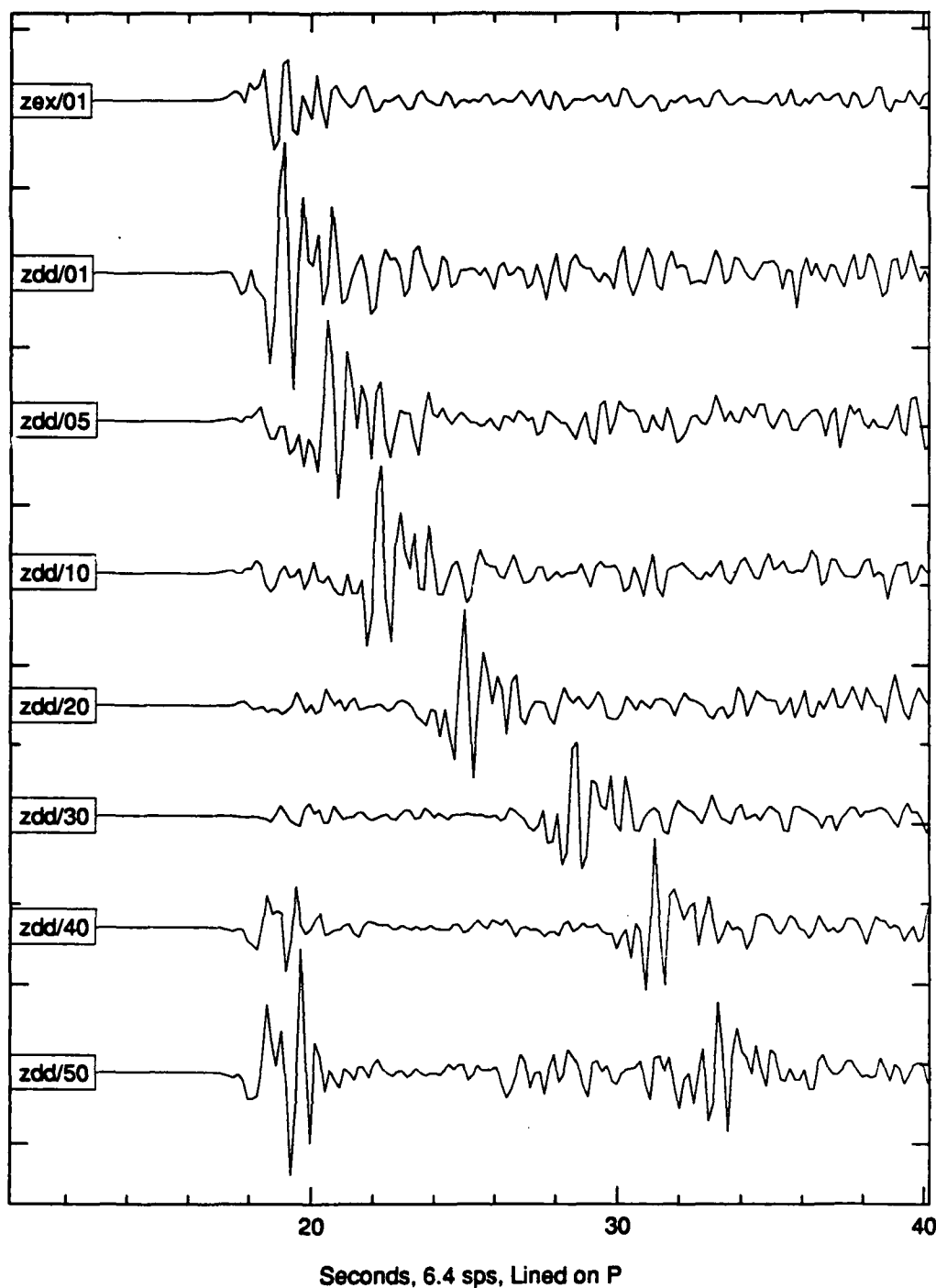


Figure 18c. Broadband velocity vertical component P synthetics for an explosion source at 1 km depth, and the 45° dip-slip (DD) Green's source at 1, 5, 10, 20, 30, 40, and 50 km depth. The moveout of the sP phase for the earthquake source is apparent, as is the weakness of pP .

Explosion Synthetics Vertical BB versus Depth

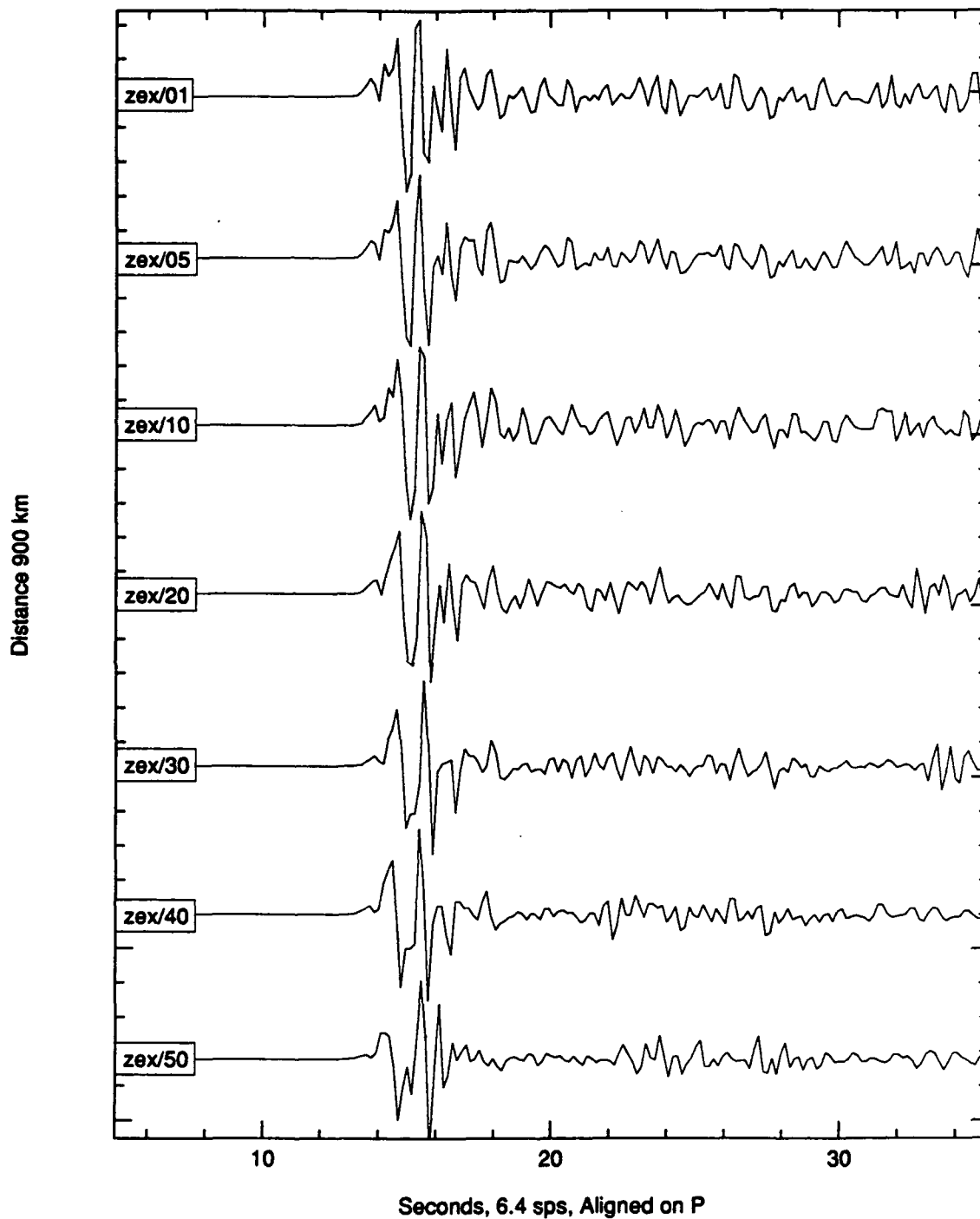


Figure 18d. Broadband velocity vertical component P synthetics for an explosion source at 1, 5, 10, 20, 30, 40, and 50 km depth. The weakness of sP and pP is apparent.

EX & EQ(SS) Synthetics, Vertical Component, BB

DSS, Toksoz Crust, 900 km, True Relative Amplitudes

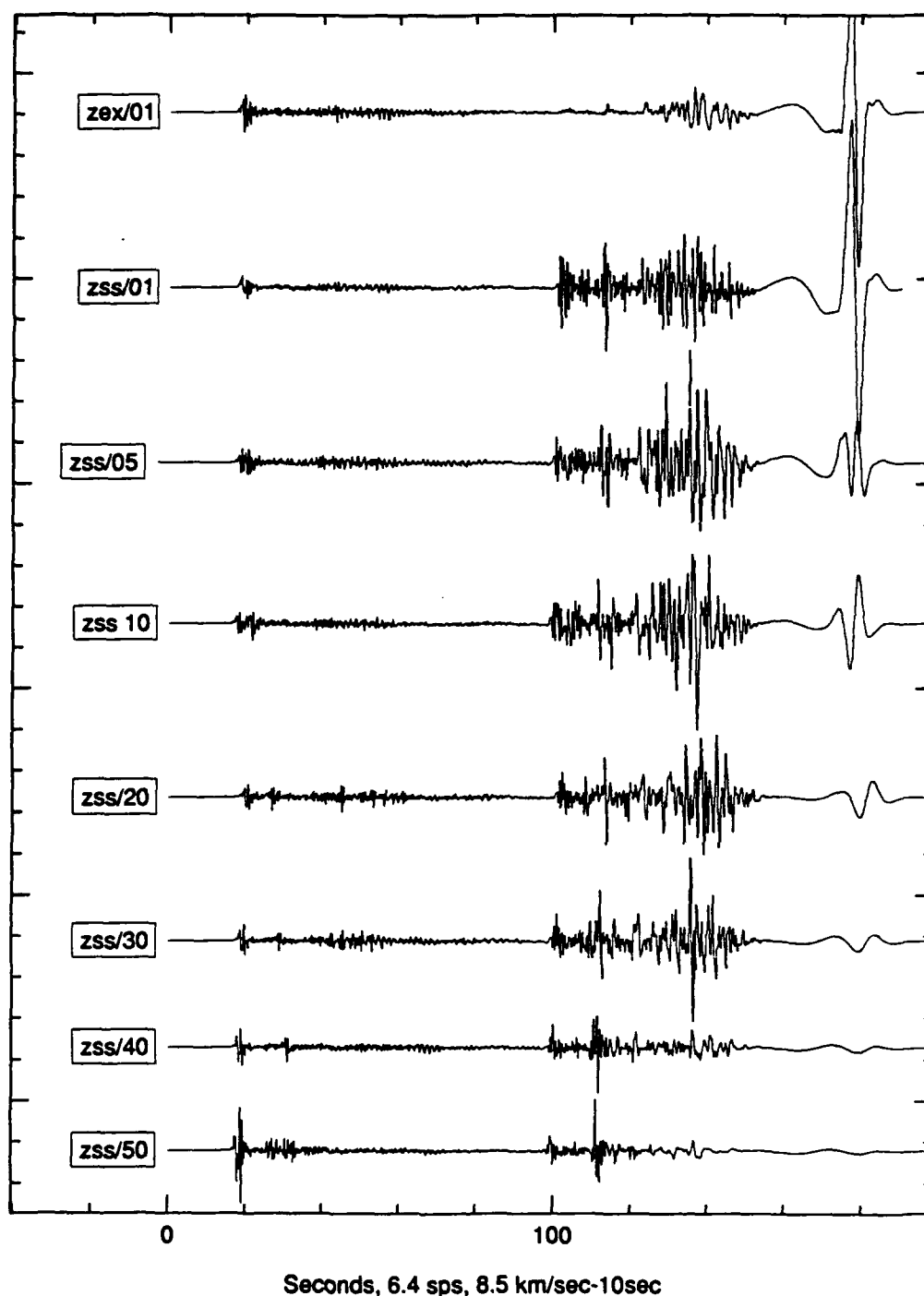


Figure 19a. Broadband velocity vertical component synthetics for an explosion source at 1 km depth, and the vertical strike-slip (SS) Green's source at 1, 5, 10, 20, 30, 40, and 50 km depth. The decrease of the Rayleigh amplitude with depth is apparent. The *Lg* amplitudes for the earthquake do not significantly decrease until the Moho is reached at 40 km. Even there the *S* wave amplitudes remain large.

EX & EQ(DS) Synthetics, Vertical Component, BB

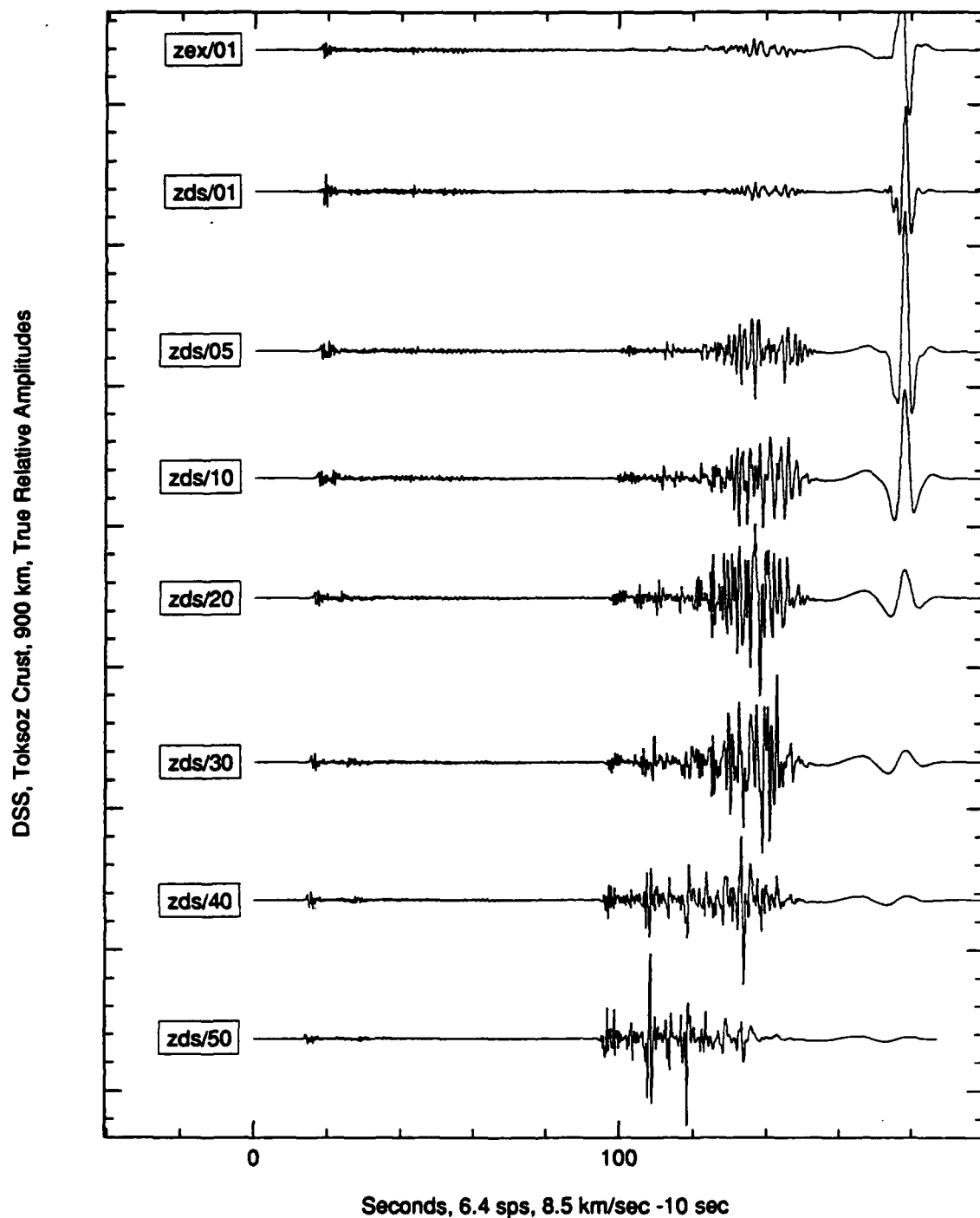


Figure 19b. Broadband velocity vertical component synthetics for an explosion source at 1 km depth, and the vertical dip-slip (DS) Green's source at 1, 5, 10, 20, 30, 40, and 50 km depth. The L_g amplitude at 1 km is low enough that the L_g to P discriminant would not work, but then increases and subsequently does not decrease until the source below the Moho is reached at 50 km. Even there the S wave amplitudes remain large and the L_g to P discriminant would likely work well.

EX & EQ(DD) Synthetics, Vertical Component, BB

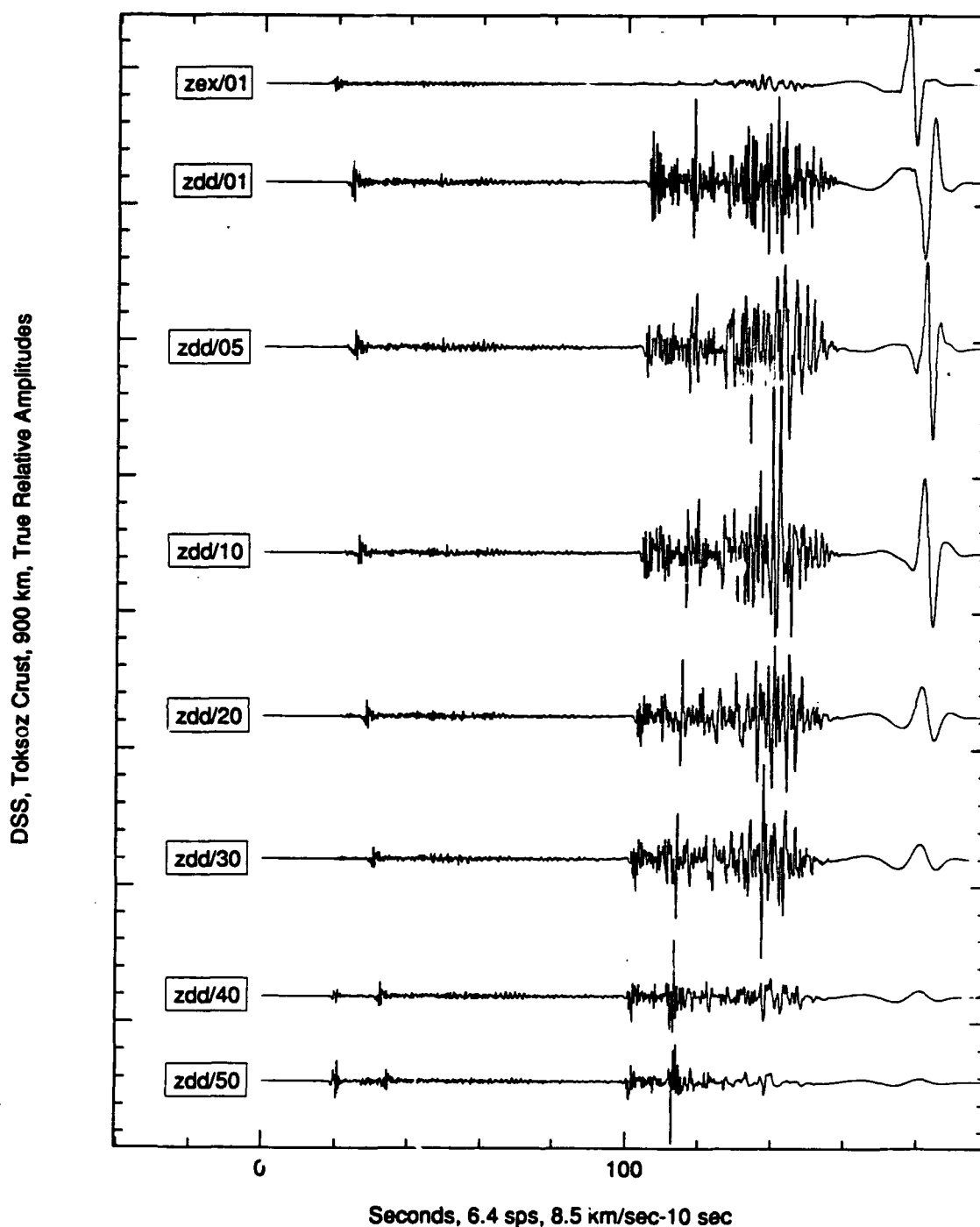


Figure 19c. Broadband velocity vertical component synthetics for an explosion source at 1 km depth, and the 45° dip-slip (DS) Green's source at 1, 5, 10, 20, 30, 40, and 50 km depth. The decrease of the Rayleigh amplitude with depth is apparent. The L_g amplitudes for the earthquake do not significantly decrease until the Moho is reached at 50 km. Even there the S wave amplitudes remain large.

Explosion and DS Synthetics, BB

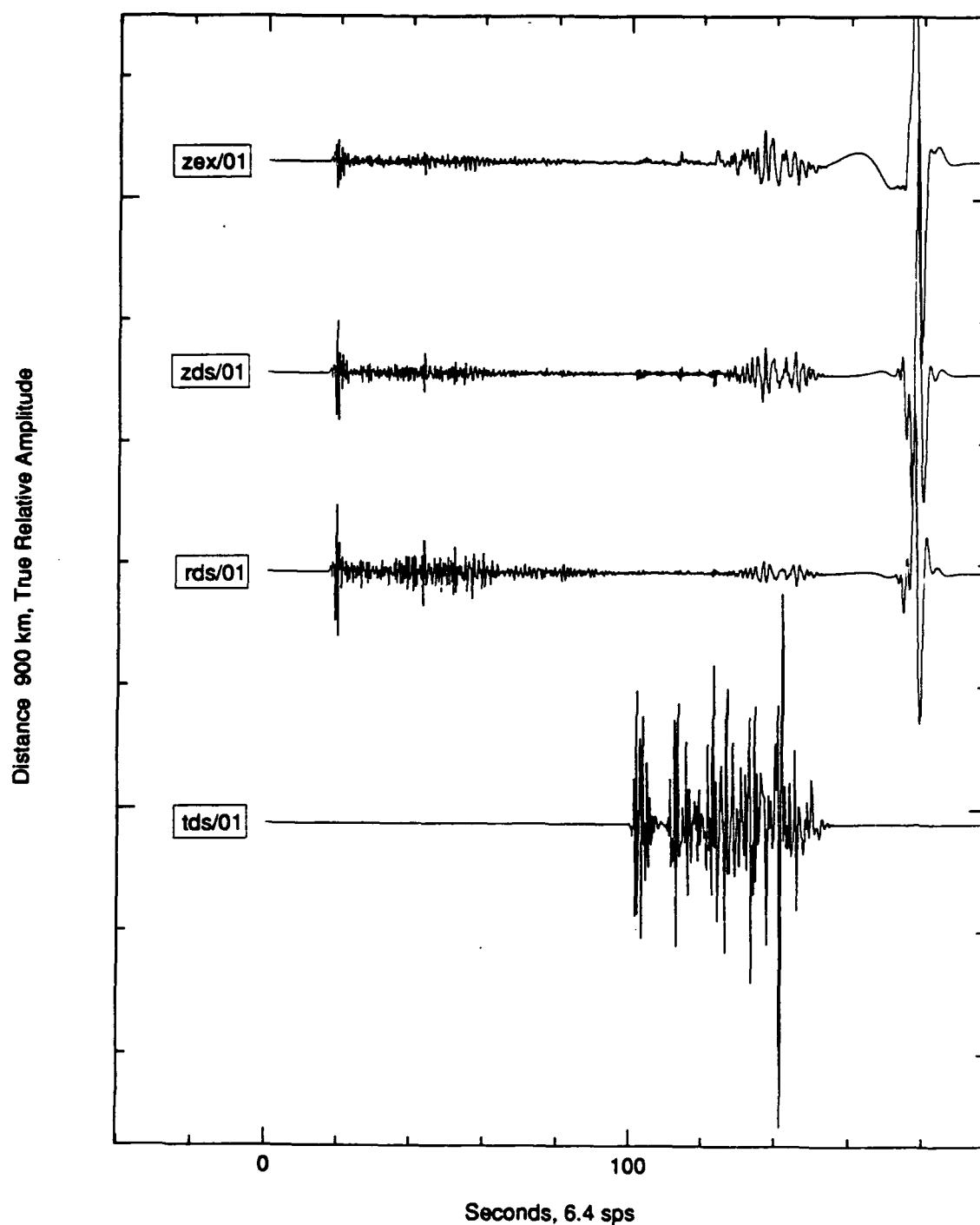


Figure 19d. Broadband velocity vertical component for an explosion source at 1 km and 3 components for the vertical dip-slip (DS) Green's source function at 1 km. While the L_g to P discriminant would not work well for the vertical components only, it is apparent that if the discriminant were applied using some average over all three components; or if the transverse component were scattered into the vertical component, then the discriminant would work.

EX & EQ(SS) Synthetics, Vertical Component, 1 Hz HP

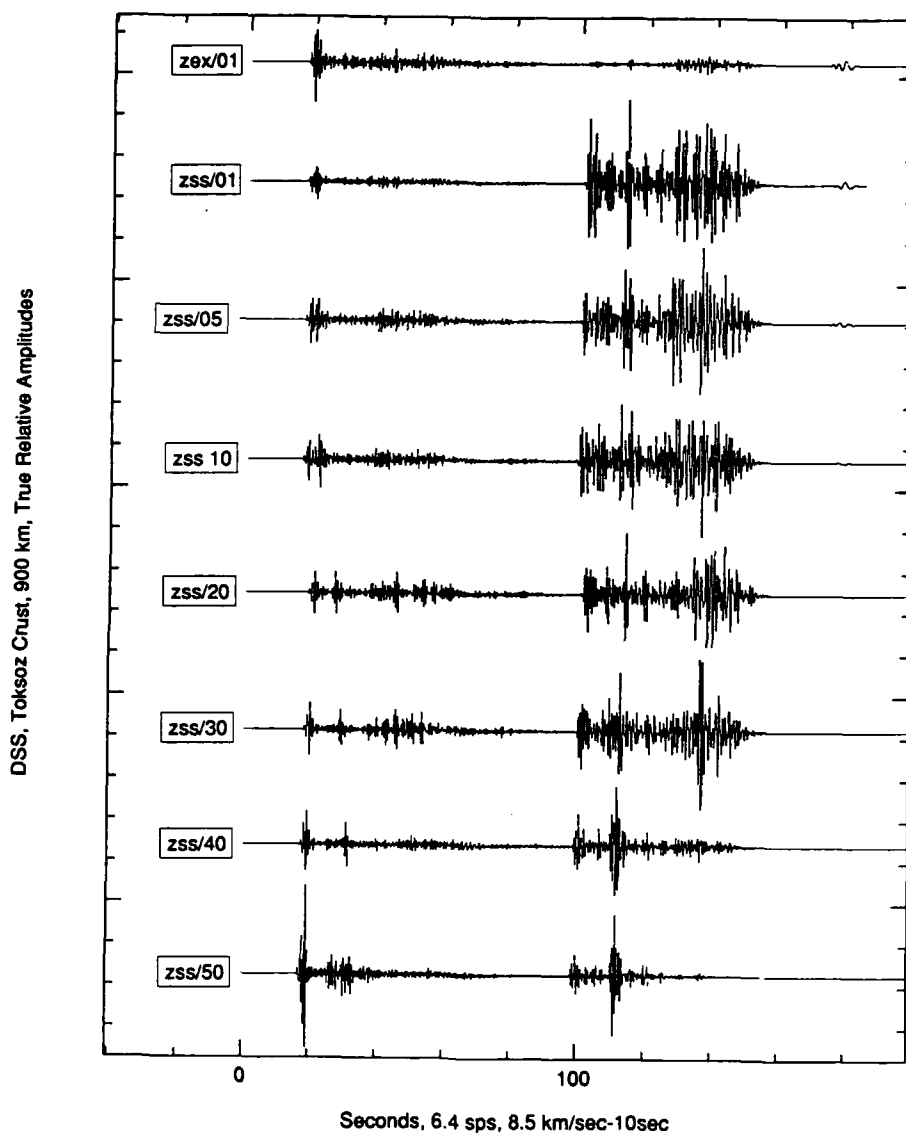


Figure 20a. 1 Hz highpass velocity vertical component synthetics for an explosion source at 1 km depth, and the vertical strike-slip (SS) Green's source at 1, 5, 10, 20, 30, 40, and 50 km depth. The L_g amplitudes for the earthquake do not significantly decrease until the Moho is reached at 40 km. Even there the S wave amplitudes remain large and a suitably defined discriminant would work.

EX & EQ(DS) Synthetics, Vertical Component, 1Hz HP

DSS, Toksoz Crust, 900 km, True Relative Amplitudes

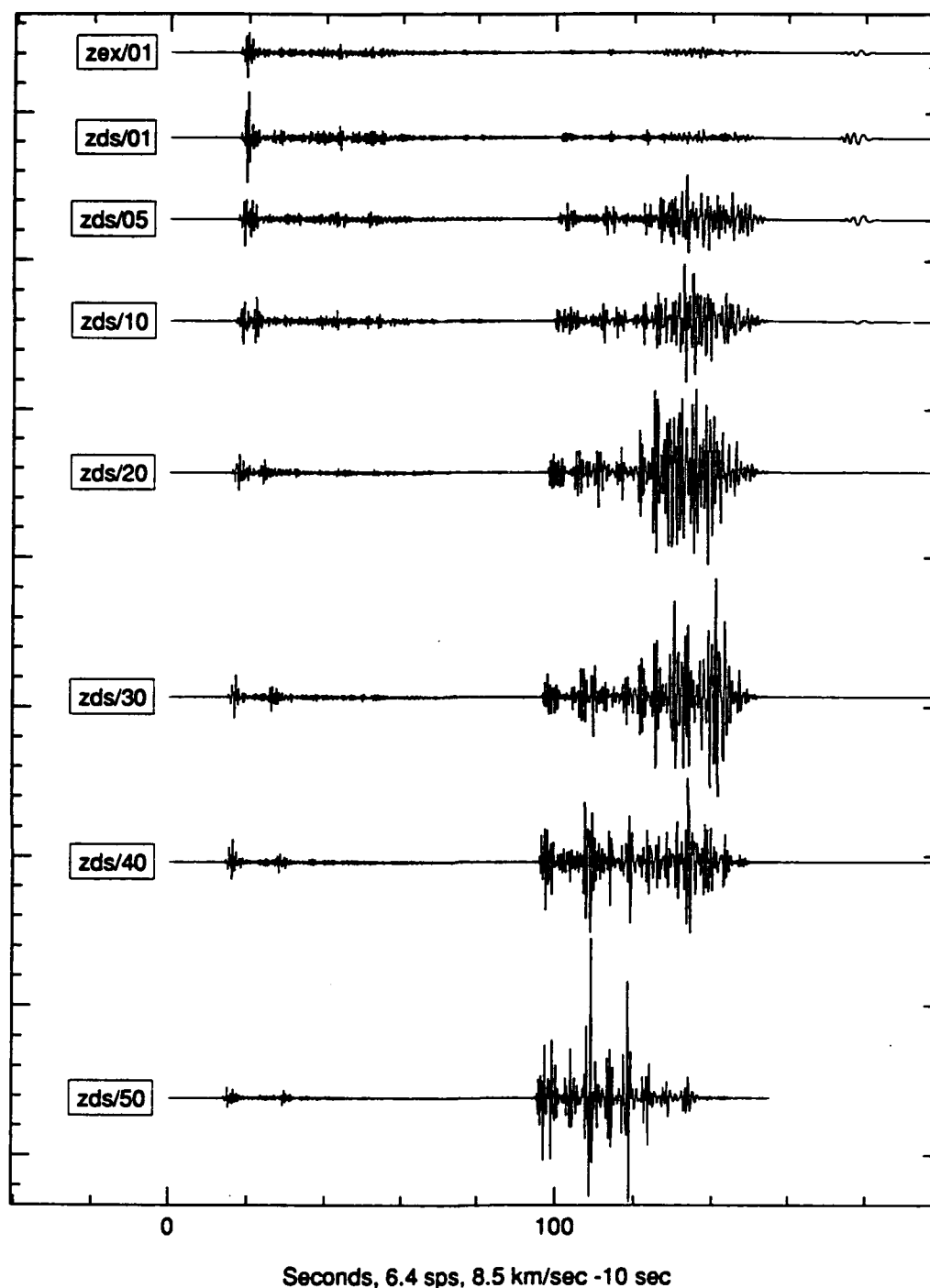


Figure 20b. 1 Hz highpass velocity vertical component synthetics for an explosion source at 1 km depth, and the vertical dip-slip (DS) Green's source at 1, 5, 10, 20, 30, 40, and 50 km depth. The L_g amplitude at 1 km is low enough that the L_g to P discriminant would not work, but then increases and subsequently does not decrease until the source below the Moho is reached at 40 km. Even there the S wave amplitudes remain large and a suitably defined discriminant would work.

EX & EQ(DD) Synthetics, Vertical Component, 1Hz HP

DSS, Toksoz Crust, 900 km, True Relative Amplitudes

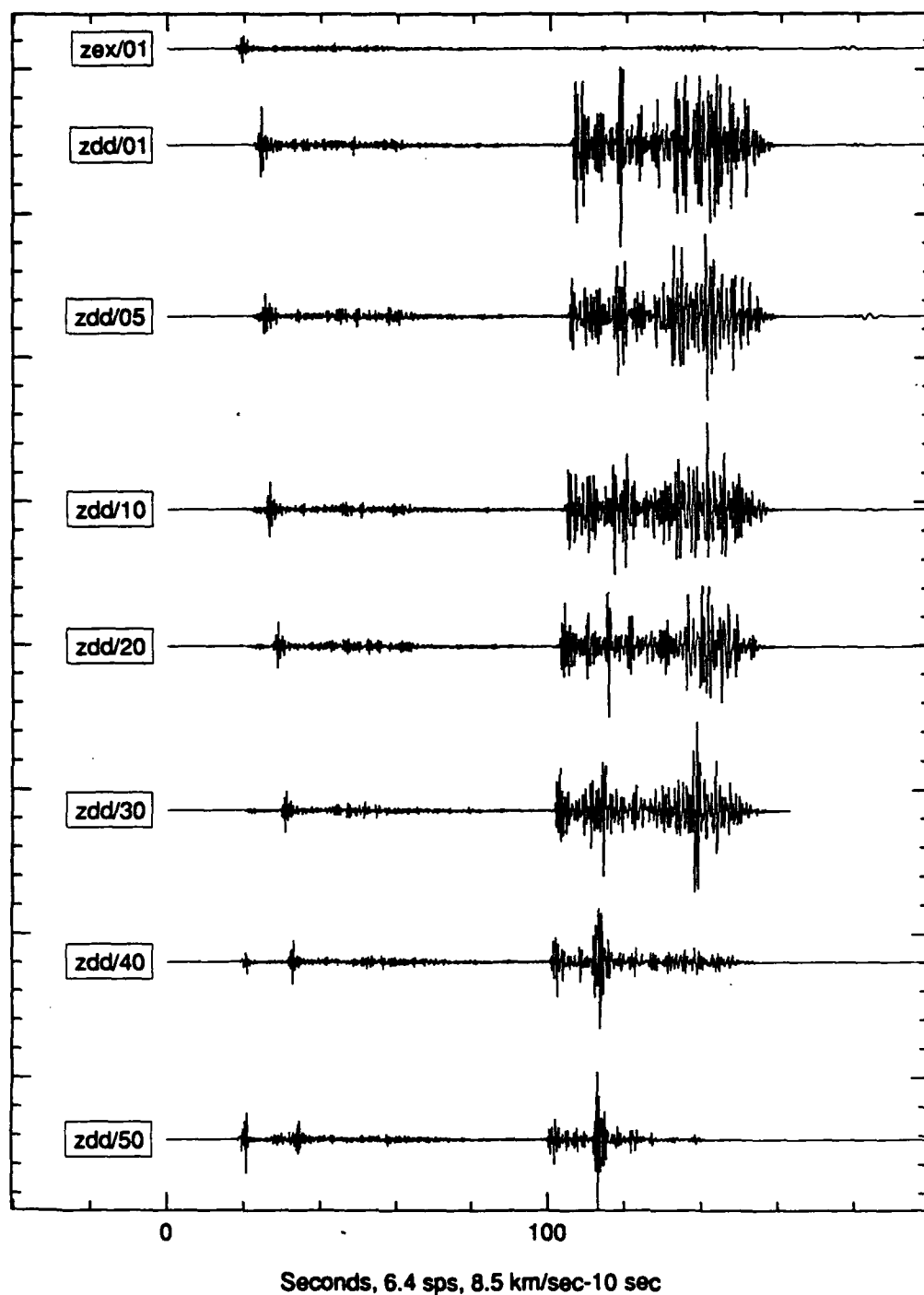


Figure 20c. 1 Hz highpass velocity vertical component synthetics for an explosion source at 1 km depth, and the 45° dip-slip (DD) Green's source at 1, 5, 10, 20, 30, 40, and 50 km depth. The L_g amplitudes for the earthquake do not significantly decrease until the Moho is reached at 40 km. Even there the S wave amplitudes remain large and a suitably defined discriminant would work.

Conclusions

The study has shown, both by the examination of actual regional data and by calculation of regional synthetics, that many earthquakes in Scandinavia will have at least one P wave signal in a network of observations which is more emergent than any from an explosion.

To make use of this insight in order to develop a routine practical discriminant, a number of additional steps must be taken. To guard against an explosion being discriminated as an earthquake because a later P triplication or reflection creates an emergent signal in certain distance intervals, (see e.g., Figure 12), quarry blasts and other known explosions should be used to detect these phenomena and synthetics should be constructed to model them so that they may be anticipated from new locations. When these phenomena are understood the windows which define complexity can be properly designed. In such research, and in application, strong constraints on S/N must be maintained to ensure that explosion signals are not determined to be complex when all that is occurring is that the low-amplitude coda of the signal is being enhanced in amplitude by the noise, or that earthquakes are determined to be impulsive because the P_n onset has been missed.

Applications to smaller events than those treated in this study can be carried out using P wave beams from arrays. Discrimination using P array beams as contrasted to analyses using single instruments must also be emphasized because this should result in simpler signals for those arrivals which are truly simple since beamforming will minimize the energy scattered near the receiver which leads to more complex signals. For this application, research and development should be carried out on linear maximum-likelihood frequency-wavenumber techniques in order to minimize such signal generated noise to a greater degree than can be achieved by simple beamforming.

Since the principal obstacle to successful implementation of a complexity discriminant is the degree to which explosion signals may be emergent, a careful study should be made of regional P -wave array beams from explosions to discover the degree to which they may be emergent. Studies of single elements may also be useful but may incorrectly reach a more pessimistic conclusion with respect to the applicability of the complexity discriminant than would studies using array beams.

Since the actual observed signals typically peak at 5 Hz and are, of course, in a real earth which is more complex than the Ryaboy-Toksoz model used in this study, theoretical modeling should be extended to higher frequencies and more complex models. This can be done for P waves, the appropriate phase, by using the wavenumber integration techniques used in this study and making use of wavenumber filtering. To the extent that the appropriate ray paths can be specified, Gaussian beam techniques may be used in complex media which are not horizontally uniform.

In addition, it seems very likely that a true duplication of the emergent character of earthquakes cannot be achieved without fully 2D, or perhaps even 3D, calculations. These would likely consist of double couple sources in a 2D or 3D medium with calculations performed by finite difference.

It is important to recognize that any research on complexity discrimination statistics cannot be based on the hypothesis of two populations with equal covariance matrices but different means. The assumed covariance matrices should not even be simple multiples of one another. It is clear on theoretical grounds that the earthquake signal population can have members which appear just as simple as explosions. It is only the upper tail of high-complexity earthquakes which can be discriminated. Thus the very concept of two populations which can be optimally separated in hyperspace is inappropriate. Explosions and simple earthquakes will have to be placed in an undecided category unless more careful visual examination of a sample of simple earthquake signals reveals details of the signals which can be characterized as complexity and which are different from explosion signals. However, since in practice there are many more earthquakes than explosions to discriminate, assuming thresholds of M_L 2.5 and on-site inspection of quarries which detonate such large blasts, such a discriminant will be very useful in practice.

It is also important to recognize that application of complexity on a network basis can, in theory, give results superior to that available from a single station. The explosion signal should be similarly simple at every station of the network, while an earthquake may be simple at most stations but a single complex signal identifies it. A suitably subtle statistical discrimination procedure will recognize this fact from the beginning; it will not be satisfactory to average complexity over the network, just as it is not satisfactory to average first-motions. In principle, a single good S/N negative first motion will identify an event as an earthquake despite many other positive first motions.

The study has also confirmed the results of earlier workers showing that in theory the L_g to P amplitude discriminant should work well. The fact that it does not, in practice, appear to work as well as theoretically predicted has also been shown, following the lead of earlier workers, to possibly be due to the fact that spall from quarry blast events enhances the explosion L_g , making quarry blasts look more like earthquakes. Thus one would expect the L_g to P ratio discriminant to work better for well contained explosions, such as decoupled explosions, than for quarry blasts. In this sense, also, complexity can be seen to be to some degree independent of, and thus complementary to, the L_g to P discriminant since in theory explosion and spall sources have equal complexity.

We have also seen, Figures 19b and 19d, that a shallow (1 km) vertical dip-slip earthquake could be incorrectly classified as an explosion using the L_g to P discriminant on the vertical component only. It is also clear from Figure 18b that such an event at 1 km depth cannot be discriminated using complexity. However, it appears that the transverse L_g component from such an event is very large so that if the L_g amplitude is defined as an average over all components, or over the vertical and transverse components, or if scattering converts the transverse component into the vertical, that the L_g to P discriminant may work in this case where the complexity discriminant cannot. Of course the usual caveats with respect to the L_g to P discriminant must be observed: one must ensure that a missing L_g is not due to blockage.

This study has suggested that, in building a discrimination database, earthquakes in the ocean should be carefully treated since reverberation in the water layer may make them appear more complex, or possibly simpler, than earthquakes on land; thus unduly complicating the problem of discriminating those earthquakes on land which are the true problem of interest.

The analysis has also shown that explosions, but not spall, are expected to have a lower frequency L_g than most earthquakes. Thus, again, the L_g spectral discriminant is expected to work better for contained explosions which have very little spall than for quarry blasts which may have a large amount of spall. It is interesting that this result confirms conclusions reached by earlier researchers but is not due to non-linear effects of spall but rather to linear considerations which result in the L_g from an explosion source being lower frequency than that from a deeper earthquake source even when they have the same source-time function.

There have been suggestions in the study that observations would show that shear arrival times can be better estimated on the vertical or transverse component than on the radial, and that well-contained explosions would show more emergent S arrivals than would earthquakes or other explosions with significant spall such as quarry blasts or other shallowly buried explosions. However, further observational studies are needed on these points.

REFERENCES

- Barker, B.W. and J. Murphy (1992). A lithospheric velocity anomaly beneath the Shagan River test site. Part 1. Detection and location with network magnitude residuals, *Bull. Seism. Soc. Am.*, **82**, 980-998.
- Barker, J. S. (1991). Analysis of regional bodywave phases from earthquakes and explosions in Eastern Asia, in *Papers Presented at 13th Annual PL/DARPA Seismic Research Symposium*, Phillips Laboratory, 64-70.
- Barley, B.J. (1977). The origin of complexity in some P seismograms from deep earthquakes, *Geophys. J. Roy. astr. Soc.*, **33**, 195-221.
- Bennett, J. and J. Murphy (1986). Analysis of seismic discrimination capabilities using regional data from western United States events, *Bull. Seism. Soc. Am.*, **76**, 1069-1086.
- Bennett, J., B. Barker, K. McLaughlin, and J. Murphy (1989). Regional discrimination of quarry blasts, earthquakes, and underground nuclear explosions, SSS-TR-89-10835, GL-TR-89-0114, ADA223148.
- Bennett, J., A. Campanella, J. Murphy, and J. Scheimer (1990). Regional discrimination research and methodology implementation: analyses of CDSN and Soviet IRIS data, SSS-TR-90-11757, GL-TR-90-0194, ADA230251.
- Bennett, J., A. Campanella, J. Scheimer and J. Murphy (1992). Demonstration of regional discrimination of Eurasian seismic events using observations at Soviet IRIS and CDSN stations, SSS-FR-92-13150, PL-TR-92-2090.
- Blandford, R. (1977). Discrimination between earthquakes and underground explosions, in *Annual Reviews of Earth and Planetary Sciences*, Annual Reviews Inc., 111-122.
- Blandford, R. (1981). Seismic discrimination problems at regional distances, in *Identification of Seismic Sources - Earthquake or Underground Explosion*, E. S. Husebye and S. Mykkeltveit (Editors), D. Reidel Publishing Company, 695-740.
- Blandford, R., R. Hartenberger, and R. Naylor (1981). Regional amplitude-distance relations, discrimination and detection (VSC-TR-81-15), Teledyne Geotech, Alexandria VA, ADA105722.
- Blandford, R. (1985). Regional detection, location, discrimination and yield determination, in *The Vela Program*, Ann Kerr (Editor), Executive Graphic Services 85-080931, 787-816.
- Bouchon, M. (1981). A simple method to calculate Green's functions for elastic layered media, *Bull. Seism. Soc. Am.*, **71**, 959-971.
- Bouchon, M. (1982). The complete synthesis of seismic crustal phases at regional distances, *J. Geophys. Res.*, **87**, 1735-1741.

Campillo, M., M. Bouchon and B. Massinon (1984). Theoretical study of the excitation, spectral characteristics, and geometrical attenuation of regional seismic phases, *Bull. Seism. Soc. Am.*, **74**, 79-90.

Campillo, M., J. Plantet, and M. Bouchon (1985). Frequency-dependent attenuation in the crust beneath Central France from *Lg* waves: Data analysis and numerical modeling, *Bull. Seism. Soc. Am.*, **75**, 1395-1411.

Carpenter, E.W. (1963). Explosion seismology, *Science*, **147**, 363-373.

Chan, W.W., R. Baumstark and R.K. Cessaro (1990). Spectral discrimination between explosions and earthquakes in Central Eurasia, *GL-TR-90-0217*, Teledyne Geotech.

Chapman, C.H. and J.A. Orcutt (1985). The computation of body wave synthetic seismograms in laterally homogeneous media, *Reviews of Geophysics*, **23**, 105-163.

Cullen, E.A. and A. Douglas (1975). P-wave seismograms from three seismic sources in SW USSR, *Geophys. J. Roy. astr. Soc.*, **41**, 11-28.

Day, S.M., N. Rimer and J. T. Cherry (1983). Surface waves from underground explosions with spall analysis of elastic and nonlinear source models, *Bull. Seism. Soc. Am.* **73**, 247-264.

Day, S. M. and K. L. McLaughlin (1991). Seismic source representations for spall, *Bull. Seism. Soc. Am.*, **81**, 191-201.

Douglas, A. (1967). P-signal complexity and source radiation patterns, in *VESIAC Report 7885-1-X*. University of Michigan.

Douglas, A., P.D. Marshall and D.J. Corbishly (1971). Absorption and the complexity of P signals, *Nature*, **233**, 50-51.

Douglas, A., P.D. Marshall, P.G. Gibbs, J.B. Young and C. Blamey (1973). P signal complexity re-examined, *Geophys. J. R. astr. Soc.*, **33**, 195-221.

Douglas, A., J.B. Young and J.A. Hudson (1974). Complex P-wave seismograms from simple earthquake sources, *Geophys. J. R. astr. Soc.*, **37**, 141-150.

Douglas, A. (1981). Seismic source identification: a review of past and present research efforts, in *Identification of Seismic Sources - Earthquake or Underground Explosion*, E. S. Husebye and S. Mykkeltveit (Editors), D. Reidel Publishing Company, 1-48.

Douglas, A., J.A. Hudson and B.J. Barley (1981). Complexity of short period seismograms: what does scattering contribute?, *AWRE Report No. O 3/81*, H. M. Stationery Office.

Douglas, A., L. Richardson and M. Hutchins (1990). Surface reflections and S-to-P conversions on P seismograms, *Geophys. J. Int.*, **100**, 303-314.

- Douglas, A., A.F. Sheehan and R.C. Stewart (1992). Northern Chile earthquake of 26 May 1980: evidence of unilateral fracture, *Geophys. J. Int.*, **110**, 201-210.
- Dysart, P. and J.J. Pulli (1990). Regional seismic event classification at the NORESS array: seismological measurements and the use of trained neural networks, *Bull. Seism. Soc. Am.*, **80**, 1910-1933.
- Fisk, M.D., and G.D. McCartor (1991). The phase screen method for vector elastic waves, *J. Geophys. Res.*, **96**, 5985-6010.
- Fisk, M.D., E. Charrette and G.D. McCartor (1992). A comparison of phase screen and finite difference calculations for elastic waves in random media, *J. Geophys. Res.*, **97**, 12409-12423.
- Greenfield, R. J. (1971). Short period P-wave generation by Rayleigh wave scattering at Novaya Zemlya, *J. Geophys. Res.*, **76**, 7988-8002.
- Gupta, I.N. and J. A. Burnetti (1981). An investigation of discriminants for events in western USSR based on regional phases recorded at station Kabul, *Bull. Seism. Soc. Am.*, **71**, 263-274.
- Gupta, I.N. and R.R. Blandford (1983). A mechanism for generation of short period transverse motion from explosions, *BSSA*, **73**, 571-592.
- Gupta, I.N., C.S. Lynnes, T.W. McElfresh, and R.A. Wagner (1990). F-K analysis of NORESS array and single station data to identify sources of near-receiver and near-source scattering, *Bull. Seism. Soc. Am.*, **80**, 2227-2241.
- Gupta, I.N. and R.A. Wagner (1992). Evidence for *Rg*-to-*P* scattering in teleseismic *P* coda of East Kazakh explosions, *Bull. Seism. Soc. Am.*, **82**, 2139-2152.
- Herrmann, R.B. and C.Y. Wang (1985). A comparison of synthetic seismograms, *Bull. Seism. Soc. Am.*, **75**, 41-56.
- Herrmann, R.B. and B. Mandal (1986). A study of wavenumber integration techniques, *Earthquake Notes*, **57**, 33-40.
- Kelly, E.J. (1968). A study of two short period discriminants, *Technical Note 1968-8*, Massachusetts Institute of Technology, Lincoln Laboratory.
- Key, F.A. (1968). Some observations and analyses of signal generated noise, *Geophys. J. R. astr. Soc.*, **15**, 377-392.
- Lynnes, C., and R. Baumstark (1991). Phase and spectral ratio discrimination in North America, *PL-TR-91-2212(II)*, Teledyne Geotech.
- Marshall, P.D. (1972). Some seismic results from a world wide sample of large underground explosions, *AWRE Report No. O 49/72*, H. M. Stationery Office.
- McLaughlin, K.L., D.W. Rivers and M.A. Brennan (1983). Pearce focal sphere analysis of explosion and earthquake mechanisms, *TGAL-TR-83-4*, Teledyne Geotech.

- McLaughlin, K.L. (1985). Evaluation of small events using the Pearce focal plane algorithm, *TGAL-85-11a*, Teledyne Geotech.
- McLaughlin, K.L., and L.M. Anderson (1987). Stochastic dispersion of short-period P-waves due to scattering and multipathing, *Geophys. J. R. astr. Soc.*, **89**, 933-963.
- McLaughlin, K. L., T. G. Barker, S. M. Day, B. Shkoller, and J. L. Stevens (1988). Effects of depth of burial on explosion and earthquake regional seismograms: regional discrimination and yield estimation, *SSS-R-88-9844*, S-Cubed.
- McLaughlin, K. L., J. Murphy, and B.W. Barker (1992). A lithospheric velocity anomaly beneath the Shagan River test site. Part 2. Imaging and inversion with amplitude transmission tomography, *Bull. Seism. Soc. Am.*, **82**, 999-1017.
- Murphy, J.R. and T.J. Bennett (1982). A discrimination analysis of short-period regional seismic data recorded at Tonto Forest Observatory, *Bull. Seism. Soc. Am.*, **72**, 1351-1366.
- Pearce, R.G. (1977). Fault plane solutions using relative amplitudes of P and pP, *Geophys. J. Roy. astr. Soc.*, **50**, 381-394.
- Pearce, R.G. (1980). Fault plane solutions using relative amplitudes of P and surface reflections: further studies, *Geophys. J. R. astr. Soc.*, **60**, 459-487.
- Pearce, R.G. (1981). Complex P waveforms from a Gulf of Aden earthquake, *Geophys. J. R. astr. Soc.*, **64**, 187-200.
- Pearce, R.G., J.A. Hudson and A. Douglas (1988). On the use of P-wave seismograms to identify a double-couple source, *Bull. Seism. Soc. Am.*, **78**, 651-671.
- Pooley, C.I., A. Douglas and R.G. Pearce (1983). The seismic disturbance of 20 March 1976 east Kazakhstan: earthquake or explosion?, *Geophys. J. R. astr. Soc.*, **74**, 621-631.
- Priestly, K. (1992). Regional seismic studies in Central Asia, *PL-TR-92-2127*, Phillips Laboratory.
- Riviere-Barbier, F. and L.T. Grant (1992). Cluster analysis of closely spaced mining blasts as a method of event location, *PL-TR-92-2006*, Phillips Laboratory.
- Ruud, B.O., E.S. Husebye and R.S. Hestholm (1992). On crustal, short-period Rg-propagation using array records from 4 continents, in *Seismic Surveillance - Nuclear Test Ban Verification*, *PL-TR-92-2095*, E. S. Husebye and B. O. Ruud (Editors), Phillips Laboratory, 119-153.
- Ryaboy, V. (1990). Upper mantle structure along a profile from Oslo (NORESS) to Helsinki to Leningrad, based on explosion seismology, *Bull. Seism. Soc. Am.*, **80**, 2194-2213.
- Ryaboy, V. (1992). Regional phase identification in the IMS, in *Center for Seismic Studies Semiannual Technical Report March-October 1992* by Carter, J., Coyne, J., Grant, L., Henson, A., Israelsson, H., Riviere, F. and Ryaboy, V. *CSS 92-04*, SAIC.

Saikia, C.K. and L.J. Burdick (1991). Fine structure of P_{nl} waves from explosions, *J. Geophys. Res.*, **96**, 14,383-14,401.

Sereno, T.J. and J.W. Given (1990). P_n attenuation for a spherically symmetric earth model, *Geophys. Research Letters*, **17**, 1141-1144.

Sereno, T.J., G.B. Patnaik, and M.J. Mortell (1992). Data to test and evaluate the performance of neural network architectures for seismic signal discrimination: Data sets #2-3, *PL-TR_92-2218(I)*, Phillips Laboratory.

Shumway, R. and R. Blandford (1974). An examination of some new and classical short period discriminants, *SDAC-TR-74-10*, Teledyne Geotech, Alexandria VA.

Smart, E. and K.L. McLaughlin (1985). Discrimination by detection of the relative polarity of the entire P waveform, *TGAL-85-12*, Teledyne Geotech.

Taylor, S.R., N.W. Sherman, and M.D. Denny (1988). Spectral discrimination between NTS explosions and western United States earthquakes at regional distances, *Bull. Seism. Soc. Am.*, **78**, 1563-1579.

Taylor, S.R. and G.E. Randall (1989). The effects of spall on regional seismograms, *Geophysical Research Letters*, **16**, 211-214.

Taylor, S.R., M.D. Denny, E.S. Vergino, and R.E. Glaser (1989). Regional discrimination between NTS explosions and western U.S. earthquakes, *Bull. Seism. Soc. Am.*, **79**, 1142-1176.

Thirlaway, H.I.S. (1963). Earthquake or Explosion? *New Scientist*, **18**, 311-315.

Thirlaway, H.I.S. (1966). Interpreting array records: explosion and earthquake P-wave trains which have traversed the deep mantle, *Proc. Roy. Soc. A.*, **290**, 385-395.

Toksoz, M.N., B. Mandal and A.M. Dainty (1990). Frequency dependent attenuation in the crust, *Geophysical Research Letters*, **17**, 973-976.

Tsvang, S.L., V.I. Pinsky, and E.S. Husebye (1993). Enhanced seismic source discrimination using NORESS recordings from Eurasian events, *Geophys. J. Int.*, **112**, 1-14.

UKAEA (1965). The detection and recognition of underground explosions, United Kingdom Atomic Energy Authority, HMSO, London.

Vogfjörd, K.S., C.A. Langston and B. Yan (1992). Composition of short period regional phases inferred from Fennoscandian array data, *PL-TR-92-2024*, Phillips Laboratory.

Wuster, J. (1992). Discrimination of chemical explosions and earthquakes in Central Europe--A case study (Expanded Abstract), in *Proceedings of the GERESS Symposium on Regional Seismic Arrays June 22-24, 1992*, 1-9.

DISTRIBUTION LIST

DEPARTMENT OF DEFENSE

ARPA/NMRO

ATTN: Dr R. Alewine & Dr A. Ryall
3701 North Fairfax Drive
Arlington VA 22203-1714

Defense Intelligence Agency

ATTN: Dr D. Glover
DIA/DT-1B
Washington DC 20350-6158

Defense Nuclear Agency

ATTN: Dr M. Shore/SPSS
6801 Telegraph Road
Washington DC 20305-1000

Defense Technical Information Center

Cameron Station
Alexandria VA 22314

DEPARTMENT OF THE AIR FORCE

AFOSR/NP

ATTN: Col J.J. Perrizo
Building 410, Room C222
Bolling AFB
Washington DC 20332-6448

AFTAC/CA(STINFO)/TT/TTR/TTD

1030 South Highway A1A
Patrick AFB FL 32925-3002

AFWL/NTESG

Kirtland AFB NM 87117-5000

PL/GPEH

ATTN: Mr J. Lewkowicz
Hanscom AFB MA 01731-5000

DEPARTMENT OF ENERGY

US Department of Energy

ATTN: Mr Max Koontz/DP-5
Forrestal Building
1000 Independence Avenue, SW
Washington DC 20585

Lawrence Livermore National Laboratory

ATTN: Dr J. Hannon & Dr K. Nakanishi
University of California
PO Box 808
Livermore CA 94550

Los Alamos Scientific Laboratory

ATTN: Dr C. Newton
PO Box 1663
Los Alamos NM 87544

Sandia National laboratory

ATTN: Mr P. Stokes, Dept. 9110
PO Box 5800
Albuquerque NM 87185

OTHER GOVERNMENT AGENCIES

CIA/OSWR/NED

ATTN: Dr L. Turnbull
Room 5G48
Washington DC 20505

US Arms Control and Disarmament Agency

ATTN: Dr M. Eimer, Room 4953
Verification and Intelligence Bureau
Washington DC 20451

OTHER GOVERNMENT AGENCIES CON'T

US Arms Control and Disarmament Agency
ATTN: Mr R. Morrow, Room 5741
320 21st Street, NW
Washington DC 20451

US Geological Survey
ATTN: Dr W. Leith
Mail Stop 928
Reston VA 22092

DEPARTMENT OF DEFENSE CONTRACTORS

Center for Seismic Studies
ATTN: Mr Rick Perez, Dr J. Carter, &
Dr S. Bratt
1300 North 17th Street, Suite 1450
Arlington VA 22209-3871

ENSCO, Inc.
ATTN: Dr R. Kemerait
445 Pineda Court
Melbourne FL 32940

ENSCO, Inc.
ATTN: Mr J.R. Stevenson, Dr Z. Der, &
Dr D.R. Baumgardt
5400 Port Royal Road
Springfield VA 22151-2388

Mission Research Corporation
ATTN: Dr M. Fisk & Dr W. Wortman
735 State Street
PO Drawer 719
Santa Barbara CA 93102

Pacific Sierra Research
ATTN: Dr R. Fritzel
1401 Wilson Boulevard, Suite 1100
Arlington VA 22209

S-Cubed, A Division of Maxwell Laboratories
ATTN: Mr J. Murphy, Suite 1112
11800 Sunrise Valley Drive
Reston VA 22019

S-Cubed, A Division of Maxwell Laboratories
ATTN: Dr K.L. McLaughlin
PO Box 1620
La Jolla CA 92038-1620

Science Horizons, Inc.
ATTN: Dr T. Cherry
710 Encinitas Boulevard., Suite 200
Encinitas CA 92024

Science Application International Corporation
ATTN: Dr T. Bache, Jr., & Dr T.J. Sereno
10260 Campus Point Drive
San Diego CA 92121-1578

Teledyne Geotech
ATTN: Mr W. Rivers
314 Montgomery Street
Alexandria VA 22314

Sierra Geophysics, Inc.
ATTN: Dr G. Mellman
11255 Kirkland Way
Kirkland WA 98033

Woodward-Clyde Consultants
ATTN: Dr L. Burdick
566 El Dorado Street
Pasadena CA 91109-3245

Teledyne Geotech
ATTN: Mr M. Browne
3410 Shiloh Road
Garland TX 75041

NONGOVERNMENT CONTRACTORS/UNIVERSITIES

California Institute of Technology
ATTN: Prof T. Ahrens & Dr D.V. Helmberger
Division of Geological and Planetary Sciences
Seismological Laboratory, 252-21
Pasadena CA 91125

Cornell University
ATTN: Prof B. Isacks & Prof M. Barazangi
Department of Geological Sciences
SNEE Hall
Ithaca NY 14850

The Pennsylvania State University
ATTN: Prof C.A. Langston
Geosciences Department
403 Deike Building
University Park PA 16802

Southern Methodist University
ATTN: Dr E. Herrin & Dr B. Stump
Institute for the Study of Earth and Man
Geophysical Laboratory
Dallas TX 75275

University of California
ATTN: Prof L.R. Johnson &
Prof T.V. McEvilly
Seismographic Station
Berkeley CA 94720

University of California (UCLA)
ATTN: Dr P.M. Davis
Department of Earth and Space Sciences
Los Angeles CA 90024

University of California
ATTN: Dr T. Lay & Dr S. Schwartz
Institute of Tectonics
Earth Sciences Board
Santa Cruz CA 95064

Virginia Polytechnic Institute
ATTN: Dr G.A. Bollinger
Department of Geological Sciences
21044 Derring Hall
Blacksburg VA 24061

Columbia University
ATTN: Prof A. Lerner-Lam, Prof P. Richards,
& Prof C.H. Scholz
Lamont-Doherty Geological Observatory
Palisades NY 10964

Massachusetts Institute of Technology
ATTN: Dr R. LaCross, M-200B
Lincoln Laboratory
PO Box 73
Lexington MA 02173-0073

San Diego State University
ATTN: Dr S. Day
Department of Geological Sciences
San Diego CA 92182

University of Arizona
ATTN: Prof T.C. Wallace
Department of Geosciences
Building 77
Tucson AZ 85721

University of California
ATTN: Prof J. Berger, IGPP, A-025
Scripps Institution of Oceanography
La Jolla CA 92093

University of California
ATTN: Prof S. Flatts
Applied Sciences Building
Santa Cruz CA 95064

University of Illinois
ATTN: Prof F.K. Lamb
Department of Physics
1110 West Green Street
Urbana IL 61801

FOREIGN GOVERNMENTS/UNIVERSITIES

Institute of Advanced Studies
 ATTN: Prof B.L.N. Kennett
 Research School of Earth Sciences
 GPO Box 4
 Canberra 2601
 AUSTRALIA

Geological Survey of Canada
 ATTN: Dr P. Basham & Dr R. North
 Earth Sciences Branch
 1 Observatory Crescent
 Ottawa, Ontario
 CANADA K1A 0Y3

University of Toronto
 ATTN: Dr K.Y. Chun
 Geophysics Division
 Physics Department
 Ontario
 CANADA M5S 1A7

Ruhr University, Bochum
 ATTN: Prof Hans-Peter Harjes
 Institute for Geophysik
 PO Box 102148
 4630 Bochum 1
 GERMANY

Federal Institute for Geosciences and National
 Resources
 ATTN: Dr M. Henger
 Postfach 510153
 D-3000 Hanover 51
 GERMANY

National Defense Research Institute
 ATTN: Ms E. Johannisson
 Senior Research Officer
 PO Box 27322
 S-102 54 Stockholm
 SWEDEN

Ministry of Defense
 ATTN: Dr P. Marshall
 Procurement Executive
 Blacknest, Brimpton
 Reading RG7 4Rs
 UNITED KINGDOM

(This page intentionally left blank)